Radiation-induced luminescence mechanisms on quartz and their application to dating

Takashi YAWATA

Ph. D. Thesis

Graduate School of Science and Technology
Niigata University, Niigata, Japan
(Feb. 2007)

Radiation-induced luminescence mechanisms on quartz and their application to dating

(石英からの放射線誘起ルミネッセンス現象の機構解明と年代測定への応用)

Takashi YAWATA

Ph. D. Thesis

Graduate School of Science and Technology
Niigata University, Niigata, Japan

PREFACE

First of all, I wish to express my sincere gratitude to my supervisor and promoter, Prof. Tetsuo Hashimoto (Niigata University) for introducing me to this field of research and for many valuable suggestions and discussions for whole studies.

I would like to also thank Prof. Kiyoshi Sawada (Niigata University), Prof. Tsuneyoshi Horigome (Niigata University), Dr Hisaaki Kudo (Niigata University), and Dr. Shinichi Goto (Niigata University) for critical reading of this manuscript.

This work is largely indebted to the continuous help of many researchers. Dr. Shinichi Goto (Niigata University), Dr. Koki Yamazaki (Niigata Prefectural Radiation Monitoring Center), and Dr. Hisanobu Sakaue (Niigata Prefectural Radiation Monitoring Center) helped me to calibrate HPGe detector. Dr. Keiichi Sato (Niigata University) and Mr. Takashi Sato (Niigata University) gave me helpful advice for ICP-MS measurements. Dr. Sumiko Tsukamoto (University of Wales Aberystwyth) offered me to use the RISØ reader for OSL and TL measurements and gave me helpful advice for Radial plot. Prof. Geoff, Duller (University of Wales Aberystwyth) gave me an opportunity to visit his laboratory and gave me helpful suggestions. Dr. Atushi Tani (Osaka University) gave me helpful advice for ESR measurements. Prof. Ganzawa (Hokkaido University of Education) and Dr. Ryuta Hataya (Central Research Institute of Electric Power Industry) gave me samples and their informations. I am very grateful to all mentioned above and all members in Hashimoto laboratory (Niigata University), especially Dr. Akihiro Takeuchi, Dr. Hiroki Fujita, Dr. Hisanobu Sakaue, Dr. Yukihisa Sanada, Mr. Naoki Mitamura, Mr. Nobuhiro Shimizu, Mr. Yasuhiro Tajika, Mr. Tomoyuki Takeuchi, Mr. Tomohiro Shibutani, Ms. Sachiko Nomura, Ms. Yuko Nakata, and Ms. Mizuho Tamaki.

This work was supported by the grant for Research Fellowships of the Japan Society for the Promotion of Science (JSPS) for Young Scientists (No. 17-902, 2005-2007) and I greatly appreciate it to concentrate in my work completely for these three years.

Takashi YAWATA

Contents

General introduction

Chapter 1

Optimal luminescence measuring conditions

for single-aliquot regenerative-dose (SAR) method

Table

Figure

Chapter 2

Dependence of luminescence properties on impurity contents in quartz

Table

Figure

Chapter 3

Determination of internal radioactivity in quartz grains using a multiple pulse time interval analysis (MTA) technique and its contribution on annual dose for RTL dating

Table

Figure

† *General introduction* †

For the Late Quaternary dating, there are a number of radiation dosimetry and dating methods which can establish the formation time covered wide ranges using organic and inorganic materials. However direct dating methods are relatively few. From the archaeological point of view, the radiocarbon (^{14}C) dating technique is predominant for successive sediment layers and ruin sites when remains of human occupation, or even human remains, are contained therein. Owing to commercially use of accelerated mass spectrometry (AMS) for $^{14}C/^{12}C$ ratio determination, the upper and lower age limits are currently extending towards a 55,000 BP. and a few tens years ago, respectively. The radiocarbon technique has a strong role in this respect using organic materials such as charcoal, or fossil plants and shells. However, there needs to be any indications that growth was in situ soon after deposition and this is not always the case. Furthermore, several reservoir effects, such as marine reservoir effect, northern to southern hemisphere effect and hard-water effect, result in an apparent increase in the ^{14}C age and are difficult to assess true ^{14}C age (Wagner, 1995). On the other hand, fission track dating method can be applied to the inorganic material, such as mica and quartz elapsed beyond about 200,000 years. Thus, there are circumstances when the existing dating methods are restricted due to the validity, accuracy and materials.

In such situations, the luminescence methods, including thermoluminescence (TL) and optically stimulated luminescence (OSL), is principally proving to be increasingly advantageous (Aitken, 1985; 1998). The characteristic of this method that makes it important to geoscientists and archaeologists is that ‘clock’ of natural minerals can be set to zero by heating or exposure to light. Because, both heating in the course of heated events and daylight exposure in the course of deposition are important for several aspects of Quaternary research. For both luminescence phenomena, the minerals of main interest are grains of quartz and feldspar, which are abundant in natural. The dosimetry/dating ranges and their examples are shown in Fig. 1 and Table 1, respectively. These examples also have other connotations: for instance, the sand deposited by a tsunami wave can help elucidate the chronology of past earthquakes; bracket lava is used to date volcanic activity; several deposits can document environmental transitions. The upper and lower limit to the radiation dosimetry and dating are found to be greatly dependent on kind of the each luminescence; OSL of quartz can be applied to the range from a few years (mGy order) to ten thousand years (up to 100 Gy);

OSL of feldspar, called infrared stimulated luminescence (IRSL), has linear relationship between luminescence and applied doses from a few years (mGy order) to hundred thousand years (up to 1 kGy), however IRSL phenomena are greatly suffered from extremely fading rate (anomalous fading effect); TL of quartz (red TL; RTL and blue TL; BTL) can be applied to the range from a thousand years (Gy order) to a million years (up to 10 kGy). However, it should be noted that both limits are dependent on sample type, circumstance, and technique.

In particular, the RTL phenomena, which were initially reported by Hashimoto et al. (1986, 1994), have recognized to show dominantly in quartz grains from volcanic samples and burnt archaeological samples (Ganzawa et al., 1997; Nakagawa and Hashimoto, 2003) and to be preferable for the equivalent dose determination because of possessing the excellent properties of RTL (Hashimoto et al., 1993; Fattahi and Stokes, 2003; Stokes and Fattahi, 2003). However, owing to high thermal background the RTL-measurements had been limited to relatively old samples rather than BTL-measurements. As the high background is a major source of error in estimating the equivalent doses, it is important to retard this background as low as possible (Bøtter-Jensen, 1997; Yawata and Hashimoto, 2004; Ganzawa et al., 2005).

For the luminescence mechanism, some of defect sites due to impurity atoms in natural quartz can operate as luminescent centres when quartz is exposed with ionizing radiations (McKeever, 1988). In general, the impurities in dielectric materials give rise to localized energy levels within the forbidden energy gap, which are crucial to the luminescence process. So, the properties of luminescence emission from quartz are well known to be particularly sensitive to the trace amounts of impurities. Several researchers have reported that the recombination of electrons with $[AlO_4/h]^0$ centres give rise to BTL emission (at 470 nm). Additionally, other centres related to UV emission (250-400 nm) have been identified to be electron recombination with holes trapped at the family of $[AlO_4/h]^0$ centres or at $[AlO_4/M^+]$ (M^+: alkali ions) centres. On the other hand, hole centres of RTL emission (620-630 mn) have not been cleared yet.

Accordingly, the aim of this thesis is to study the RTL properties and to construct the preferable RTL hole centre model. This area has not been explored well and there are many interesting topics. This thesis can be divided to three parts, measuring-system part, basic study part and application part. In chapter 1,

for the sake of low-level and high-reproducible RTL-measurements, the measuring conditions were optimized from the view points of irradiation part and detection part. In Chapter 2, thirty synthetic and natural quartz samples were subjected to measure TL-coloration, TL-sensitivities, concentrations of impurity, and $\alpha-\beta$ phase inversion break temperatures. From these relationships, preferable RTL hole centre model was discussed. Chapter 3 is a geological application to estimate an equivalent dose and an annual dose using volcanic ash samples originated in the Toya-volcano activity, which were estimated the age of at around 100-120 ka (Machida and Arai, 2003). For accurate annual dose calculation, liquid scintillation counting combined with pulse time interval technique was developed for determination of radioactive nuclides in quartz (namely internal dose-rate).

Reference

Aitken M. J., Thermoluminescence Dating. Academic press, London, 61-86 (1985).

Aitken M. J., An introduction to optical dating. Oxford university press, 39-47 (1998).

Bøtter-Jensen L., Luminescence techniques: Instrumentation and Method. Radiat. Meas., **27**, 749-768 (1997).

Fattahi M., and Stokes S., Dating volcanic and related sediments by luminescence methods: a review. Earth Sci. Reviews. **1280**, 1-36 (2003).

Ganzawa Y., Watanabe Y., Osani F., Hashimoto T., TL color images from quartzes of loess and tephra in China and Japan. Radiat. Meas., **27**, 383-388 (1997).

Ganzawa Y., Furukawa H., Hashimoto T., Sanzelle S., Miallier D. and Pilleyre T., Single grains dating of volcanic quartz from pyroclastic flows using red TL. Radiat. Meas., 39, 479-487 (2005).

Hashimoto T., Koyanagi A., Yokosaka K., Hayashi Y., Sotobayashi T., Thermoluminescence color images from quartz of beach sands. Geochem. J., **20**, 111-118 (1986).

Hashimoto T., Kojima M., Shirai N. and Ichino M., Activation energies from blue- and red-thermoluminescence (TL) of quartz grains and mean lives of trapped electrons related to natural red-TL. Nucl. Tracks Radiat. Meas., **21**, 217-223 (1993).

Hashimoto T., Sakaue S., Aoki H. and Ichino M., Dependence of TL-property changes of natural quartzes on aluminium contents accompanied by thermal annealing treatment. Radiat. Meas. **23**, 293-299 (1994).

Machida H. and Arai F., Atlas of tephra in and around Japan (in Japanese). University of Tokyo Press, 94-165 (1992)

McKeever S. W. S., 1988. Thermoluminescence of solids. Cambridge University Press. Cambridge.

Nakagawa T., Usuda H., Hashimoto T., Optically stimulate luminescence (OSL) and thermoluminescence (TL) properties of red TL (RTL) quartz using a new automated OSL/TL measuring system. J. Radioanal. Nucl. Chem., **255**, 355-358 (2003).

Stokes S. and Fattahi M., Red emission luminescence from quartz and feldspar for dating applications: an overview. Radiat. Meas., **37**, 383-395 (2003).

Yawata T., Hashimoto T., Identification of the volcanic quartz origins from dune sand using a single-grain RTL measurement. Quat. Sci. Rev., **23**, 1183-1186 (2004).

Wagner G.A., Age Determination of Young Rocks and Artifacts; Physical and Chemical Clocks in Quaternary Geology and Archaeology. Springer-Verlag Berlin Heidelberg, New York, 144-145 (1995).

Table 1 Some typical luminescence dating examples using quarz and feldspar grains

Method	sample	Material	Location	Age range (ka)	stimulation	Authors
Blue-TL	Quartz (?)	Pottery		>1.0		Kennedy and Knopff, 1960
Blue-TL	Quartz	Pottery	Japan	12-13		Ichikawa and Nagatomo, 1978
Blue-TL	Polymineral	Under lava flows	Idaho	2-100		Forman et al., 1994
Blue-TL	Polymineral	Loess, Tephra	Central Asia	190±20		Berger et al., 1996
Blue-TL	Polymineral	Loess bracketing tephra	Washington and Oregon	15-40		Richardson et al., 1999
Red-TL	Quartz	Pumice	Japan	60-200		Hashimoto et al., 1991
Red-TL	Quartz	Baked soil	France	8.5-9.5		Montret et al., 1992
Red-TL	Quartz	Primary volcanic deposit (Ignimbrite)	NewZealand	300-1200		Fattahi and Stokes, 2000
OSL	Quartz	Dune sand	USA	4-10	Green laser	Gaylord, 1993
OSL	Quartz	Sand from rock shelter at Nauwalabila	Australia	0.3-60	Green laser	Roberts et al., 1994
OSL	Quartz	Dune sand	Zimbabwe	9-115	Green laser	Stokes et al., 1997
IRSL	K-feldspar	Tsunami-sand	British Columbia	0.2-1.3	IR-diodes	Huntley and Clague, 1996
IRSL	K-feldspar	Colluvial deposit	Africa	13-96	IR-diodes	Clarke et al., 1996
IRSL	Polymineral	Loess	USA	2-11	IR-diodes	Lian, 1997

This table was modified from references (Aitken, 1998; Fattahi and Stokes, 2003)

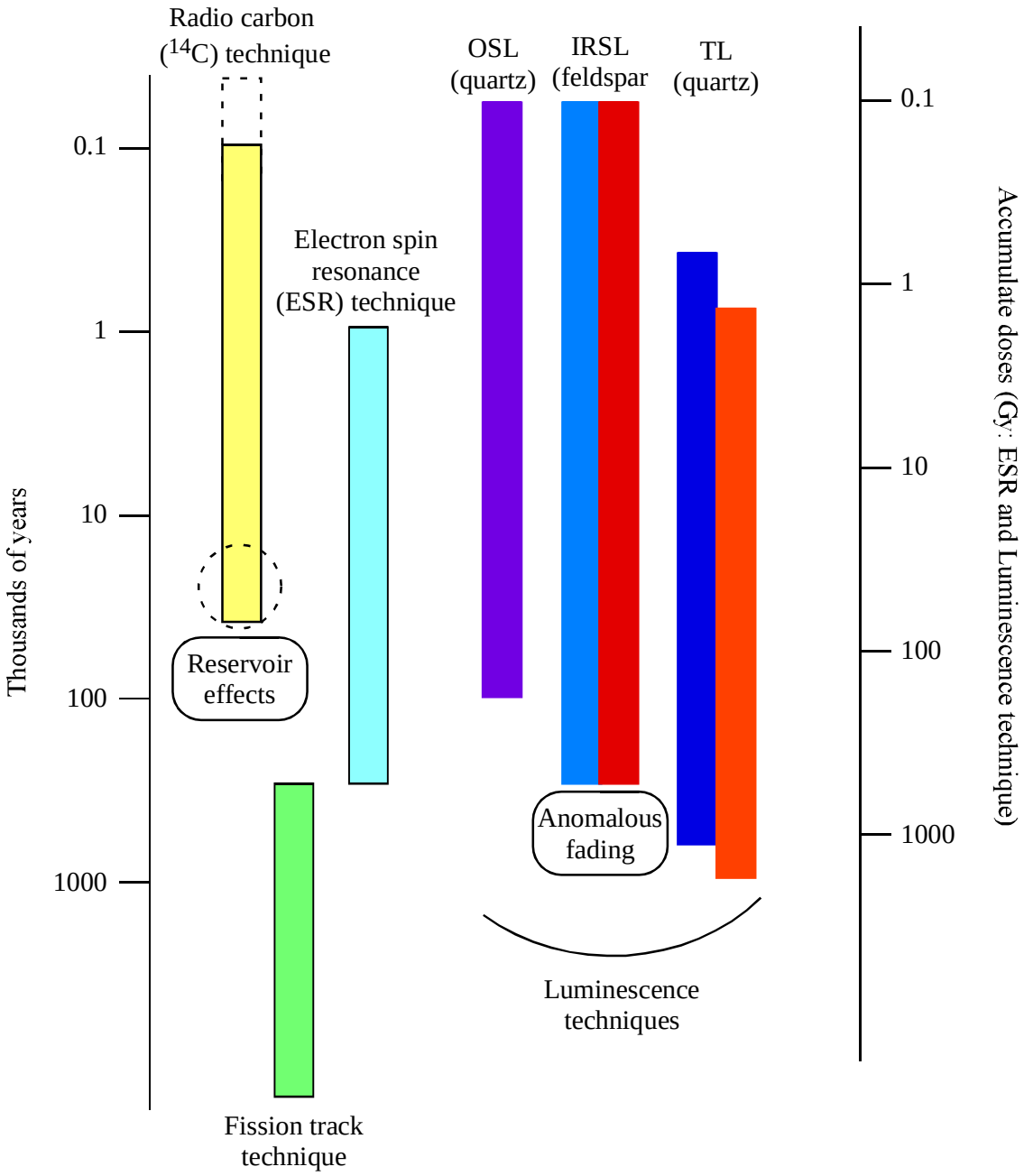

Fig. 1 Conceptual view of radiation dosimetry/dating ranges of several techniques. Actual limits are dependent on sample type and technical development

† *Chapter 1* †

Optimal luminescence measuring conditions

for single-aliquot regenerative-dose (SAR) method

Abstract

For accurate equivalent dose determination using single-aliquot regenerative-dose (SAR) method, it is necessary to achieve high reproducibility for detection of luminescence as well as for a fixed artificial irradiation. Therefore, the luminescence measuring conditions for the equivalent dose determination were optimized from the view points of irradiation part and detection part.

Radiation induced luminescence was measured using a small X-ray generator (Varian VF-50J) as a natural radiation dose simulator. Assessment of the optimal X-ray irradiation conditions include consideration of the irradiation dose rate change and the thickness variations of Al-absorber in the equivalent dose determination when simulating the dating process with laboratory dosed quartz samples. As a result, the equivalent doses were found to be greatly dependent on both the thickness of Al-absorber and the X-ray dose rate. Consequently, the optimal X-ray irradiation conditions for an accurate luminescence dating work were obtained by applying the following conditions: (i) use of the Al-absorber with a thickness of approximately 200 μm and (ii) X-ray dose rates of 0.38 Gy/min to 2.9 Gy/min.

Red thermoluminescence (RTL) of natural quartz grains has been recognized to offer preferable properties for the Quaternary chronology and archaeological dating. However, the most inevitable obstacle on the RTL-measurements is high background due to high thermal background according to black-body radiation on heating up. To eliminate the thermal background as low as possible, the suitable combination of optical filters, a silver sample disc covered with biotite plate, and the use of light guide and cluster-heater have been applied, so that the thermal background decreased from $2x10^4$ cps into 1000 cps in the temperature ranges of 350-380^oC. Accordingly, RTL detection limit was realized till about 100 cps.

1. Introduction

Radiation induced luminescence phenomena, including thermoluminescence (TL) and optically stimulated luminescence (OSL), arise from the recombination of luminescent holes with electrons, which are released from the metastable energy levels within dielectric materials, such as ceramics and natural minerals. These luminescence intensities connected with naturally accumulated radiation defects can be applicable to dosimetry and age determination of geological and archaeological samples (Aitken, 1985, 1998). In general, the naturally accumulated dose (radiation defects) is called the 'equivalent dose', which has been recently estimated by the single-aliquot regenerative-dose (SAR) method (Wintle and Murray, 2000). A generalized measurement procedure of the SAR method (Table 1-1) involves repeated measurements of the same aliquot in order to construct a dose response curve. After measuring the natural signal (heated (TL) or bleached (OSL)), larger laboratory regeneration doses are successively administered and the consequent TL/OSL signals are measured. Sensitivity changes during the successive TL/OSL measurements are corrected using the luminescence response by a subsequent small radiation dose which keeps constant dose throughout the experiment. A plot of luminescence intensities against laboratory given doses enables natural luminescence intensity to make evaluation of an equivalent dose. In this protocol, an artificial irradiation source as a standard dose-simulator with a fixed irradiation geometry in place of natural radiations needs to determine the equivalent doses.

For the accurate equivalent dose determination, therefore, it is necessary to achieve high reproducibility for detection of luminescence photons as well as for artificial irradiation. In this thesis, all luminescence measurements were carried out using an automated OSL/TL measuring system installed with a small X-ray generator (Hashimoto et al., 2002; Nakagawa et al., 2003). Therefore, in this chapter, I optimized luminescence measuring conditions for the equivalent dose determination from the view points of (1) irradiation part (see Section 2) and (2) detection part (see Section 3).

2. Optimal X-ray irradiation conditions

Firstly, in order to obtain a good reproducibility of X-ray irradiation, optimal X-ray irradiation conditions including the thickness of Al-absorber and dose rates are discussed in terms of the equivalent dose determination using SAR protocols. In this section, the investigation was carried out using OSL/SAR technique due to lower background contribution in comparison with TL-measurements (see the section 3 in details).

2-1. Introduction of a small X-ray generator (Varian VF-50J)

Insofar, the 40 mCi ^{90}Sr-^{90}Y beta source has been commonly installed on the luminescence measuring system for luminescence dating works (Bøtter-Jensen et al, 2000), although they provide only a fixed dose rate and require a heavy shielding to protect bremsstrahlung X-rays from the ^{90}Sr-^{90}Y source. In order to overcome these problems, the preferred use of a small X-ray generator (Varian VF-50J), which has a maximum power of 50 W at 50 kV and 1 mA, instead of the ^{90}Sr-^{90}Y beta source as a standard radiation source, was proposed because of the following advantages; (i) a good linearity between tube currents and X-ray dose-rates, (ii) a wide dynamic range of applicable dose rates and (iii) a highly uniform irradiation property to the sample area (Hashimoto et al., 2002; Andersen et al., 2003). The photon energies emitted from X-ray generator are well known to produce continuous energy spectrum as well as the electron energies from beta sources. In Fig. 1-1, the X-ray energy spectrum from this small X-ray generator consists of both low- and high-energy components, having an energy peak of 9 keV, assigned characteristic X-ray from target material (tungsten target) and a main peak at 35 keV, respectively. (Yawata and Hashimoto, 2004; Hong et al., 2005). From the mass-attenuation coefficients, the half-layer value for quartz is calculated about 5 mm Al thickness for 35 keV photons. This means that the high energy components at 35 keV generated from the small X-ray generator will completely penetrate into typical quartz samples such as a monolayer coarse grains (75-150 μm). However, the low-energy parts of X-rays at 9 keV are too week to pass through whole of coarse grains due to their short ranges within quartz (half-layer value for quartz: 150 μm), so

that inhomogeneous ionization may occur within grains. Consequently, the incomplete ionizing parts should give rise to different luminescence intensities and lead the scatter of equivalent doses. To eliminate the low-energy components, a use of appropriate Al-absorber was recommended from the X-ray spectrum and etching test (Yawata and Hashimoto, 2004a; Hong et al., 2005).

2-2. Measuring system and conditions

All luminescence measurements were carried out by using an automated OSL/TL measuring system installed with a small X-ray generator (Varian VF-50J) (Hashimoto et al., 2002; Nakagawa et al., 2003). In order to obtain a good reproducibility of irradiation, the X-ray tube was mounted on a lead collimator with a hole of 12 mm diameter. The distance between X-ray tube window and sample was fixed at a distance of 50 mm. Since the X-rays arise from collision of the accelerated electrons to the tungsten target, the energy spectrum of the X-rays consists of main Bremsstrahlung radiation accompanied with a line spectrum due to characteristic L-shell X-ray at about 9 keV (Fig. 1-1). Any characteristic K-shell X-rays do not appear, because the threshold energy needs above 50 keV for tungsten target. In addition, the X-ray photons with energies below a few keV are removed by Beryllium thin window. The X-ray generator using thermionic cathodes was known to delay a few seconds for the actual start of X-ray emission because the filling of a condenser with electrons. To evaluate this dead time, the X-ray photons were counted by using both the high-efficiency Ge semiconductor (EGSP 2800-30-R) and the multi-channel analyzer (MCA) as seen in Fig. 1-2. From this measurement, the dead time was estimated to be approximately two seconds at the tube current of 0.01 mA at 50 keV. In order to estimate the contribution of this dead time on the equivalent dose determination, an investigation was carried out without any mechanical shutter, although the use of mechanical shutter was more preferred.

In the OSL measurements, quartz grains were stimulated by 16 LEDs with 11.8 mW/cm^2 at the sample position. The photon signals were recorded every 0.2 second intervals by keeping the sample at 125^oC during light exposure, after the preheating procedure for 5 min at 220^oC. The signals

were integrated for the first one second of the decay curve, in calibrating the X-ray dose-rates as well as in determining the equivalent doses. The quartz samples were uniformly fixed on silver discs (a diameter of 10 mm) using silicone oil to distribute a monolayer of coarse grains.

2-3. Calibration of X-ray dose-rates

The quartz sample was prepared from "acid washed sand" (supplied by BDH Co. Ltd.) quartz, which was heated for 5 min at 500^{o}C to eliminate the residual natural doses and to enhance OSL signals. With the quartz sample treated in such a way, a 5 Gy of irradiation was administered using a calibrated ^{137}Cs source, and the X-ray dose rates for tube currents were then determined using SAR method. The sequence was as follows: the first one second of the OSL signal from the 5 Gy quartz sample was measured and the subsequent SAR growth curve was constructed as a function of X-ray irradiation time. Sensitivity changes were carefully monitored. With the X-ray irradiation time equivalent to an absorbed dose of 5 Gy, the dose rates were calculated by changing both the tube currents and the thicknesses of Al-absorber. Table 1-2 and Fig. 1-3 represent the results of the estimated dose rates. The experimental errors were derived from four or five aliquot analyses. Note that the dose rates in Table 1-2 were not corrected the dead time contribution from the X-ray generator.

2-4. Simulation of equivalent dose determination

Determination of a natural equivalent dose was simulated by using three sets of heated quartz samples, which were dosed to 10 Gy, 20 Gy and 50 Gy by using a calibrated ^{137}Cs source. These samples simulated the natural samples, and the SAR protocol was applied to determine the initial doses. Comparison of the given initial doses with the estimated doses may then give some guidelines for determining optimal conditions for the use of the X-ray generator.

In this simulation, the X-ray dose rates at the X-ray tube currents of 0.02 mA, 0.04 mA, 0.08 mA, 0.15 mA and 0.30 mA were employed. To check the influence of low-energy photons around 9 keV from the X-ray generator, the determination of equivalent doses were carried out under

employment of various Al-absorber thicknesses (without Al-absorber and with Al-absorber thicknesses of 50 μm, 100 μm, 150 μm and 200 μm). A measurement with an Al-thickness greater than 200 μm was not performed, since the thickness of 200 μm was enough to absorb completely the low-energy components (Fig. 1-1). The results were summarized in Table 1-3 and Fig. 1-4.

2-5. Results and discussion

2-5-1. X-ray dose-rates

Table 1-2 is summarized the X-ray dose rates as a function of X-ray tube currents and Al-absorber thicknesses. The table shows the highest precision at the measurement of 200 μm Al-absorber thickness. The X-ray dose rates with an Al-absorber (200 μm) and without an Al-absorber were plotted as a function of tube currents in Fig. 1-3, in which a good linear relationship is illustrated between X-ray dose rates and X-ray tube currents ranging of 0.2 mA ~ 3.0 mA. This means that the desirable dose rates (0.38 Gy/min ~ 22.1 Gy/min) can be conveniently obtained by means of changing the thicknesses of Al-absorber, along with change of the X-ray tube currents. In addition, the higher or lower X-ray dose-rates can be obtained by adjusting the distance changes between X-ray window and sample.

In Table 1-2, the experimental errors accompanied with dose rates in each condition apparently decreased as the thickness of Al-absorber increased, which was intimately correlated with good reproducibility. This tendency should be attributed to the incomplete ionizing parts due to low X-ray energy parts below 9 keV. The low-energy parts of the X-ray around 9 keV (half-layer value for quartz: 150 μm) are too weak to pass through the whole coarse grains due to the short ranges within quartz. Inhomogeneous ionization would, therefore, occur within grains. These incomplete ionizing parts may cause different luminescence intensities and can potentially be a significant source of scatter in the estimated equivalent doses. From this result, a thicker Al-absorber than 200 μm is recommended for an accurate luminescence dosimetry and dating works, although these uncertain effects can be eliminated by the use of Al-absorber with a thickness of at least 50 μm, as reported in the previous

etching tests (Yawata and Hashimoto, 2004a; Hong et al., 2005).

Figure 1-2(b) shows superior feature of the small X-ray generator providing excellent irradiation stability during irradiation. The stability scattering in X-ray photons was estimated to be only 0.6%. However, the X-ray generator also has an intrinsic dead time of about 2 sec, which is corresponding to the 2% irradiation error for the irradiation time of 100 sec. Anderson et al. (2003) have proposed the use of a mechanical shutter to eliminate the dead time. However, the dead time contribution for X-ray dose rates would contribute negligibly if the X-ray irradiation time is longer enough in comparison with the dead time. As an example, an acceptable X-ray irradiation condition was achieved when low X-ray dose rates of 0.38 Gy/min ~ 2.9 Gy/min with a long irradiation time of over 100 sec were used (see the following section 2-5-2 in details). Alternately, the dead time can be compensated by the real irradiation time by subtracting 2 sec from the actual irradiation time, since the dead time of 2 sec are unchangeable even if the applied voltage and current are changed. Bøtter-Jensen et al. (2003) reported a uniformity of the X-ray dose rate across a sample disc with a diameter of 10 mm from the same X-ray generator. By using an optimized collimator design, they obtained an improved uniformity of approximately 1%, which is much better than the result of the ^{90}Sr-^{90}Y beta source.

2-5-2. Simulation of equivalent dose determination

The simulated doses for artificially irradiated quartz samples equivalent to 10 Gy, 20 Gy, and 50 Gy were estimated by varying both X-ray tube currents (0.02 mA, 0.04 mA, 0.08 mA, 0.15 mA and 0.30 mA) and Al-absorber thicknesses (0, 50 μm, 100 μm, 150 μm and 200 μm). The dose-response curve of the quartz samples was saturated around 50 Gy, so that the estimated equivalent doses of 50 Gy were considerably scattered. As shown in Table 1-3 and Fig. 1-4, the evaluated equivalent doses with the highest precision were obtained at an Al-absorber thickness of 200 μm (8.4% for no Al-absorber, 6.9% for 50 μm, 100 μm and 150 μm Al-absorbers, and 5.1% for 200 μm Al-absorber). These results are similar to the result of the dose rate measurement. In addition, the equivalent doses

were underestimated from the use of the dose rates of over 3.0 Gy/min, compared with the initially given dose, irrespective of the thicknesses of Al-absorber. Particularly, the artificially dosed quartz samples (50 Gy) offered higher degrees of underestimation relative to the lower dosed samples (10 Gy and 20 Gy).

In order to investigate this inconsistent result, the OSL intensities were measured against the X-ray dose rates with quartz samples artificially dosed to 30 Gy. The OSL intensities rapidly increased in the dose rate range of 3.0 Gy/min to 6.0 Gy/min, as shown in Fig. 1-5. This change implies that the underestimation of the equivalent dose could be assigned to the dose rate effects. The enhanced OSL sensitivities for given high X-ray dose rates induced steeper regeneration curves and consequently resulted in the underestimation of equivalent doses. The dose and dose rate effects for TL and OSL sensitivities have been described in several studies. Valladas and Ferriera (1980) observed a 10% increase in TL sensitivity (ultraviolet emission) in the dose rate range from 8 mGy/min to 9 Gy/min, while Groom et al. (1978) reported a decrease of a factor of 5 in TL sensitivity when the applied dose rates were varied from 84 mGy/min to 19.8 Gy/min. In addition, Chawala et al. (1998) observed that TL ages for quartz with doses over 250 Gy may be underestimated when TL sensitivity was increased according to variations of the laboratory dose rate.

Concerning the causes of dose-rate and dose dependence, Bailey (2004) and Bailey et al. (2005) have investigated the dose rate effects on the OSL dose-response curve from quartz on the basis of empirical results and a numerical model, including seven electron trapping sites and four recombination centers. They suggested that dose rate dependence can probably be caused by an increased competition of the electrons from the conduction band during the laboratory irradiation in comparison with natural irradiation. They concluded the competition was attributed to relatively thermally unstable recombination centre, which is effectively absent at natural irradiation rates. In general, the TL/OSL defects behave competitively with free electrons and holes which are created during irradiation. The recombination of defect pair should result in the production of radio-luminescence (RL). Recently, Shimizu et al. (2006) have investigated an experimentally

competitive relationship between blue TL and blue RL sources, based on the irradiation temperature dependence. A greater number of TL/OSL/RL measurements as a function of irradiation/stimulation temperature dependence are required to characterize the thermally unstable recombination centre. Much attention should be paid on the construction of an optimal OSL model for these relationships.

According to these results, the regenerated dose response curves on some quartz samples could be susceptible to X-ray dose rate effects. This dose rate dependence may arise due to the competition for electrons, during irradiation, from the relatively thermally unstable recombination centre. However, the dose rate dependence on luminescence should be further studied for luminescence works to obtain a more accurate luminescence doses result and a suitable luminescence model.

2-6. Conclusions (Irradiation part)

It was recognized that a small X-ray generator (VF-50J) possesses several excellent properties, such as irradiation stability and desirable X-ray dose rates. These advantageous properties could be attained by adjusting both the irradiation time and the thickness of Al-absorber. For an accurate luminescence dating work, the use of Al-absorber with a thickness of approximately 200 μm was recommended since this thickness could eliminate low-energy components which induced scattered data in the equivalent dose values. In the simulation of equivalent dose determination, the regenerated dose response curves of quartz samples used in this study were found to be greatly dependent on the X-ray dose rate and to show agreement to the initially given dose in the dose rate range of 0.38 Gy/min to 2.9 Gy/min. As a result, it was found that optimal X-ray irradiation conditions for accurate luminescence dosimetric work were achieved by applying following conditions: (i) use of the Al-absorber beyond 200 μm thickness, (ii) longer time irradiation over 100-200 sec, and (iii) relatively low X-ray dose-rates of 0.38-2.9 Gy/min.

3. Optimal detection conditions for red TL (RTL)-measurements

Red TL (RTL) properties of natural quartz grains have been recognized to provide the preferable properties for the equivalent dose determination owing to high signal stability and good dose-response (Hashimoto et al., 1993; Fattahi and Stokes, 2003; Stokes and Fattahi, 2003). However, the most inevitable obstacle on the RTL-measurements is high background due to black-body radiation from heating portion of sample and sample disc. As the high background component must be a major source of error in estimating the equivalent doses, it is important to retard this background as low as possible (Bøtter-Jensen, 1997; Yawata and Hashimoto, 2004b; Ganzawa et al., 2005). Insofar, owing to high thermal background, the RTL-measurements had been limited to relatively old samples, which accumulate doses over 50 Gy (Miallier et al, 1991). Recently, Hashimoto et al. (2002) developed an automated OSL/TL measuring system having high sensitivity detection for RTL, enabling to detect doses below 10 Gy.

An OSL dosimetry from single quartz grain has been initially attempted by Roberts et al. (1997) and Murray and Roberts (1997) using a laser beam stimulation. Additionally, reliable OSL-measurements combined with single grain technique have been utilized for the age determination using several age models (Galbraith and Laslett, 1993; Duller et al., 2000). Nowadays, the single grain technique becomes necessary to assess the uncertainty associated with equivalent dose distribution. Besides the OSL-measurements with single grain technique (McFee and Tite, 1994; Olley et al., 1999; Duller et al., 2000), a little attention has been paid to the RTL-measurements using single quartz grain method (Yawata and Hashimoto, 2004b; Ganzawa et al., 2005) because of high thermal background during the sample heating.

In this section, the RTL-measurements combined with single grain technique were developed for quartz grains in terms of eliminating the thermal background. Additionally, this allows the lower RTL equivalent dose limits with high reproducibility for aliquot samples (~5mg) to be extending toward a few Gy (equivalent from hundreds years to a thousand years).

3-1.Sample and sample preparation

The quartz grains were collected from volcanic ash layers (Medeshima tephra layer, Miyagi, Japan), which show typically RTL properties (see Fig. 2-2(b)) from TL color image and TL-spectrometry (Hashimoto et al., 1989, 1997). Sample preparation was carried out using standard procedure as follows; samples were washed and treated with 6M HCl and 6M NaOH to remove carbonates and organic materials. Remains were etched for 60 min with 46 % HF at 50^{o}C under an ultrasonic agitator to remove the alpha-dosed surface of the grains. After drying, the samples were sieved to obtain the 250-500 μm diameter fraction for the single-grain measurements and 75-150 μm diameter fraction for the determination of optimal RTL-measurement conditions, respectively. A flow diagram of extraction procedure is shown in Fig 1-6. In these procedures, quartz crushing procedure was not applied since the mechanical crushing will cause uncertain effects, such as formation of surface disordered layer (Takeuchi et al., 2006).

3-2. Determination of optimal RTL-measuring conditions

Since a high thermal background is originated from in the vicinity of heating part during the RTL-measurement, the following causes of thermal background can be considered, such as (i) heating unit, (ii) sample disk, and (iii) detection parts.

(i) Heating unit

The heater unit should be most intensive cause of background in the TL measuring system, namely almost thermal photons must generate at the higher heater-temperature beyond 300 ^{o}C. In order to suppress the black-body radiation, a small cluster ceramic-heater (32W x 4), possessing an edge-part with the highest heating-power, was wrapped with brass plate and used by restricting the small heater-area down to about 10^2 mm^2 faced to the PMT surface. Furthermore, to eliminate the stray light, this heating unit is surrounded with an aluminum plate.

(ii) Sample disc

Silver disc is preferable for the TL measurements since high thermal conductivity lead to

small thermal lag between disc and quartz samples. The schematic sample disc for single grain measurements is shown in Fig. 1-7(a). The silver disc plate of 8 mm in diameter is covered by a biotite 10 mm in diameter with a small hole of 0.8 mm diameter, into which a single quartz grain is placed. As seen in Fig. 1-7(b), the thermal background tends to increase rapidly with increment of hole diameter. Such setting of a biotite cover is preferable to eliminate effectively black-body radiation owing to its preferable property of the poor thermal conductivity in vertical direction of the biotite plate layers as well as no transmission of light in the visible light region. When a biotite plate, having a sample hole with less than 2 mm diameter, was employed, the thermal background could reduce to be approximately a part of seventh relative to uncovered sample disc.

(iii) Detection parts

Dark noise of the PMT with multi-alkali surface (Na-K-Sb-Cs) was suppressed by installing in cooling box which was kept at -20^{o}C. As shown in Fig. 1-8. The holding PMT at -20^{o}C allows great reduction of background counts from 200 cps to 30 cps. Since the storage of PMT in the cooling box brings on the long distance between the PMT surface and sample, the poor light collection became serious problem. To improve the light collection efficiency, a core-rod type light guide (65mm in length and ϕ=11mm) was inserted between the sample and the PMT surface. Transmittance of a light guide over 320-800 nm is illustrated with Fig. 1-9(a). Fig. 1-9(b) shows differences of RTL glow-curves with and without the light guide using two quartz aliquots (5 mg), which are irradiated with a fixed dose. The light collection efficiency using light guide improved in a factor of 40 by comparing without a light guide.

In order to detect selectively RTL photons, suitable optical filter combinations were searched in terms of signal to noise ratio for RTL measurements. The quartz grains of 5 mg were irradiated with a fixed dose (60 Gy) of X-ray. Then, the samples were initially subjected to a measurement of first glow-curve, followed to a black-body curve. The first glow-curve are subtracted from the black-body curve, the remainder is defined as an RTL glow-curve. Both RTL glowcurve and black-body curve were integrated over 350-380 ^{o}C, assignable to either RTL signal or to background, respectively. The

experimental errors were derived from three different disc analyses. The detection windows and signal to noise ratio for selected filter combinations are summarized in Fig. 1-10 and Table 1-4. Four IR-cut (CF-50E (Asahi techno), IRC-65L (Kenko), IR-cut (eagle), and UCF-22 (Kureha)) and three long wavelength pass (O-56 (HOYA), SC-54 (Fuji), and R-60 (Toshiba)) filters were applied to the present tests. It is efficient to remove the contribution of black-body radiation (690-700 nm) down to 3%, whereas the combination of O-56 and CF-50E allows to transmit only about 30% of the RTL signal in the wavelength range of 620-630 nm. In contrast, the O-56 and IRC-65L offer the highest transmission of RTL signal (c. 75%), giving relatively good heat rejection ability to PMT sensitive surface by cutting infra-red region with 5%. In Table 1-4, O-56 and CF-50E combination are considered to be most favorite filter combination for RTL/single grain measurements in spite of low transmission of RTL signal. It should be emphasized again that reproducibility of RTL measurements is prominently influenced by thermal background events rather than the objective luminescence signals.

On the basis of these experimental results, the final measuring conditions can attain the excellent reproducibility of RTL signal even from single quartz grain. The thermal background apparently reduced from $2x10^4$ cps to 1000 cps in the temperature ranges of 350-380^oC, which is commonly identified RTL peaks, by eliminating the black-body radiation. The detection limit of RTL-glow curve was estimated for the single grain by applying regeneration procedure composed of artificial irradiation with known doses and RTL measurements. As a result, the weakest RTL-glowcurve peak has a detection limit of about 100 cps for low level X-ray irradiation (4 Gy) of single grains (250-500 μm). Note that this detection limit should be greatly dependent on RTL sensitivities, which are strongly dependent on impurity contents (see Chapter 2 for details).

3-3. Equivalent dose determination using RTL/single-grain measurements

In order to check the reproducibility of RTL/single-grain measurements for the equivalent dose determination, the SAR protocol was applied for three aliquot samples (~5 mg) and 50

single-grain samples under the optimal detection conditions as described above. For aliquot analyses, biotite-uncovered sample disc was used. In RTL-measurements, the natural samples were measured from 50°C to 450°C at heating rate 1°C/sec with a preheat at 220°C for 3 min. Resultant equivalent doses from 50 grain analyses are plotted into a radial plot (Galbraith, 1990) as seen in Fig. 1-11.

The estimated equivalent doses from three aliquots and 50 single-grain samples are 98.7±3.7 Gy and 95.7±16.6 Gy, respectively. These equivalent doses are in good agreement with previous results (Hashimoto et al, 1991). For 50 single grain analyses, using optimal measuring conditions, the equivalent doses even from single-grain were confirmed to be evaluated within 20% errors. In addition, concerning the aliquot analyses, a high reproducibility was verified for equivalent dose determination. In fact, the equivalent doses of an ancient roof tile, which accumulates doses of approximately a few of Gy, was estimated using aliquot samples under these optimal detection conditions (Hashimoto et al., 2005)

3-4. Conclusions (Detection part)

On the bases of the use of new sample disk, cluster heater, light guide and carefully selected optical filter combinations, the thermal background greatly decreased down to approximately 1000 cps at temperatures ranging from 350 to 380 °C. Accordingly, the RTL-measurements were realized even for a single quartz grain with accumulated dose close to 4.0 Gy. Consequently, this allows the lower RTL equivalent dose limits with high reproducibility for aliquot samples to be extending toward a few Gy.

4. Reference

Aitken M.J., Thermoluminescence Dating. Academic press, London, 61-86 (1985).

Aitken M.J., An introduction to optical dating. Oxford university press, 39-47 (1998).

Andersen, C.E., Bötter-Jensen, L., Murray, A.S., A mini X-ray generator as an alternative to a $^{90}Sr/^{90}Y$ beta source in luminescence dating. Radiat. Meas., **37**, 557-561 (2003).

Bailey, R.M., Paper I-simulation of dose absorption in quartz over geological timescales and its implications for the precision and accuracy of optical dating. Radiat. Meas., **38**, 299-310 (2004).

Bailey, R.M., Armitage, S.J., Stokes, S., An investigation of pulsed-irradiation regeneration of quartz OSL and its implications for the precision and accuracy of optical dating (Paper II). Radiat. Meas., **39**, 347-359 (2005).

Bøtter-Jensen L., Luminescence techniques: Instrumentation and Method. Radiat. Meas., **27**, 749-768 (1997).

Bøtter-Jensen L., Bulur E., Duller G.A.T., Murray A.S., Advances in luminescence instrument systems. Radiat. Meas., **32**, 523-528 (2000).

Bøtter-Jensen L., Anderson C.E., Duller G.A.T., Murray A.S., Developments in radiation, stimulation and observation facilities in luminescence measurements. Radiat. Meas., **37**, 535-541 (2003).

Chawla S., Gundu Rao T.K., Singhvi A.K., Quartz thermoluminescence: dose and dose-rate effects and their implications. Radiat. Meas., **29**, 53-63 (1998).

Duller G. A.T., Bøtter-Jensen L., Murray A. S., Optical dating of single sand-sized grains of quartz: sources of variability. Radiat. Meas., **32**, 453-457 (2000).

Fattahi M., Stokes S., Dating volcanic and related sediments by luminescence methods: a review. Earth Sci. Reviews, **1280**, 1-36 (2003).

Galbraith R.F., The radial plot: Graphical assessment of spread in ages. Nucl. Tracks and Raiat. Meas., **17** 207-214 (1990).

Galbraith R.F., Laslett G.M., Statistical models for mixed fission track ages. Radiat. Meas., **21**, 459-470 (1993).

Ganzawa Y., Furukawa H., Hashimoto T., Sanzelle S., Miallier D., Pilleyre T., Single grains dating of volcanic quartz from pyroclastic flows using red TL. Radiat. Meas., **39**, 479-487 (2005).

Groom, P.J., Durrani, S.A., Khazal, K.A.R., McKeever, S.W.S., The dose-rate dependence of the thermoluminescence response in quartz. PACT 2, 200-210 (1978).

Hashimoto T., Yokosaka K., Habuki H., Hayashi Y., Provenance search of dune sand using thermoluminescence colour images (TLCIs) from quartz grains. Nucl. Tracks Radiat. Meas., **16**, 3-10 (1989).

Hashimoto T., Kojima M., Sakai T., Age determination of pre-historical sites in Japan using red-thermoluminescence measurements from quartz grains (in Japanese). Archaeology and Natural Science, **23**, 13-25 (1991).

Hashimoto T., Kojima M., Shirai N., Ichino M., Activation energies from blue- and red-thermoluminescence (TL) of quartz grains and mean lives of trapped electrons related to

natural red-TL. Nucl. Tracks Radiat. Meas., **21**, 217-223 (1993).

Hashimoto T., Sugai N., Sakaue H., Yasuda K., Shirai N., Thermoluminescence (TL) spectra from quartz grains using on-line TL-spectrometric system. Geochem. J., **31**, 189-201 (1997).

Hashimoto T., Nakagawa T., Hong D.G., Takano M., An automated system for both red/blue thermoluminescence and optically stimulated luminescence measurements. J. Nucl. Sci. Tech., **39**, 108-109 (2002).

Hashimoto T., Nakata Y., Yawata T., Naturally accumulated radiation doses and dating of archaeologically burnt materials using luminescence from white minerals. Proceedings of the 5HLNRRA, International Congress Series, **1276**, 231-232 (2005).

Hong, D.G., Kim, M.J., Yawata, T., Hashimoto, T. Optimum aluminum absorber thickness of a small X-ray irradiator for equivalent dose determination. J. Radioanal. Nucl. Chem., **265**, 495-498 (2005).

McFee C.J., Tite M. S., Investigations into the thermoluminescence properties of single quartz grains using an imaging photon detector. Radiat. Meas., **23**, 355-360 (1994).

Murray A.S., Roberts R.G., Determining the burial time of single grains of quartz using optically stimulated luminescence. Earth Planet. Sci. Let., **152**, 163-180 (1997).

Miallier D., Faïn J., Montret M., Pilleyre Th., Sanzelle S., Soumana S., Properties of the red TL peak of quartz relevant to thermoluminescence dating. Nucl. Tracks Radiat. Meas., **18**, 89-94 (1991).

Murray A.S., Wintle A.G., Luminescence dating of quartz using an improved single-aliquot regenerative-dose protocol. Radiat. Meas., **32**, 57-73 (2000).

Nakagawa T., Usuda H., Hashimoto T., Optically stimulated luminescence (OSL) and thermoluminescence (TL) measurements on red TL (RTL) quartz samples using a new automated OSL/ TL measuring system. J. Radioanal. Nucl. Chem., **255**, 355-358 (2003).

Olley J.M., Caitcheon G.G., Galbraith R.F., The origin of dose distributions in fluvial sediments, and the prospect of dating single grains from fluvial deposits using optically stimulated luminescence. Radiat. Meas., **30**, 207-127 (1999).

Roberts R., Walsh G., Murray A., Olley J., Jones R., Morwood M., Tuniz C., Lawson E., Macphail M., Bowdery D., Naumann I., Luminescence dating of rock art and past environments using mud-wasp nests in northern Australia. Nature, **387**, 696-699 (1997).

Shimizu N., Mitamura N., Takeuchi A., Hashimoto T., Dependence of radioluminescence on TL-properties in natural quartz. Radiat. Meas., **41**, (2006) 831.

Stokes S., Fattahi M., Red emission luminescence from quartz and feldspar for dating applications: an overview. Radiat. Meas., **37**, 383-395 (2003).

Takeuchi A., Nagahama H., Hashimoto T., Surface resetting of thermoluminescence in milled quartz grains. Radiat. Meas., **41**, 826-830 (2006).

Valladas, G., Ferriera, J., On the dose-rate dependence of thermoluminescence response in quartz. Nucl. Instrum. Methods, **175**, 216-218 (1980).

Yawata T., Hashimoto T., Availability of a small X-ray tube combined with Al-absorber as a new irradiator for luminescence researches. Radioisotopes, **53**, 207-212 (2004a) (in Japanese).

Yawata T., Hashimoto T., Identification of the volcanic quartz origins from dune sand using a single-grain RTL measurement. Quat. Sci. Rev., **23**, 1183-1186 (2004b).

Table 1-1 Single-aliquot regenerative-dose (SAR) protocol compensating for cut heating. (see Murray and Wintle, 2000)

STEP	Treatment	Signal
1	Give dose, D_i	-
2	Preheat (220^oC for 3min)	-
3	Stimulate for 200 sec at 125 ^oC	L_i
4	Heat to 450^oC	-
5	Give test dose, D_t	-
6	Heat to 200^oC	-
7	Stimulate for 200 sec at 125^oC	T_i
8	Heat to 450^oC	-
9	Return to step 1	-

For the first sample, i = 0, and D_0 = 0 Gy.

In step 6, the OSL signal from the test dose (2.5 Gy) can be observed. L_i and T_i are derived from the initial OSL signal minus a background estimated from the last part of the stimulation curve.

To eliminate the source of luminescence, step 4 and 8 are compensate with SAR protocol.

Table 1-2 Changes of X-ray dose-rates ($Gy \cdot min^{-1}$) from small X-ray generator as a function of X-ray tube currents and Al-absorber thickness.

Tube currents / Al thickness	0.02 mA	0.04 mA	0.08 mA	0.15 mA	0.30 mA
0	1.64 ± 0.11 (6.9%)	3.25 ± 0.20 (6.2%)	6.48 ± 0.50 (7.7%)	12.4 ± 0.4 (3.4%)	22.1 ± 1.3 (6.0%)
50 μm	0.96 ± 0.06 (6.7%)	2.00 ± 0.10 (5.0%)	4.02 ± 0.18 (4.5%)	6.91 ± 0.06 (0.9%)	13.8 ± 1.0 (7.2%)
100 μm	0.70 ± 0.04 (5.4%)	1.47 ± 0.05 (3.3%)	2.80 ± 0.09 (3.3%)	5.37 ± 0.13 (2.4%)	9.94 ± 0.35 (3.5%)
150 μm	0.48 ± 0.02 (3.3%)	0.97 ± 0.04 (4.0%)	2.00 ± 0.11 (5.3%)	3.69 ± 0.07 (1.9%)	6.70 ± 0.17 (2.5%)
200 μm	0.38 ± 0.02 (4.4%)	0.82 ± 0.03 (3.4%)	1.62 ± 0.04 (2.6%)	2.93 ± 0.02 (0.8%)	5.74 ± 0.31 (5.4%)

Table 1-3 Changes of the equivalent doses as a function of both applied X-ray dose-rate and thickness of Al-absorber. Equivalent doses and their errors are calculated from four to six aliquots.

Average applied X-ray dose-rate (Gy/min)	Thickness of Al-absorber (μm)	Evaluated equivalent doses (Gy) from artificial irradiated quartz		
		10 Gy	20Gy	50Gy
0.4	200	9.7 ± 0.6 (6.3%)	20.1 ± 1.2 (6.0%)	
0.5	150	9.6 ± 0.5 (5.2%)	17.5 ± 1.0 (5.7%)	41.6 ± 2.7 (6.5%)
0.7	100	8.8 ± 0.9 (9.8%)	20.9 ± 1.9 (9.0%)	46.7 ± 5.4 (11.7%)
0.8	200	10.6 ± 0.5 (4.9%)	21.1 ± 0.8 (3.7%)	
1.0	50	10.2 ± 0.4 (3.9%)	16.9 ± 0.9 (5.3%)	46.0 ± 3.3 (7.1%)
1.0	150	9.8 ± 0.7 (7.0%)	19.0 ± 1.3 (6.9%)	44.7 ± 3.4 (7.6%)
1.5	100	10.4 ± 0.8 (7.3%)	20.3 ± 1.5 (7.2%)	47.4 ± 4.8 (10.1%)
1.6	200	9.3 ± 0.7 (7.4%)	19.5 ± 1.2 (6.1%)	44.3 ± 1.6 (3.7%)
1.6	0	10.5 ± 0.4 (3.9%)	20.1 ± 0.6 (2.9%)	50.2 ± 9.2 (18.3%)
2.0	150	10.3 ± 0.8 (7.8%)	20.0 ± 1.5 (7.5%)	43.3 ± 3.0 (6.9%)
2.0	50	10.5 ± 0.6 (5.3%)	20.2 ± 1.2 (5.8%)	41.2 ± 4.3 (10.4%)
2.8	100	10.0 ± 0.6 (5.8%)	19.4 ± 0.9 (4.6%)	40.6 ± 2.9 (7.1%)
2.9	200	9.9 ± 0.1 (1.0%)	19.9 ± 0.4 (2.1%)	43.7 ± 4.4 (10.0%)
3.2	0	10.1 ± 0.1 (9.6%)	16.5 ± 1.1 (6.7%)	46.5 ± 6.5 (13.9%)
3.7	150	10.3 ± 0.6 (5.8%)	19.0 ± 1.5 (7.9%)	44.7 ± 3.1 (6.9%)
4.0	50	9.8 ± 0.5 (5.3%)	18.5 ± 1.2 (6.3%)	42.8 ± 3.2 (7.6%)
5.4	100	10.3 ± 0.4 (4.3%)	17.9 ± 0.6 (3.3%)	48.6 ± 3.9 (7.9%)
5.7	200	9.9 ± 0.7 (6.6%)	18.1 ± 1.2 (6.8%)	42.7 ± 3.5 (8.1%)
6.5	0	9.2 ± 0.9 (9.8%)	17.4 ± 1.3 (7.6%)	42.9 ± 4.4 (10.4%)
6.7	150	9.1 ± 0.3 (3.3%)	16.8 ± 0.7 (4.2%)	37.8 ± 7.4 (19.6%)
6.9	50	9.7 ± 0.2 (2.6%)	17.7 ± 0.7 (4.2%)	46.0 ± 1.4 (3.1%)
9.9	100	10.2 ± 0.5 (4.9%)	17.7 ± 1.5 (8.5%)	42.8 ± 5.1 (11.9%)
12.4	0	10.2 ± 0.7 (6.7%)	18.5 ± 0.9 (4.7%)	48.5 ± 5.1 (10.5%)
13.8	50	10.3 ± 0.8 (7.9%)	17.1 ± 1.9 (10.9%)	39.6 ± 4.7 (11.9%)
22.1	0	8.8 ± 1.1 (12.4%)	17.6 ± 1.5 (8.7%)	41.0 ± 3.3 (8.0%)

Table 1-4 Comparison of signal/noise ratios for RTL-detection according to different filter combinations

Filter combination	Detection range (nm)	Transmittance (%)		signal ($\times 10^5$ counts)	Background ($\times 10^5$ counts)	S/N ratio
		620-630 nm	690-700 nm			
R-60 + IR-cut (Toshiba) (eagle)	600-700	83.8	68.5	42.2	8.18	5.2
O-56 + UCF-22 (Hoya) (Kureha)	560-640	38.6	6.40	35.2	2.37	14.9
Sc54 + IRC65L (Fuji) (Kenko)	540-650	75.6	4.23	39.1	1.97	19.8
O-56 + IRC65L (Hoya) (Kenko)	560-650	74.2	4.13	47.2	2.18	21.7
O-56 + CF-50E (Hoya) (Asahi-techno)	560-625	28.6	2.59	25.2	0.86	29.3

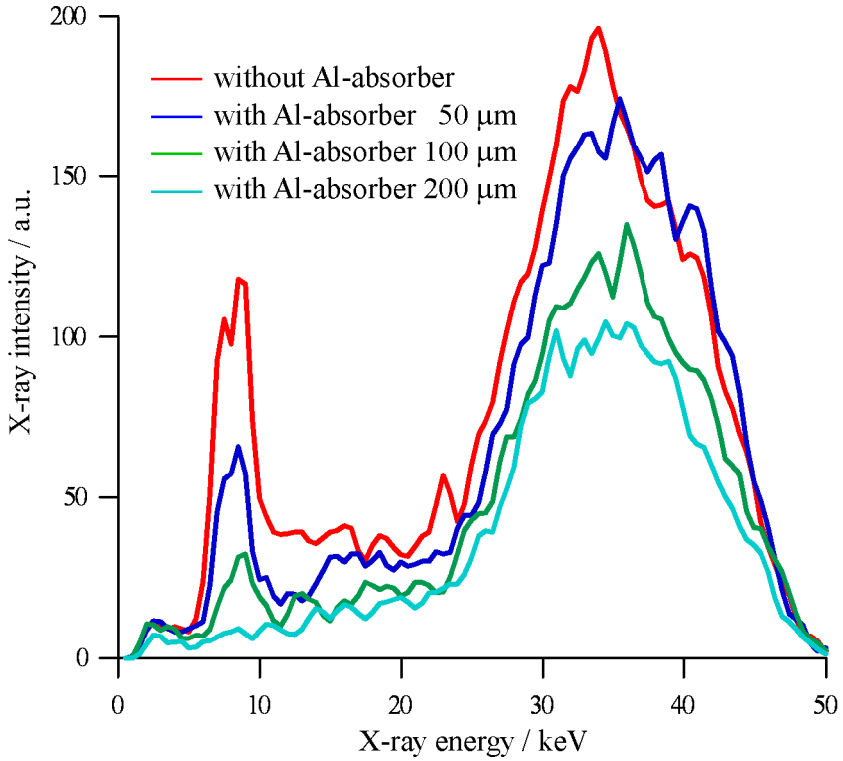

Fig. 1-1 X-ray energy spectra from a small X-ray generator (Varian VF-50J) using the Ge detector (EGSP2800-30-R) and the multi-channel analyzer (MCA).

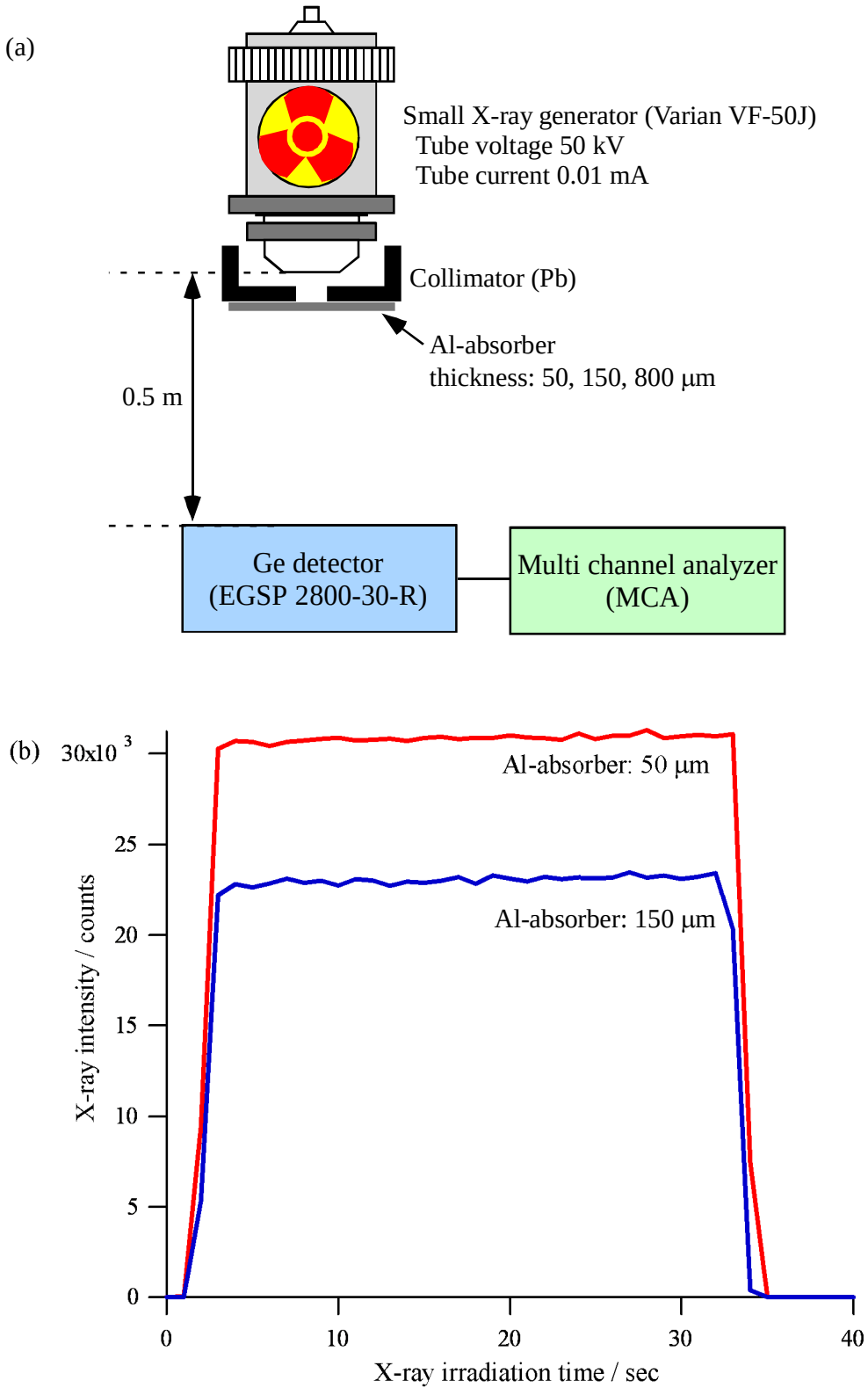

Fig. 1-2 X-ray irradiation stability of small X-ray generator (Varian VF-50J) using the multi-channel analyzer (MCA). (a) Conceptual view of the experimental configuration and (b) Generated X-ray photons as a function of X-ray irradiation time.

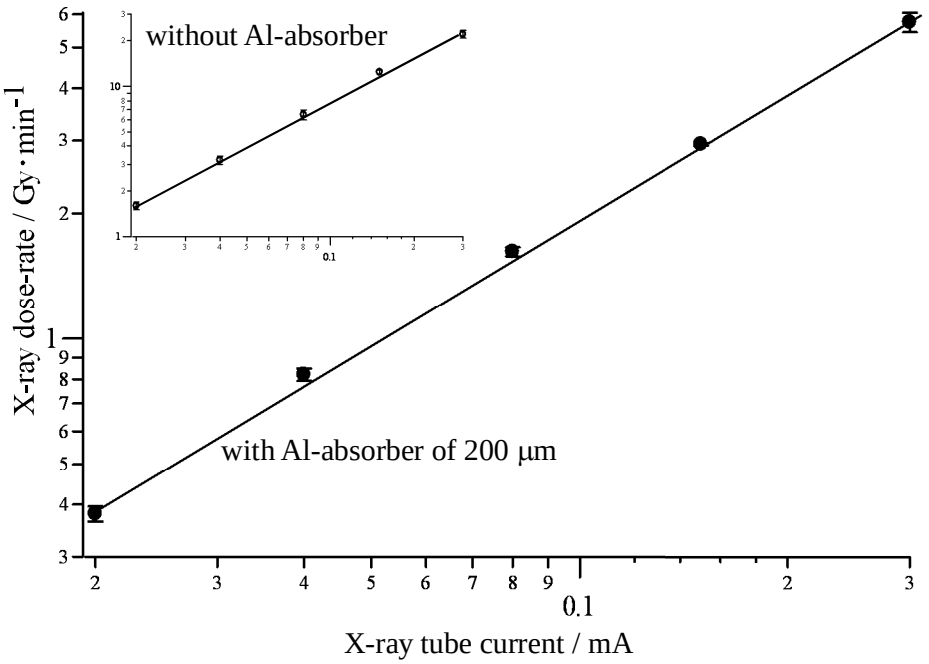

Fig. 1-3 Relationship between X-ray tube currents and X-ray dose rates. The X-ray dose rates were calibrated by comparing a standard irradiation (5 Gy) of quartz with a ^{137}Cs gamma ray source. Inset shows a case for absence of Al-absorber.

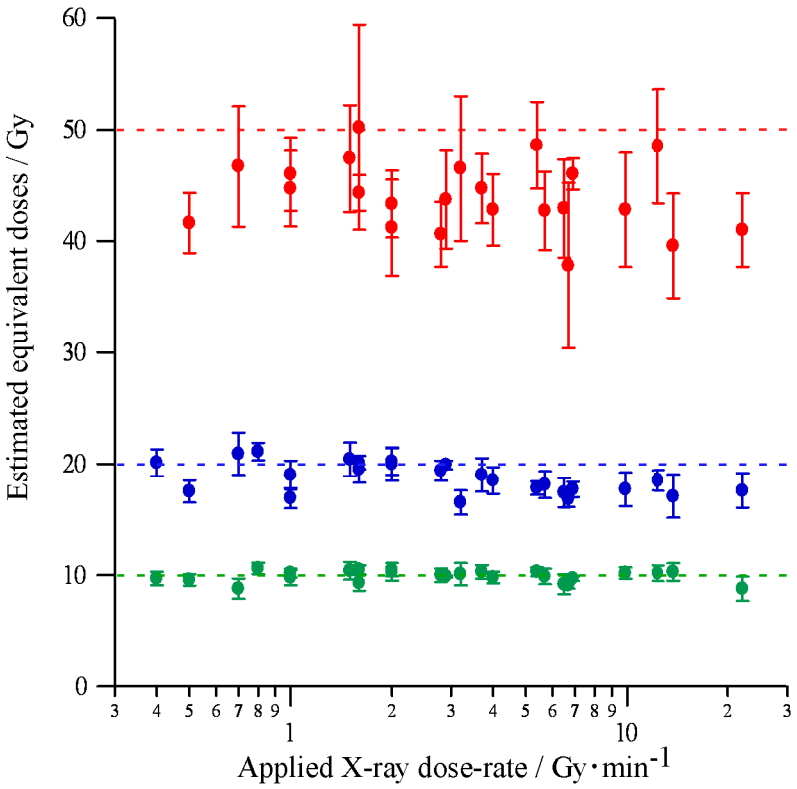

Fig. 1-4 Equivalent doses estimated as a function of the applied X-ray dose rates.
Dotted lines indicate each artificial irradiation doses of 10 Gy, 20 Gy and 50 Gy.

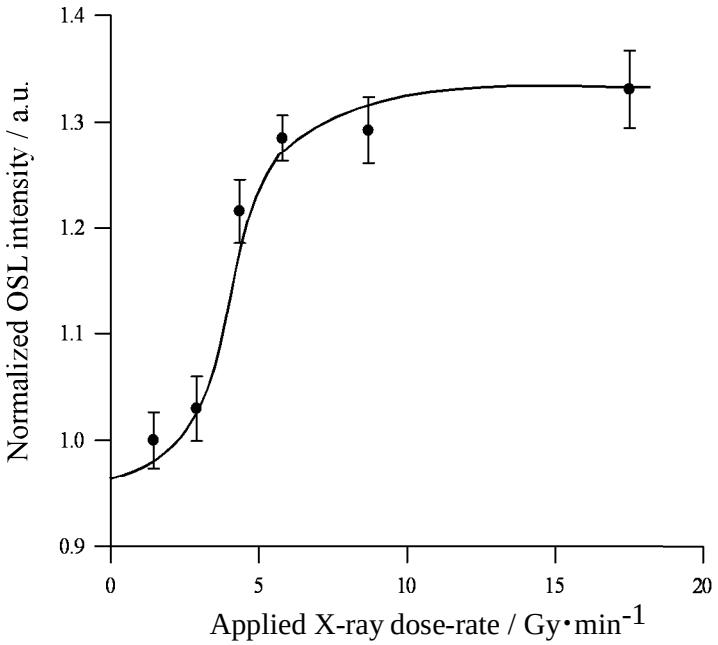

Fig. 1-5 Dependence of OSL intensities on the applied X-ray dose rate.

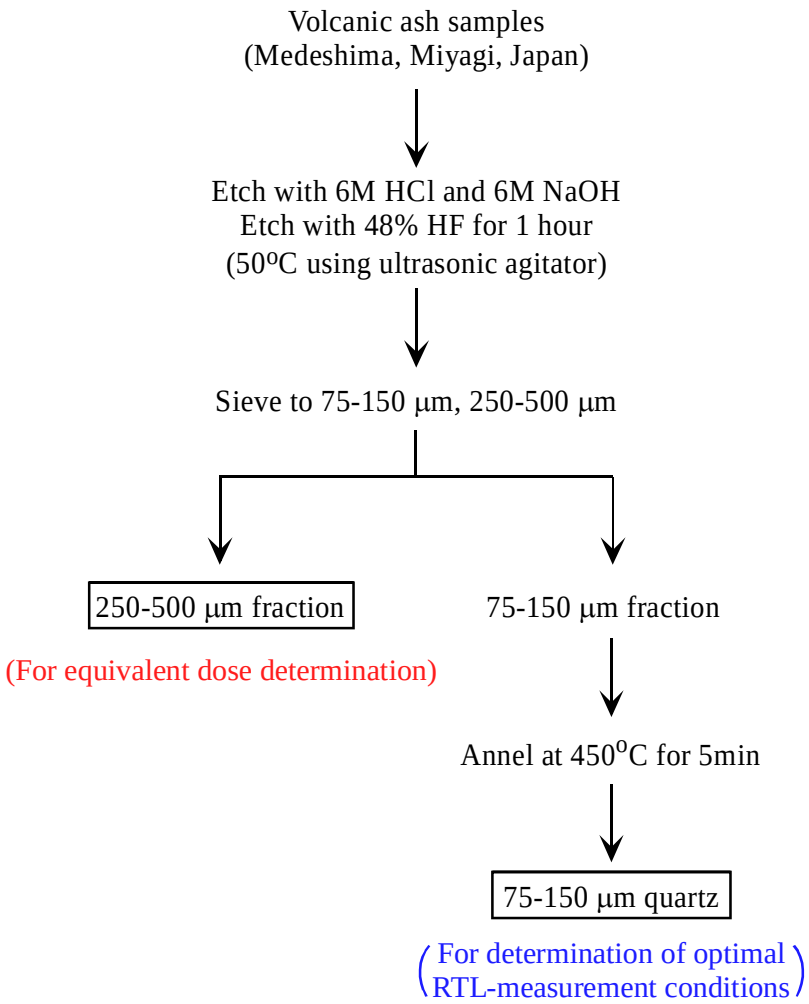

Fig. 1-6 Flow diagram of extraction for quartz grain samples

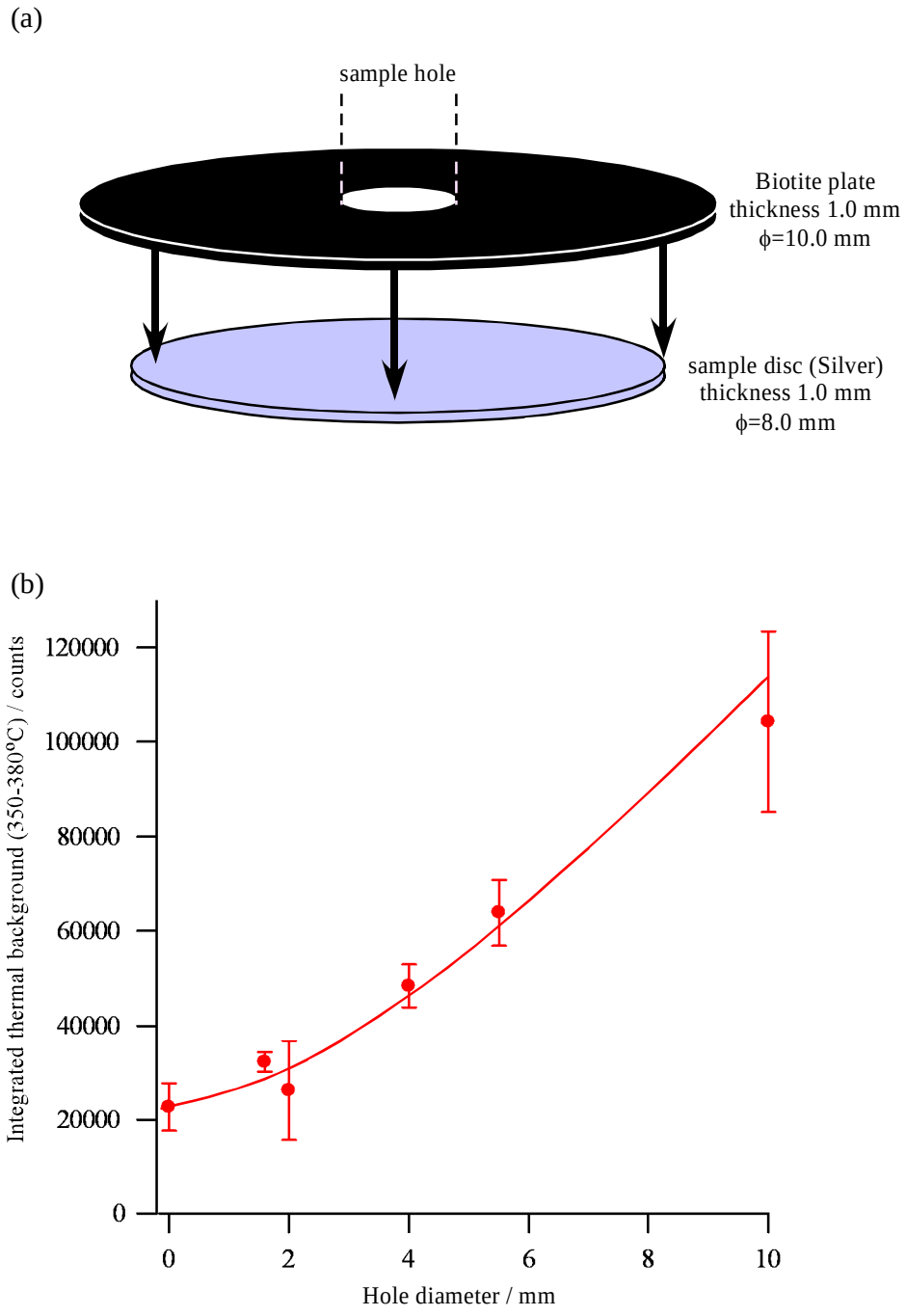

Fig. 1-7 A schematic illustration of new sample disc (a), and changes of thermal background* with hole diameter

*thermal background was integrated from 350-380°C

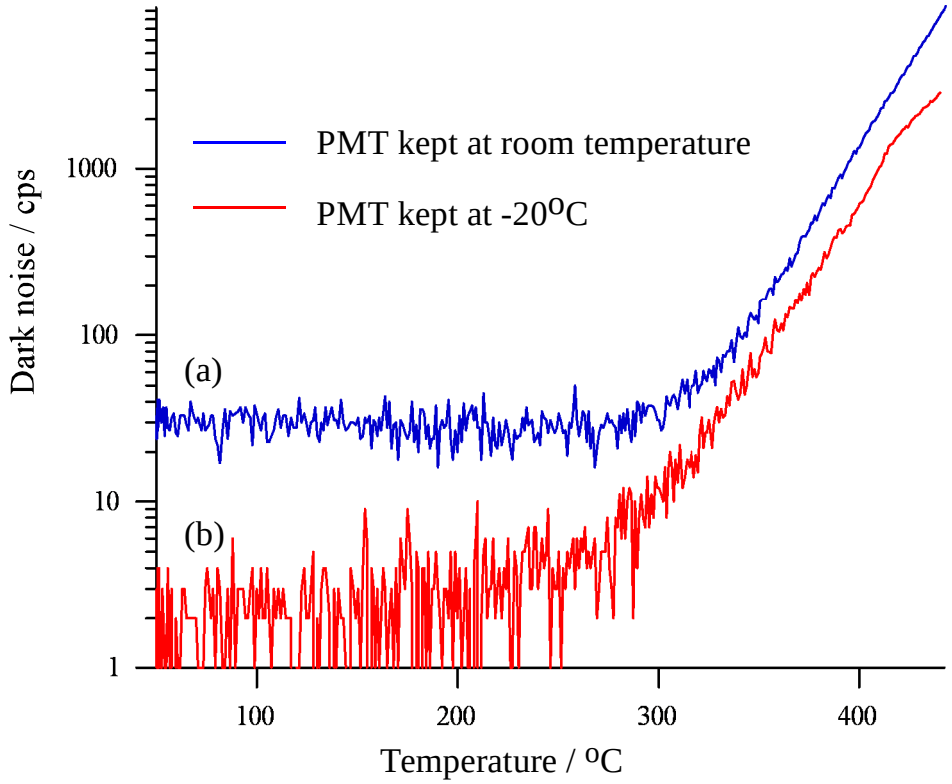

Fig. 1-8 Dark noise curve from photomultiplier tube (Hamamatsu: R649S) kept at room temperature (a) and at -20°C (b)

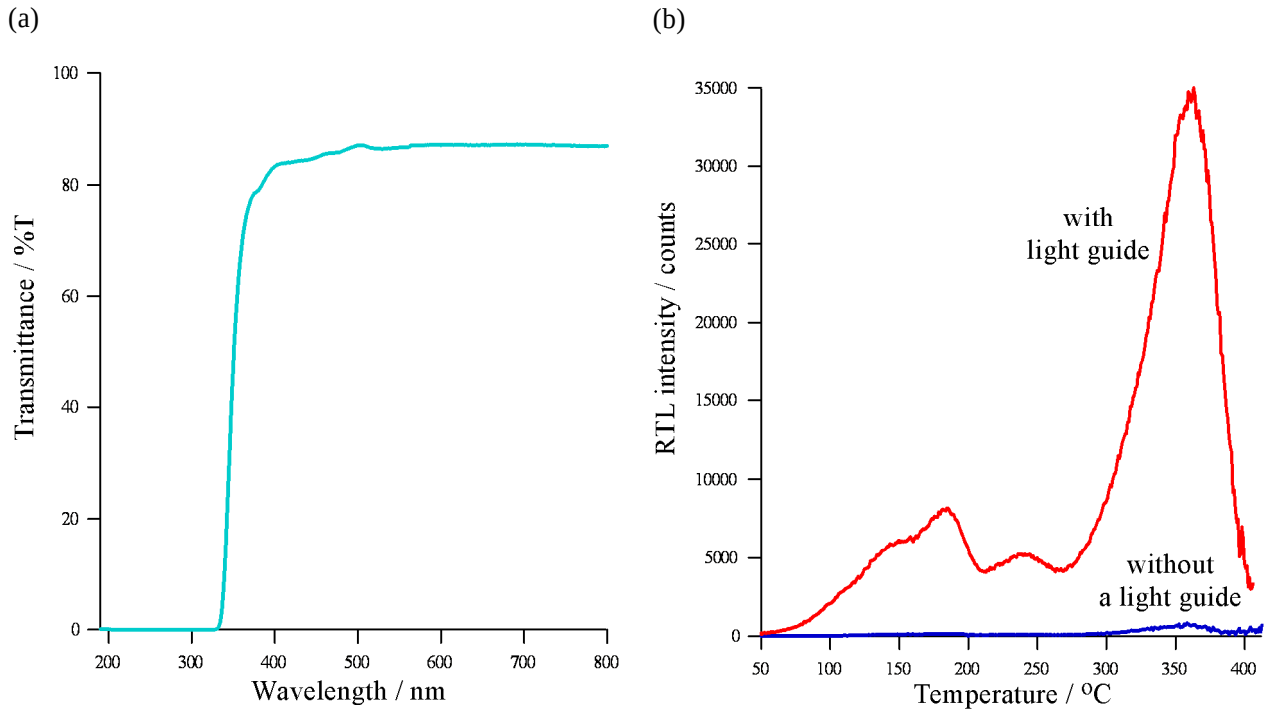

Fig. 1-9 Transmittance of light guide with a clad-rod type made by glass (a), and TL glow-curve differences between the use of light guide and without light guide (b).

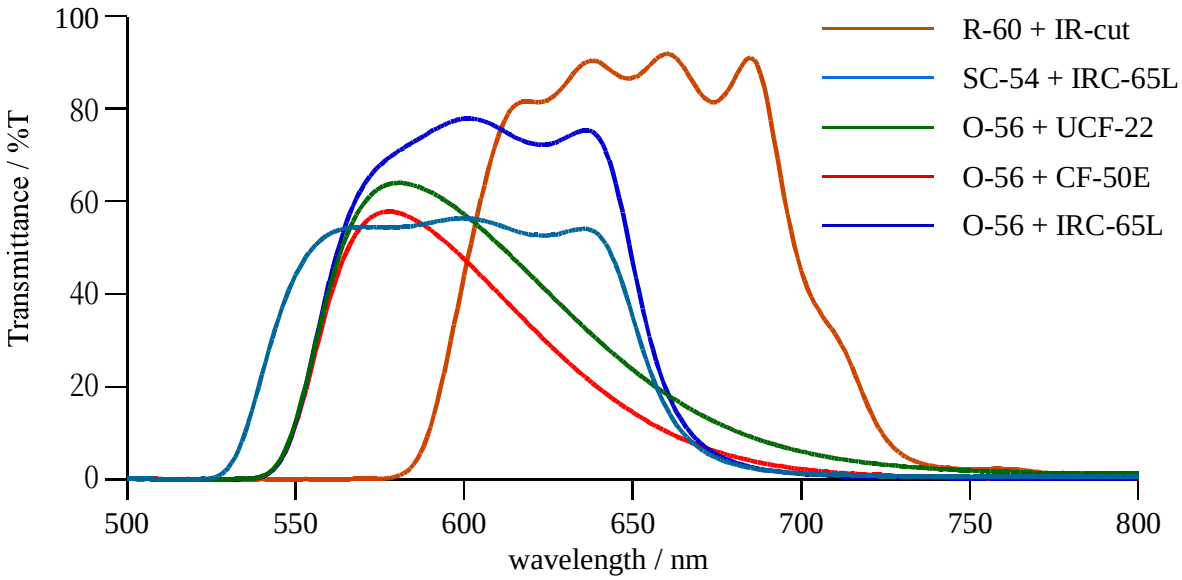

Fig. 1-10 Transmission in % versus wavelength for some filter combinations for detection of RTL emission.

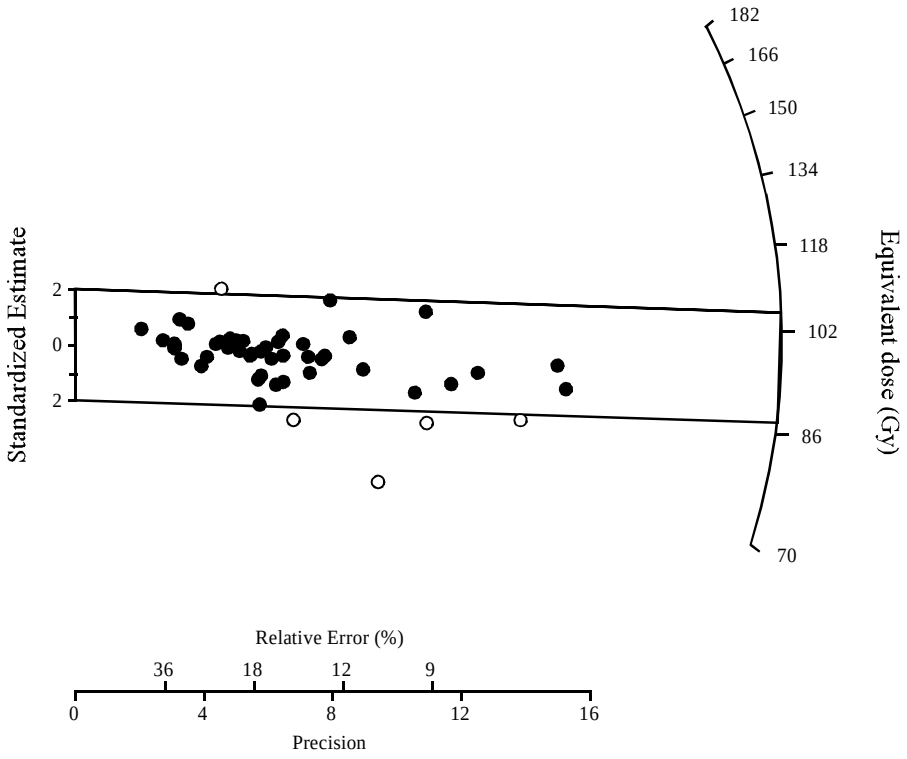

Fig. 1-11 Radial plot from natural quartz grains.
This plot is comprised of data from approximately 50 grains.

† *Chapter 2* †

Dependence of luminescence properties on impurity contents in quartz

Abstract

To elucidate the luminescence characteristics, including differences in luminescence sensitivity and TL color (red-TL; RTL and blue-TL; BTL), synthetic and 32 natural quartz samples from different origins were investigated with respect of impurity contents (Al, Ti, Li, Fe, Mg, Cu, Ge and -OH related impurity) and α–β phase inversion break temperatures. Concerning the color of TL emission, the TL coloration was apparently dependent on Al impurity content and an approximately inverse correlation was found between the Al contents (> few tens ppm) and the inversion break temperatures. In the region of low Al impurity content (< 300 ppm), quartz samples exhibit BTL property. In contrast, samples with Al-impurity content beyond 300 ppm showed RTL without any exception. Consequently, the RTL- and BTL-quartz were classified at Al content of 300 ppm and at a boundary inversion break temperature of 572 ^{o}C.

The luminescence mechanism was found to be quite different between BTL- and RTL-quartz. The BTL sensitivity generally shows a negative relationship with the Al content above an impurity concentration of a few tens of ppm, probably attributed to quenching effects at radiolysis products, derived from molecular water concentration and OH related impurity quenching effects. In contrast, the RTL sensitivity showed a correlation with the square of Al impurity content, strongly suggesting that the structurally distorted defect sites associated with neighboring two Al impurities act as a RTL hole centre.

1. Introduction

Natural quartz has defect sites due to impurity atoms, such as Al, Ti, Fe, OH, and monovalent ions (H^+, Li^+, Na^+ and K^+) during mineral formation, as well as in the rapid cooling processes crossing the α–β phase inversion break temperature (573^{o}C), and subsequent radiation damage. Some of these defects can operate as luminescent centres when quartz is exposed with ionizing radiations (McKeever, 1988). In general, the impurities in dielectric materials give rise to localized energy levels within the forbidden energy gap, which are crucial to the luminescence process. Therefore, sensitivities of thermoluminescence (TL), including blue-TL (BTL) and red-TL (RTL), and optically stimulated luminescence (OSL) should be affected by trace amounts of impurities. So, luminescence emission from quartz is well known to be particularly sensitive to the trace amounts of impurities. Several researchers have reported that the recombination of electrons with $[AlO_4/h]^0$ centres give rise to BTL emission at 325^{o}C (470 nm; Yang and McKeever, 1990; Woda et al., 2002), whereas Hashimoto et al. (1994) reported a negative correlation of the BTL emission with Al content. The OSL emission in the violet range (360-380 nm; Huntley et al., 1991) has been concluded to be attributable to the H_3O_4 hole trapping centre based on the observation of "pre-dose effect" (Zimmermann, 1971) and electron spin resonance (ESR) signals (Yang and McKeever (1990)). Additionally, other centres related to UV emission (250-400 nm) have been identified to be electron recombination with holes trapped at the family of $[AlO_4/h]^0$ centres (Martini et al., 1995) or at $[AlO_4/M^+]$ (M^+: alkali ions) centres (Vartanian et al., 2000). On the other hand, hole centres of RTL emission (620-630 mn) at 375^{o}C, which were initially reported by Hashimoto et al. (1986a, 1994), are still uncertain. Hashimoto et al. (1996) suggested the thermal history, particularly its cooling rate from molten state to solid and atmospheric condition at heating process, had greatly affected on the RTL colorations of quartz.

Quartz has two crystalline modifications, assigned into low quartz (or α-quartz) or high quartz (or β-quartz) and the α–β phase inversion at 573 ^{o}C is changeable within narrow temperature-ranges depending on the existence of Al-, Li- and OH related-impurities (Keith and Turtle, 1952). However, a little attention has been paid so far to the relationship between the α–β phase inversion break

temperature and luminescence properties of quartz specimens.

The aim of this chapter is to propose hole centre models associated with RTL emission. For this purpose, luminescence sensitivities from irradiated samples at a fixed dose of 20 Gy, were measured to monitor differences in the population of the recombination centres. The impurity concentrations and their configurations in quartz were determined by induced coupled plasma mass spectrometry (ICP-MS), Fourier transform infrared spectrometry (FT-IR) and electron spin resonance (ESR) spectrometry. The α–β inversion temperatures are compared with the impurity content in quartz samples of different origins and from these relationships, the influence of impurity concentration on the luminescence characteristics, including color properties and sensitivities is examined. Based on these characteristics, we will discuss the impurity configurations in quartz.

2. Samples

2-1. Extraction procedure

Natural and synthetic quartz specimens of 30 types were collected from a large variety of sources. Natural quartz grains were extracted from volcanic material, granite, pegmatite, hydrothermal crystals, plutonic rock, and soil or sandy sediment, while synthetic quartz was cut into each grown part, each having different Al impurity content. Quartz grains were prepared by a following standard procedure (Hashimoto et al., 2005). The samples were washed and then treated with 6M hydrochloric acid. The fractions were etched with hydrofluoric acid (46%) for 60 min under an ultrasonic agitator to remove alpha-dosed rinds of quartz grain surface. After drying, the samples were sieved to obtain the 75-150 μm sized fractions. Half of each sample was heated at 450 ^{o}C for 5 min to erase the naturally accumulated dose, followed by irradiation with X-rays (20 Gy). The remainder was used to measure the TL spectrometry, α-β phase inversion break temperature (T_c), chemical analysis (Al, Ti, Li, Fe, Mg, Cu and Ge) and ESR measurements. One natural quartz specimen (Madagascan quartz rock), which exhibit BTL property, was prepared a Z-cut slice of which surface was mirror-polished into 1 mm in thickness. The slice sample was irradiated with γ-ray of 20 kGy. Based on color centre intensities,

dense color parts and faint color parts were defined as “color parts” and “colorless parts”, respectively. The slice sample was subjected to IR-mapping and TL color image observation using 3-CCD camera.

2-2. Thermoluminescence color images (TLCIs) and TL-spectrometry using Image-Intensifier Photo-Diode Array (IPDA)

The TL emission spectra from the quartz grains were obtained using TLCI photography (Hashimoto et al., 1986b) and TL-spectrometry (Hashimoto et al., 1997). The photographic system consists of a camera (Nikon F3) with color film (Fuji SUPERIA 400). The TL emissions from quartz grains were photographed in the temperature range of 80-450^{o}C at a heating rate, 1^{o}C/sec. To obtain more quantitative information, TL-spectrometry was carried out using an Image-Intensifier Photo-Diode Array (IPDA). Some typical contour expression of TL-spectra shows in Figs. 2-1, 2-2. On the basis of the TLCI and the TL-spectrometric results, RTL, BTL and OSL detection ranges were selected as 600-650 nm, 420-500 nm and 300-400 nm, respectively. The combination of detection filters and photomultiplier tube (PMT) were as follows; i) RTL: a R-60 (Toshiba) with two IR-cut filters (Eagle, Asahi Techno) and Hamamatsu R649S PMT, ii) BTL: a B-390 (Hoya) with a GG-420 (Schott) filters and Hamamatsu R585S PMT, and iii) OSL: a DUG-11 (Schott) filter and Hamamatsu R585S PMT, because in the present experiment, red- and blue-emissions from quartz should strictly restricted.

3. Method

3-1. TL/OSL measuring system

All luminescence measurements were carried out using an automated OSL/TL measuring system installed with a small X-ray irradiator as described in the previous chapter. In all TL-measurements, the samples were measured from 50 ^{o}C to 450 ^{o}C at a heating rate of 1 ^{o}C/s after preheating for 5 min at 220 ^{o}C. Both RTL and BTL signals were integrated over the temperature ranges 350-380 ^{o}C and 250-400 ^{o}C, respectively. For OSL-measurements, the signals were recorded

during 0.2 sec intervals at a sample temperature of 125 ^{o}C during light exposure, following preheating for 5 min at 220 ^{o}C. The signals were integrated for the first 1.0 sec of the decay curve. In this chapter, these luminescence signals were defined as luminescence sensitivities.

3-2. α–β phase inversion break temperature measurements

All α-β phase inversion break temperatures for quartz samples were recorded on heating (T_h) and on cooling (T_c) using a differential scanning calorimeter system (DSC; MAC SCIENCE DSC3300). However, T_c values were employed because of offering good reproducibility of the measurements. A α–β phase inversion break temperature of 573 ^{o}C is due to synthetic quartz grains with negligible low impurity content and in fact, this value of T_c was obtained for the Z-region from the pure synthetic quartz. In contrast, the T_c values of natural quartz moved towards lower temperatures, ranging from 570.8 to 572.8 ^{o}C. The change in T_c values of natural quartz with Al content is plotted in Fig. 2-3. In this figure, the correlation between Al content and T_c value shows a roughly negative relationship. According to Hummel (1951) and Keith and Tuttle (1952), the solubility of impurities such as Al, Li and OH tends to vary linearly in temperatures below 573 ^{o}C. Therefore, the scatter in T_c values observed with Al content (Fig. 2-3) could be attributed to other impurities for T_c values below 573 ^{o}C and giving rise to complicated interactive effects between some of the impurities. In general, however, the inversion temperatures were considered to reflect changes in luminescence properties.

3-3. Chemical analysis

Seven elements, including Al, Ti, Li, Fe, Mg, Cu and Ge, were detected in all quartz specimens, and Al and Ti were major impurity elements in all specimens. These impurities occupy substitutional silicon sites of the SiO_2 structure, forming an Al hole trapping centre (Yang and McKeever et al., 1990; Ikeya 1993) or a Ti electron trapping centre (Fujita et al., submitted; Ikeya 1993) after irradiation. Li impurity is main charge compensators since the Al hole centres at room

temperature require monovalent ions for charge neutralization in the crystal. We will discuss these impurity configurations in detail (see Section 3-5). Owing to a one-to-one ratio between Al and total alkali ion content (Iwasaki and Iwasaki, 1993), the other alkali ions, especially the Na ion, should also be act as a charge compensator. Other impurities, such as Fe and Mg, have large concentrations in all specimens, while Cu was detected in volcanic quartz with low concentration, and Ge impurity as a electron trapping impurity was not detected in any of the specimens.

The luminescence sensitivities of RTL, BTL and OSL are summarized in Table 2-1, together with results of chemical analysis and inversion temperatures. The experimental errors were derived from two or three aliquot analyses.

3-4. Mapping measurements (IR-mapping and 3-CCD image)

For the Madagascar quartz slice sample, IR absorption spectrometry and IR mapping measurements were carried out using a Fourier transform infrared (FT-IR) microscopic spectrometer (PERKIN ELMER Spectrum GX FT-IR system & AutoIMAGE system) with a 100 x 100 μm^2 aperture size at room temperature (Hashimoto et al., 2003). The IR spectrum was repeatedly measured 20 times (for mapping measurements; 5 times) at the same point in a wavenumber range of 4000-500 cm^{-1}. The peak determinations were made under a 1 cm^{-1} resolution in a wavenumber. Typical IR absorption spectra from color and colorless part were shown in Fig. 2-4. In this figure, there appears many sharp absorption bands, including two peaks at 3378 cm^{-1} and 3307 cm^{-1} assignable to the Al-OH bands, and ones at 3481 cm^{-1}, corresponding to Li-dependent OH (Iwasaki and Iwasaki, 1993). From this result, microscopic scanning image of Al-OH (at 3378 cm^{-1}) was extracted for a square part; scanning area is 10 mm x 10 mm (see. Fig. 2-14) on the slice sample with 100 μm x 100 μm aperture.

Furthermore, to obtain the quantitative mapping measurements for TL spectra, a high sensitive 3-CCD camera (Hamamatsu C7780-20) was used for the same Madagascan quartz slice after IR mapping measurements. Its photosensitive sensor (1344 x 1024 pixels, 8.67 x 6.60 mm size) has a quantum efficiency of more 60 % in the visible light ranges. The CCD camera sensor was cooled at

0^{o}C to reduce the background as low as possible. The color images from quartz sample were separated into 12 bit RGB data (12 bit x 3 = 36 bit) using optical combinations of two prisms and optical filters. To obtain sufficient light from sample, two standard 35 mm camera lens were fixed between CCD sensor and quartz sample. The effective focal rations of the optics were f/1.2 and f/2.3, respectively. In this manner, a good balance between resolution and light collection was achieved. The systematic configuration was shown in Fig. 2-5. TL measurements were carried out from 50-450^{o}C at heating rate of 1.0^{o}C/s and TL data were integrated every 2 sec. RGB data from TL emissions were averaged 2x2 pixels (76 x 76 μm) to enhance the signal-to-noise ratio.

Along with the two mapping observations (FT-IR and 3-CCD image), BTL intensities (Blue-data) were plotted against to the Al-OH absorbance to clarify the quantitative relationship between Al-OH and BTL-sensitivities.

3-5. Electron spin resonance (ESR) spectrometry

Natural quartz samples contain considerable Al- and Ti-impurities, which are accompanied with monovalent ions (M^{+}) due to charge neutralization as mentioned above (Table 2-1). For a trivalent aluminum ion (Al^{3+}), Al^{3+} is easily substituted into Si^{4+} site of SiO_2 lattice by accompanied with M^{+} interstitial. A cation M^{+} at the interstitial site give rise to a $[AlO_4/M^{+}]$ centre. When this centre traps a hole (h^{+}) after irradiation at room temperature, the cation M^{+} diffuses away by leaving $[AlO_4/h]^{0}$ centre. On the other hand, Ti^{4+} also substitutes to Si^{4+} site of SiO_2 lattice. However, its electron affinity (ionization potential) is considerably high, resulting in $[TiO_4 \cdot e^{-}]^{-}$ after irradiation at room temperature. Owing to charge neutralization, this defect part attracts an interstitial monovalent cation M^{+} to form stable $[TiO_4/M^{+}]^{0}$ centre. Both Al hole and Ti electron trapping centre are detected by ESR measurements.

Prior to ESR measurements, all grain samples were irradiated with γ-ray of 20 kGy. It should be noticed that these saturated ESR signals should correspond to the impurity contents in quartz because the applied dose of 20 kGy is too high to study the dependency of RSR signal on the absorbed

doses. The irradiated quartz samples were measured with a finger Dewar vessel at 77K with ESR spectrometer (JEOL RE-1X) using 100 kHz modulation field of 0.1 mT and microwave power of 1 mW. Typical ESR spectra from BTL- and RTL-quartz are shown in Fig. 2-6.

In order to estimate the kinetic parameters of these defects, including activation energies and frequency factors, some quartz grain samples (Madagascan quartz (color centre part, colorless part), volcanic quartz (Medeshima, Tazawa, Anchi)) were subjected to the isochronal annealing experiments. In the isochronal annealing experiments, the samples were annealed at a particular temperature from 25 to 400 ^{o}C for 15 min using an electric furnace and then Al and Ti centres were measured. Each ESR signal (I(T)) was plotted as a function of annealing temperature (^{o}C) as seen in Figs 2-7, 2-8. The thermally decreasing signal was fitted to the following equation:

$$I(T) = \frac{I(298K)}{\{1 + C \cdot \exp(-W / kT)\}},$$

where C is frequency factor (s^{-1}), k is Boltzmann's constant and W represents the activation energy (eV). This equation is assumed the first-order decay kinetics (Ikeya, 1993).

The frequency factors and activation energies were calculated from Arrhenius plot.

$$\ln\left\{\frac{I(298K)}{I(T)} - 1\right\} = \ln C - W / kT$$

The frequency factors and activation energies of some quartz samples are summarized in Table 2-2, together with the kinetics parameters of electron traps related to RTL peak (300-400^{o}C) using several TL-techniques from some reference (Kojima, 1992; Ichino, 1994; Sugai, 1998).

4. Results and Discussion

4-1. Dependence of TL coloration on impurity contents

The Al and Li impurity contents for the natural quartz samples, as plotted in Fig. 2-9, show a linear relationship between the Al and the Li content due to charge neutralization in the crystal. Moreover, there is a significant difference between RTL- and BTL-quartz regarding Al content. The RTL-quartz samples of volcanic and granite origins have generally higher impurity concentrations

(beyond 300 ppm). In Fig. 2-3, the RTL- and BTL-group are also apparently distinguished for T_c=572 ^oC. That is, the values of T_c for RTL-quartz are lower than those for the BTL-quartz and this allows the TL color of natural quartz to be easily separated in terms of Al content and T_c values. Since most of the RTL-quartz has been found in volcanic quartz, the high impurity concentrations in RTL-quartz should be due to the rapid cooling rate during crystallization, such as in the events of a volcanic eruption (Hashimoto et al., 1986a). Since the impurities during the rapid formation of quartz crystals can not be excluded, the RTL-quartz of volcanic origin agrees well with the results, giving several impurities of higher concentrations compared with BTL-quartz (Table 2-1). From these results, it was confirmed that TL coloration of natural quartz is greatly dependent on Al impurity content, which causes the lowering of $\alpha-\beta$ phase inversion break temperature.

4-2. Luminescence sensitivities of natural quartz samples

The luminescence sensitivities of BTL, RTL and OSL for all quartz samples, as a function of Al content are shown in Figs 2-10, 2-11, 2-12. The results of ESR spectra at 77K and isochronal annealing curve are summarized in Figs 2-7, 2-8. The isochronal annealing curves were fitted on the basis of assumption of the first-order decay kinetics.

4-2-1. BTL sensitivities

In Fig. 2-10, it can be seen that the BTL sensitivity of synthetic quartz tends to yield explicitly a reciprocal proportion against the Al content above a few tens of ppm. In the case of natural quartz, a similarly decreasing tendency can be recognized because all natural samples contain Al of more than 26 ppm (Table 2-1). On the other hand, the BTL sensitivities of natural quartz samples rapidly increased with $[AlO_4/h]^0$ centre intensities as shown in Fig. 2-13, since the BTL emission could be responsible for the $[AlO_4/h]^0$ centres (Yang and McKeever, 1990; Woda et al., 2002). Thus, the BTL sensitivities and the $[AlO_4/h]^0$ centre intensities also gave negative correlation with Al contents. As a result, these relationships imply the existence of decreasing effects on the $[AlO_4/h]^0$ centre such as so-called concentration quenching effects (McKeever, 1988) and/or OH related

impurity quenching processes (Hashimoto et al., 2003). In particular, the BTL sensitivities were influenced on quenching effects at high Al-impurity range.

For Madagascan color (Al content of 26±3 ppm) and colorless part (Al content of 255±64 ppm), isochronal annealing experiments (Fig. 2-7, Table 2-2) revealed that no significant differences of the Al-hole centre configuration are found beyond Al-contents of 26-255 ppm. In order to clarify the quantitative relation of OH related impurity quenching effects on the BTL sensitivities, the relationship between absorbance of Al-OH and BTL sensitivities on Madagascan quartz slice is plotted as shown in Fig. 2-14. By comparing two mapping observations, the higher and lower BTL sensitivity positions corresponded to the color parts and colorless parts, respectively. In addition, it was recognized that the BTL sensitivities rapidly decreased exponentially with increasing the absorbance of Al-OH. Thus, the highly containing portions of Al-impurities in quartz structure probably possess higher degrees of distortion in comparison with the pure SiO_4 structure parts. As a result, the high Al-parts will correspond to contain a number of dangling OH-groups, including Al-OH and Li dependent OH, as well as other impurities such as monovalent ions as charge compensators and water molecules. In fact, Hashimoto et al. (1996, 1997) have reported that the thermal annealing treatment above 867^{o}C (β-quartz/tridymite phase) causes significant enhancement of sensitivity (4-5 times) for BTL in these high Al-containing parts, and concluded this enhancement probably reflecting the exclusion of water molecules from the quartz. Consequently, the OH related impurity quenching could greatly influence on the BTL sensitivities.

4-2-2. RTL sensitivities

In contrast to the BTL behavior, the RTL sensitivity steeply increases with Al and Ti impurity concentrations as seen in Figs 2-11 and 2-15, respectively. However, the sensitivity shows no meaningful relationship with other impurities. Conclusively, RTL sensitivities were confirmed to be strongly dependent on Al- and Ti-impurity contents rather than the concentrations of other impurities. Moreover, these results have proven that the RTL hole centres are not affected by the quenching

effects mentioned above. Thus, each TL mechanism is found to be significantly different between BTL- and RTL-quartz. The hole and electron trapping centre models of RTL emission will discuss in the following section 4-3.

4-2-3. OSL sensitivities

In Fig. 2-12, the OSL sensitivities increase with decreasing T_c values, although there is an obscure relationship between Al contents and OSL sensitivities. Particularly, the OSL sensitivity for RTL-quartz samples is relatively stronger than for BTL-quartz. Concerning a relationship between TL and OSL, several researchers investigated TL and OSL bleaching behavior from a view point of optical dating (Spooner et al., 1988; Spooner 1994; Franklin et al., 1995). Spooner (1994) concluded the OSL and 325^{o}C TL peak (at 420 nm; so-called rapidly bleaching peak) of quartz originated from one and the same trapped electron population, resulting in both the bleaching of the 325^{o}C TL peak and the prompt emission of OSL, proceeds by the same mechanism. However, the each luminescence sensitivity against to Al contents showed opposite tendency. As a result, the OSL hole centre should be also different from BTL ones ($[AlO_4/h]^0$ centres), although the OSL and 325 ^{o}C TL could originate from same electron traps. For the OSL hole centre model, several researchers proposed some models and process, such as H_3O_4 hole trapping centre (Yang and McKeever (1990)), the family of $[AlO_4]^0$ centres (Martini et al., 1995), $[AlO_4/M^+]$ centres (Vartanian et al., 2000) and the hole recombination with $[AlO_4]^-$ centre process (Itoh et al., 2002). However, OSL centre model was not yet cleared. The data strongly suggest that OSL sensitivities are correlated not only with Al content, but also with the interaction of several impurities, including Li and hydroxyl group. Much attention should be paid on construction of preferable OSL hole model for these relationships.

4-3. The hole and electron trapping centre model for RTL

Figure 2-8 and Table 2-2 show the isochronal annealing curves and estimated kinetics parameters for three volcanic quartz samples (Medeshima, Anci and Tazawa, respectively). Clearly,

the activation energies of Al centres offer higher thermal stabilities than those of BTL-quartz (Table 2-2). In general, the RTL sources (hole and electron trapping centre) show higher thermal stability in comparison with BTL/OSL ones; RTL sensitivity changes during repeated heating up to 450^{o}C and irradiation cycle (SAR protocol) are negligible small (Yawata and Hashimoto, 2004). Thus, the equivalent dose determination using RTL emission was preferable for burnt archaeological sample and volcanic products (Hashimoto et al., 2005; Ganzawa et al., 2005). Although these higher activation energies of Al hole centre agree with RTL properties, no one-to-one ratio between the RTL sensitivities and the Al contents are found (Fig. 2-11). As a result, the RTL hole centres may not be impurity sites similar to those in $[AlO_4]^0$ centres.

Hashimoto et al. (1994) reported that for Madagascan crystal quartz containing greater than 100 ppm of Al, the original BTL changed to RTL emission after annealing treatment above 1000 ^{o}C due to the creation of RTL hole centres. Annealing treatment above 1000 ^{o}C causes the breaking of Si-O-Si bonds, allowing other bonds, such as Si-O-O· and Si-O· to form depending on the presence of oxygen atoms. In fact, the ESR signals associated with peroxy radicals and non-bonding oxygen hole centres (NBOHC) are rapidly enhanced after annealing treatments (Stapelbroek et al., 1979). Moreover, Kalceff and Phillips (1995) suggested that the 1.95 eV (630 nm) cathodoluminescence (CL) emission from quartz during the irradiation is attributed to induced NBOHC based on the appearance of CL spectra from quartz. The RTL emission band (620-630 nm) detected in this work is in good concordance with the CL emission associated with NBOHC. Therefore, these structural bond breaking sites (such as peroxy, NBOHC and OHC) can be tentatively concerned with RTL emission. For precursors of bond breaking sites in silica, a number of different precursors have been proposed (Griscom 1985; Munekuni et al., 1990; Nishikawa et al., 1990, 1992). Griscom (1985) suggested in high-OH silica (-OH>200 ppm) the hydroxyl group could form precursors of the NBOHC according to the following reactions: ≡Si-O-H → ≡Si-O· + H^{o}. In oxygen-rich specimens the peroxy linkage provide likely a precursor for NBOHC and a number of different transformations during irradiation have been proposed (for example, ≡Si-O-O-Si≡ → ≡Si-O· + ·O-Si≡) (Munekuni et al., 1990;

Nishikawa et al., 1992). Nishikawa et al. (1990) proposed the precursors model of the “strained” silicon oxygen (Si– –O) band, which may exist due to excitation by irradiation is a possible NBOHC precursor (≡Si-O– –Si≡ → ≡Si-O・ ・Si≡) and may also result in the formation of E’ centre.

For natural quartz, the log-log plot between RTL sensitivity and Al impurity content shows a linear relationship with a gradient of 2 (Fig. 2-11(b)). This result can represent by the following equation:

$$\log D_{RTL} = 2 \log[Al] + \log C, \quad (1),$$

where D_{RTL} is the RTL hole centre density (cm^{-3}) and C is a constant; D_{RTL} is proportional to RTL intensity.

This relationship suggests that neighboring Al impurities co-operate to distort near Si-O-Si bonds and could form the precursors of structural bond breaking sites, which acts the RTL hole centres after the irradiation. As mentioned **section,** since the Al impurities in quartz could be accompanied with -OH related impurities, OH related defects, including molecular water and Si-OH, might also create the precursors of structural bond breaking sites. This model would also satisfactorily explain the RTL-enhancement results from the annealed samples, recovering the dependency on Al-concentration (Hashimoto et al., 1994). These results, however, strongly support that highly Al concentrations (>300 ppm) in natural quartz could originate the RTL hole centre alone.

For the electron trapping centre related to RTL peaks, the activation energies of electron trapping site were already estimated using several TL techniques, including initial rise method and isothermal decay. The activation energies of RTL peaks are summarized in Table 2-3. By comparing the activation energies of Ti centre, the thermal stability of Ti centres agree well with RTL peaks. In addition, Ti contents in quartz offered a one-to-one relationship with the RTL sensitivities. As a result, the electron trapping centre related to RTL could be responsible for Ti centre.

5. Conclusions

In the region of low Al impurity content (< 300 ppm), quartz samples exhibit BTL property. In contrast, samples with higher impurity content showed RTL without any exception. The color of TL from natural quartz was found to be particularly dependent on Al impurity content and an approximately inverse correlation was found between the Al contents (> few tens ppm) and T_c values. All natural samples exhibited lower T_c values compared with the standard value of T_c of 573 ^oC from pure quartz sample. In particular, low T_c values from RTL-quartz were easily distinguished from BTL-quartz samples at the boundary temperature, T_c=572.0 ^oC. Thus, the T_c values can be reflected on the luminescence properties, which are affected significantly by the various kinds of impurities.

The luminescence mechanism was found to be quite different between BTL- and RTL-quartz. The BTL sensitivity generally shows a negative relationship with the Al content above an impurity concentration of a few tens of ppm, probably attributed to quenching effects, such as concentration and OH related impurity quenching effects. In contrast, the RTL sensitivity showed a correlation with the square of Al impurity content. This result suggests that RTL hole centres are formed in the structurally distorted defect sites associated with neighboring two Al and/or OH related impurities within a short distance.

6. Reference

Franklin A.D., Prescott J.R., Scholefield R.B., The mechanism of thermoluminescence in an Australian sedimentary quartz. J. Lumin., **63**, 317-326 (1995).

Fujita H., Hashimoto T., Effects of annealing temperatures on some radiation-induced phenomena in natural quartz. Radiat. Meas., submitted for publication

Ganzawa Y., Furukawa H., Hashimoto T., Sanzelle S., Miallier D., Pilleyre T., Single grains dating of volcanic quartz from pyroclastic flows using red TL. Radiat. Meas., **39**, 479-487 (2005).

Griscom D.L., Defect structure of glasses some outstanding questions in regard to vitreous silica. J. Non-Cryst. Solids, **73**, 51-77 (1985).

Hashimoto T., Hayashi Y., Koyanagi A., Yokosaka K., Kimura K., Red and blue colouration of thermoluminescence from natural quartz sands. Nucl. Radiat. Meas., **11**, 229-235 (1986a).

Hashimoto T., Koyanagi A., Yokosaka K., Hayashi Y., Sotobayashi T., Thermoluminescence color images from quartz of beach sands. Geochem. J., **20**, 111-118 (1986b).

Hashimoto T., Sakaue S., Aoki H., Ichino M., Dependence of TL-property changes of natural quartzes on aluminium contents accompanied by thermal annealing treatment. Radiat. Meas., **23**, 293-299 (1994).

Hashimoto T., Notoya S., Arimura T., Konishi M., Changes in luminescence colour images from quartz slices with thermal annealing treatments. Radiat. Meas., **26**, 233-242 (1996).

Hashimoto T., Sugai N., Sakaue H., Yasuda K., Shirai N., Thermoluminescence (TL) spectra from quartz grains using on-line TL-spectrometric system. Geochem. J., **31**, 189-201 (1997).

Hashimoto T., Yamaguchi T., Fujita H., Yanagawa Y., Comparison of infrared spectrometric characteristics of Al-OH impurities thermoluminescence patterns in natural quartz slices at temperatures below 0^{o}C. Radiat. Meas., **37**, 479-485 (2003).

Hashimoto T., Yawata T., Takano M., Comparison of naturally accumulated radiation doses and dating of archaeological burnt materials and usefulness of RTL-dating from quartz extracts. Geochem. J., **39**, 201-212 (2005).

Hummel F.A., Thermal expansion properties of some synthetic lithia minerals. J. Am. Ceramic Soc., **34**, 235-239 (1951).

Huntley D.J., Godfrey-Smith D.I., Haskell E.H., Light-induced emission spectra from some quartz and feldspars. Nucl. Tracks and Radiat. Meas., **18**, 127-131 (1991).

Ichino M., Dependence of thermoluminescence properties and kinetic parameters for natural quartzes on thermal annealing treatment. Master thesis of Niigata University (1994).

Ikeya M., New applications of electron spin resonance: Dating, dosimetry and microscopy. World Scientific, Singapore, 271-314 (1993).

Itoh N., Stoneham D., Stoneham A.M., Ionic and electronic processes in quartz: Mechanisms of thermoluminescence and optically stimulated luminescence. J. Appl. Phys., **92**, 5036-5044 (2002).

Iwasaki F., Iwasaki H., Impurity species in synthetic and Brazilian natural quartz. Jpn. J. Appl. Phys.,

32, 893-901 (1993).

Kalceff M.A.S., Philips M. R., Cathodoluminescence microcharacterization of the defect structure of quartz. Phys. Rev. B, **52**, 3122-3134 (1995).

Keith, M.L., Tuttle, O.F., Significance of variance in high-low inversion of quartz. Am. J. Sci., **253a**, 203-280 (1952).

Kojima M., Measurements of kinetic parameters for red and blue thermoluminescence from natural quatz grains associated with TL dating. Master thesis of Niigata University (1992).

Martini M., Paleari A., Spinolo G., Vedda A., Role of $[AlO_4]^0$ centers in the 380-nm thermoluminescence of quartz. Phys. Rev. B, **52**, 138-142 (1995).

McKeever S.W.S., Thermoluminescence of solids. Cambridge University Press. Cambridge (1988).

Munekuni S., Yamanaka T., Shimogaichi Y., Tohmon R., Ohki Y., Various types of nonbridging oxygen hole center in high-purity silica glass. J. Appl. Phys., **68**, 1213-1217 (1990).

Nishikawa H., Nakamura R., Thohmon R., Ohki Y., Generation mechanism of photoinduced paramagnetic centers from preexisting precursors in high-purity silicas. Phys. Rev. B, **41**, 7828-7834 (1990).

Nishikawa H., Shiroyama T., Nakamura R., Ohki Y., Photoluminescence from defect centers in high-purity silica glasses observed under 7.9-eV excitation. Phys. Rev. B, **45**, 586-591 (1992).

Spooner N.A., On the optical signal from quartz. Radiat. Meas., **23**, 593-600 (1994).

Spooner N.A., Prescott J.R. and Hutton J.T., The effect of illumination wavelength on the bleaching of TL of quartz. Quart. Sci. Rev., **7**, 325-330 (1988).

Stapelbroek M., Griscom D.L., Fribele E.J., Sigel G.H., Oxygen-associated trapped-hole centers in high-purity fused silicas. J. Non-Cryst. Solids, **32**, 313-326 (1979).

Sugai N., Bleaching and mean lives of electron traps affecting thermoluminescence from quartz grains. Master thesis of Niigata University (1998).

Vartanian E., Guibert P., Roque C., Bechtel M., Schvoerer M., Changes in OSL properties of quartz by preheating: an interpretation. Radiat. Meas., **32**, 647-652 (2000).

Woda C., Schilles T., Riser U., Mangini A., Wagner G.A., Point Defects and the Blue Emission in Fired Quartz at High Doses: A Comparative Luminescence and EPR Study. Radiat. Protection Dosimetry, **100**, 261-264 (2002).

Yang X.H., McKeever S.W.S., Point defects and the pre-dose effect in quartz. Radiat. Protection Dosimetry., **33**, 27-30 (1990).

Yawata T., Hashimoto T., Identification of the volcanic quartz origins from dune sand using a single-grain RTL measurement. Quat. Sci. Rev., **23**, 1183-1186 (2004).

Zimmermann J., The radiation-induced increase of the 100°C thermoluminescence sensitivity of fired quartz. J. Phys. C: Solid State Phys., **4**, 3265-3276 (1971).

Table 2-1 Amounts of trace elements, α–β phase inversion break temperatures and luminescence sensitivities of quartz samples.

origin	TL coloration	Trace elements / ppm [1*]						Inversion[2*]	RTL[3*]	BTL[3*]	OSL[3*]
		Al	Ti	Li	Fe	Mg	Cu	temperature / °C	/ x10^4 counts	/ x10^4 counts	/ x10^3 counts
Volcanic	Red	768 ± 65	412 ± 62	26 ± 2	135 ± 15	41 ± 26	31 ± 4	571.3 ± 0.2	14.4 ± 1.4		6.2 ± 0.9
Volcanic	Red	709 ± 142	357 ± 51	19 ± 2	359 ± 153	267 ± 68	8 ± 2	570.8 ± 0.2	8.4 ± 0.9		37.3 ± 1.0
Volcanic	Red	691 ± 126	247 ± 30	31 ± 2	57 ± 8	215 ± 33	15 ± 2	571.2 ± 0.1	8.2 ± 0.1		16.9 ± 2.0
Volcanic	Red	683 ± 35	207 ± 28	19 ± 2	159 ± 24	53 ± 9	20 ± 4	571.7 ± 0.2	6.3 ± 0.5		0.8 ± 0.3
Volcanic	Red	643 ± 47	220 ± 16	14 ± 5	165 ± 16	66 ± 5	4 ± 0.4	571.6 ± 0.1	5.1 ± 0.4		1.6 ± 0.3
Granite	Red	619 ± 65	110 ± 11	13 ± 1	67 ± 8	28 ± 6	n.d.	571.9 ± 0	5.5 ± 0.1		4.3 ± 0.1
Volcanic	Red	580 ± 48	154 ± 4	11 ± 1	98 ± 9	40 ± 8	15 ± 2	571.0 ± 0.1	3.4 ± 0.2		40.5 ± 0.3
Granite	Red	567 ± 41	58 ± 3	14 ± 1	76 ± 23	40 ± 0.4	3 ± 0.1	571.7 ± 0.1	2.6 ± 0.3		0.3 ± 0.2
Volcanic	Red	555 ± 42	230 ± 20	16 ± 6	35 ± 6	56 ± 5	3 ± 0.2	571.8 ± 0.2	5.3 ± 0.1		2.4 ± 0.3
Volcanic	Red	540 ± 42	191 ± 30	21 ± 3	42 ± 4	36 ± 4	4 ± 3	571.8 ± 0	4.4 ± 0.4		1.7 ± 0.6
Volcanic	Red	538 ± 42	185 ± 11	16 ± 4	179 ± 45	103 ± 33	7 ± 3	571.0 ± 0.2	3.4 ± 0.6		11.7 ± 1.3
Volcanic	Red	496 ± 42	146 ± 32	42 ± 6	48 ± 16	46 ± 20	n.d.	571.9 ± 0.1	4.8 ± 0.4		1.1 ± 0.2
Volcanic	Red	450 ± 33	193 ± 58	16 ± 2	68 ± 29	165 ± 20	3 ± 2	571.3 ± 0.1	2.3 ± 0.4		2.1 ± 0.1
Volcanic	Red	457 ± 41	203 ± 21	12 ± 1	45 ± 6	124 ± 15	7 ± 2	571.8 ± 0.2	3.4 ± 0.2		1.7 ± 0.1
Volcanic	Red	426 ± 41	76 ± 20	16 ± 3	167 ± 17	177 ± 35	9 ± 3	571.7 ± 0.2	0.9 ± 0.1		3.3 ± 0.5
Volcanic	Red	324 ± 10	166 ± 16	11 ± 1	23 ± 2	58 ± 5	25 ± 2	571.8 ± 0.2	3.4 ± 0.3		1.6 ± 0.1
Crystal	Blue	255 ± 64	36 ± 23	10 ± 2	55 ± 9	44 ± 31	n.d.	572.1 ± 0		2.4 ± 0.3	1.0 ± 0.1
Crystal	Blue	231 ± 17	11 ± 0.1	20 ± 4	37 ± 3	27 ± 13	n.d.	572.4 ± 0.2		5.4 ± 0.6	8.4 ± 2.1
Plutonic rock	Blue	154 ± 16	41 ± 4	17 ± 2	11 ± 2	30 ± 8	n.d.	572.3 ± 0		0.5 ± 0.1	0.2 ± 0.2
Soil	Blue	145 ± 26	53 ± 6	4 ± 2	26 ± 13	13 ± 6	n.d.	572.7 ± 0.1		2.1 ± 0.4	2.0 ± 1.7
Soil	Blue	142 ± 28	77 ± 12	8 ± 2	19 ± 8	37 ± 11	n.d.	572.6 ± 0.1		4.4 ± 0.8	1.4 ± 0.3
Sediment	Blue	131 ± 5	145 ± 24	5 ± 1	17 ± 1	36 ± 17	n.d.	572.7 ± 0.3		3.6 ± 0.2	1.7 ± 0.3
Granite	Blue	128 ± 28	71 ± 29	4 ± 2	42 ± 5	39 ± 20	n.d.	572.4 ± 0.1		2.1 ± 1.3	2.8 ± 0.9
Vein	Blue	104 ± 7	79 ± 5	2 ± 1.2	13 ± 1	55 ± 10	n.d.	572.2 ± 0.1		12.1 ± 0.6	0.4 ± 0.1
Vein	Blue	101 ± 59	22 ± 1	3 ± 2	17 ± 3	59 ± 33	n.d.	572.7 ± 0.2		1.3 ± 0.1	1.3 ± 0.4
Vein	Blue	100 ± 7	26 ± 2	1 ± 0.4	27 ± 2	31 ± 23	n.d.	572.6 ± 0.1		0.7 ± 0.1	0.8 ± 0.2
Granite	Blue	86 ± 26	152 ± 45	6 ± 2	18 ± 5	41 ± 12	n.d.	572.6 ± 0.2		1.7 ± 1.2	0.9 ± 0.1
Soil	Blue	77 ± 24	92 ± 24	5 ± 2	13 ± 5	26 ± 12	n.d.	572.7 ± 0.1		2.0 ± 0.1	1.4 ± 0.4
Crystal	Blue	68 ± 28	37 ± 21	5 ± 2	18 ± 2	25 ± 10	n.d.	572.7 ± 0.1		0.3 ± 0.1	0.4 ± 0.1
Crystal	Blue	26 ± 3	59 ± 8	2 ± 0.1	9 ± 1	14 ± 2	n.d.	572.3 ± 0.1		25.8 ± 4.2	13.6 ± 2.0
Pegmatite	Red/Blue	279 ± 43	53 ± 3	12 ± 2	64 ± 6	86 ± 5	n.d.	572.2 ± 0.1	22.2 ± 1.0	0.9 ± 0.2	1.0 ± 0.3
Pegmatite	Red/Blue	100 ± 12	63 ± 9	6 ± 2	29 ± 6	319 ± 32	n.d.	572.1 ± 0.1	8.9 ± 1.1	0.5 ± 0.1	0.8 ± 0.3

1* Ge impurity was not detected in all specimens. 2* Inversion temperature on cooling process (Tc)

3* RTL, BTL and OSL integration: RTL (350-380°C); BTL (240-400°C); OSL(0-1.0sec) n.d. : not detected

Table 2-2 Estimated kinetics parameters of Al and Ti centres in quartz samples using isochronal annealing curves.

	Sample name	Al centre		Ti centre	
		Activation energy / eV	Frequency factor / s^{-1}	Activation energy / eV	Frequency factor / s^{-1}
BTL-quartz (Madagascar)	color parts	0.68 ± 0.02	(1.06 ± 0.46) $x10^{7}$	n.d.	n.d.
	colorless parts	0.65 ± 0.03	(1.15 ± 0.38) $x10^{7}$		
RTL-quartz	Lake Tazawa	1.22 ± 0.04	(4.30 ± 2.11) $x10^{12}$	1.08 ± 0.02	(5.87 ± 3.31) $x10^{10}$
	Anchi	1.04 ± 0.01	(7.82 ± 3.16) $x10^{10}$	1.33 ± 0.02	(6.05 ± 2.63) $x10^{12}$
	Medeshima	1.16 ± 0.05	(2.58 ± 1.54) $x10^{12}$	1.70 ± 0.04	(6.10 ± 1.56) $x10^{15}$

n.d. not detected

Table 2-3 Kinetics parameters of electron traps related to BTL/RTL most intense peak.

	Sample name	Electron traps related to BTL/RTL peak		Method and References
		Activation energy / eV	Frequency factor / s^{-1}	
BTL-quartz	Madagascar color parts Madagascar colorless parts	1.07-1.25	(0.41-1.22) $x10^{9}$	Isothermal, peak shape method (Ichino, 1994)
RTL-quartz	Lake Tazawa	1.16 ± 0.19	(1.31 ± 6.24) $x10^{8}$	Isothermal method (Ichino, 1994)
	Anchi	1.48	1.35 $x10^{11}$	Initial rise method (Sugai, 1998)
	Medeshima	1.66 ± 0.01	(1.19 ± 0.17) $x10^{12}$	Initial rise method (Kojima, 1992)

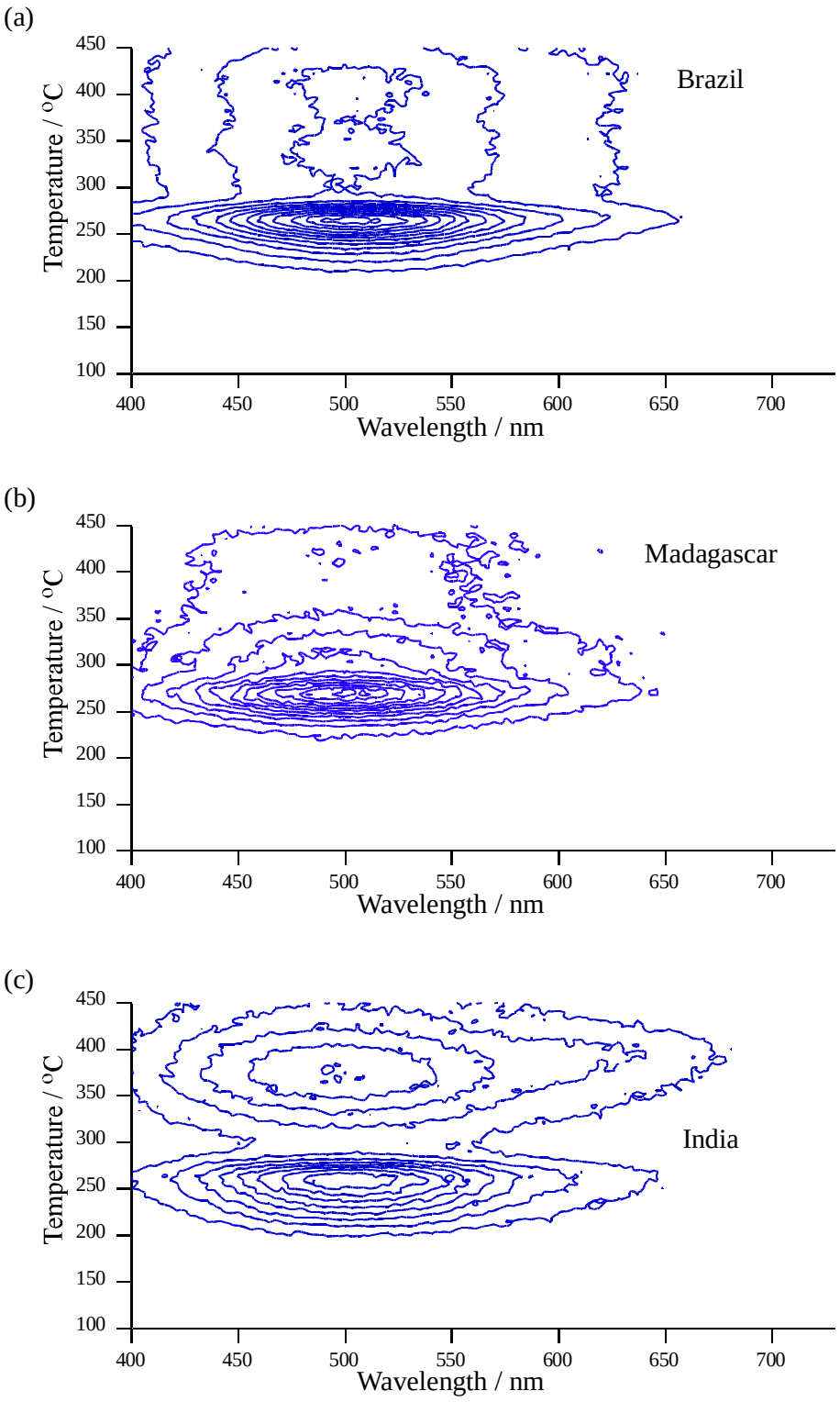

Fig. 2-1 Typical contour expression of TL-spectra from BTL-quartz grains
(a) Brazil
(b) Madagascar
(c) India
All grain samples were irradiated of 1.2 kGy by X-ray.

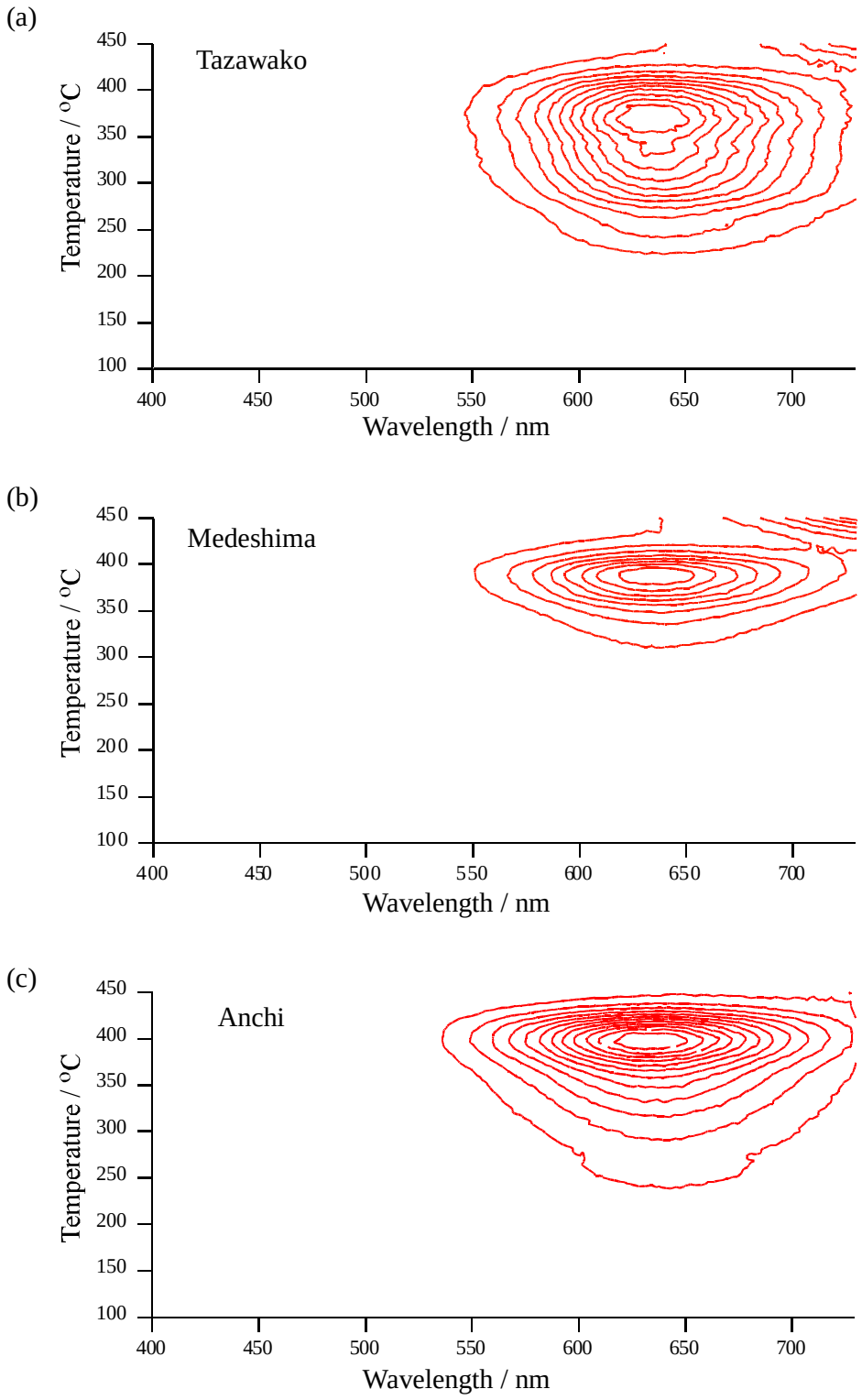

Fig. 2-2 Typical contour expression of TL-spectra from RTL-quartz grains
(a) Lake Tazawa
(b) Medeshima
(c) Anchi
All grain samples were irradiated of 1.2 kGy by X-ray.

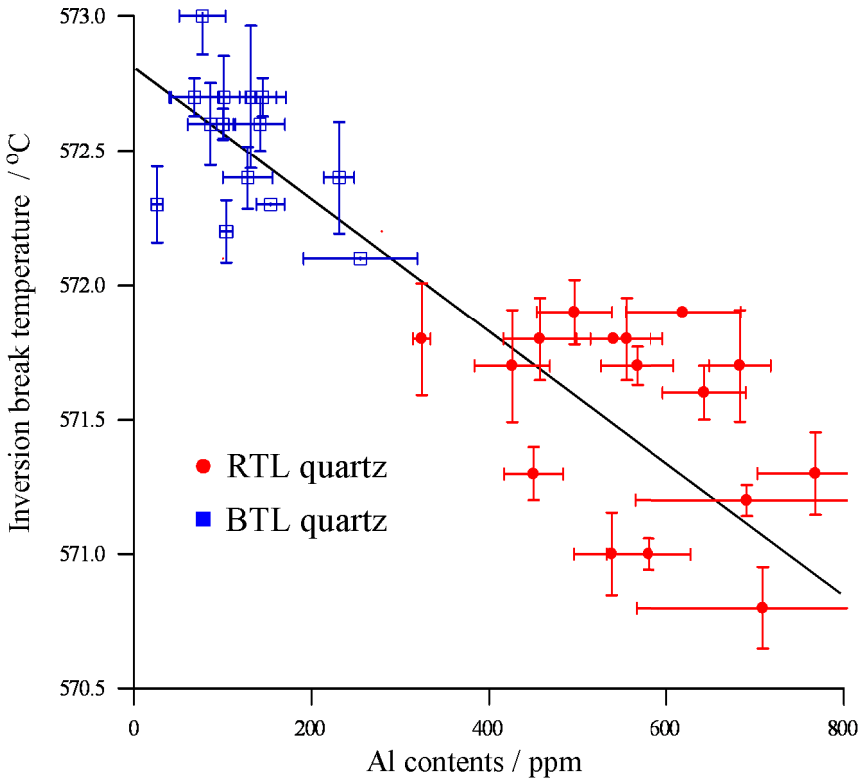

Fig. 2-3 A relationship between the Al contents and α−β phase inversion break temperatures (T_C). Each experimental error was derived from two or three aliquot analysis. The line was obtained by least square fitting.

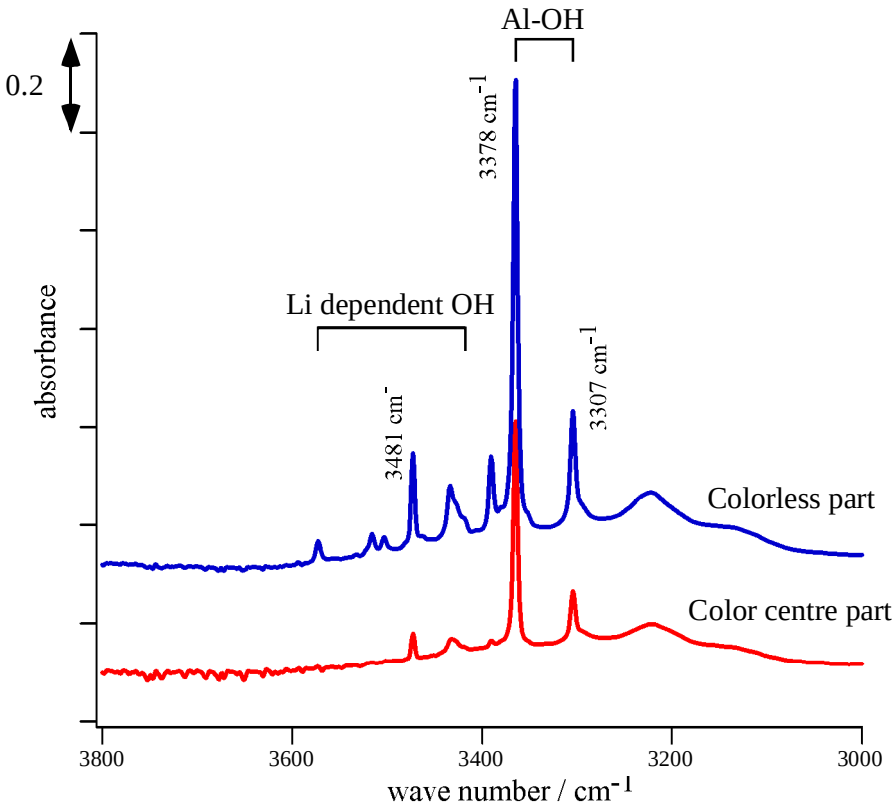

Fig. 2-4 Typical IR absorption spectra from Madagascan quartz sample.
This quartz sample was irradiated with g-ray of 20kGy.
These spectra were measured at liquid nitrogen temperature (-196^{o}C)

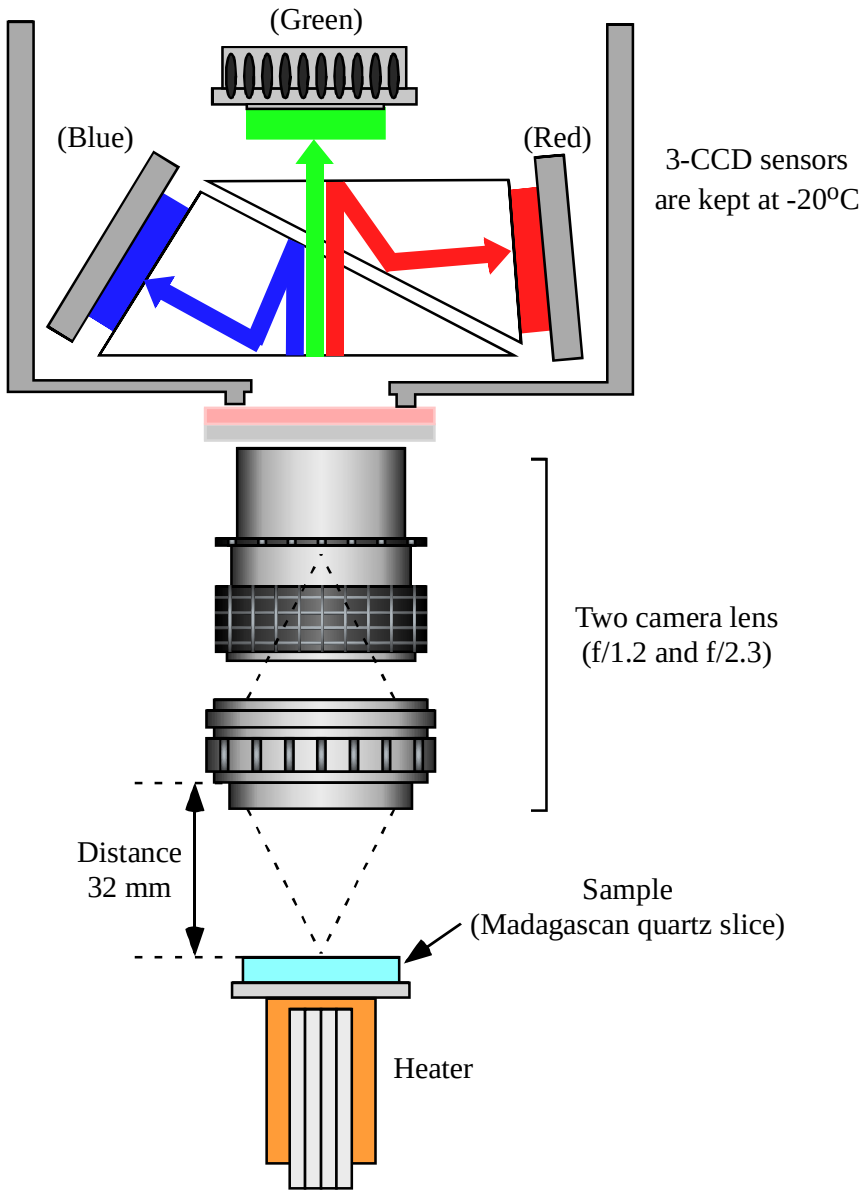

Fig. 2-5 Conceptual view of quantitative mapping measurements for TL spectra. The TL emission data from quartz sample were separated into 12 bit RGB data using prisms and optical filters.

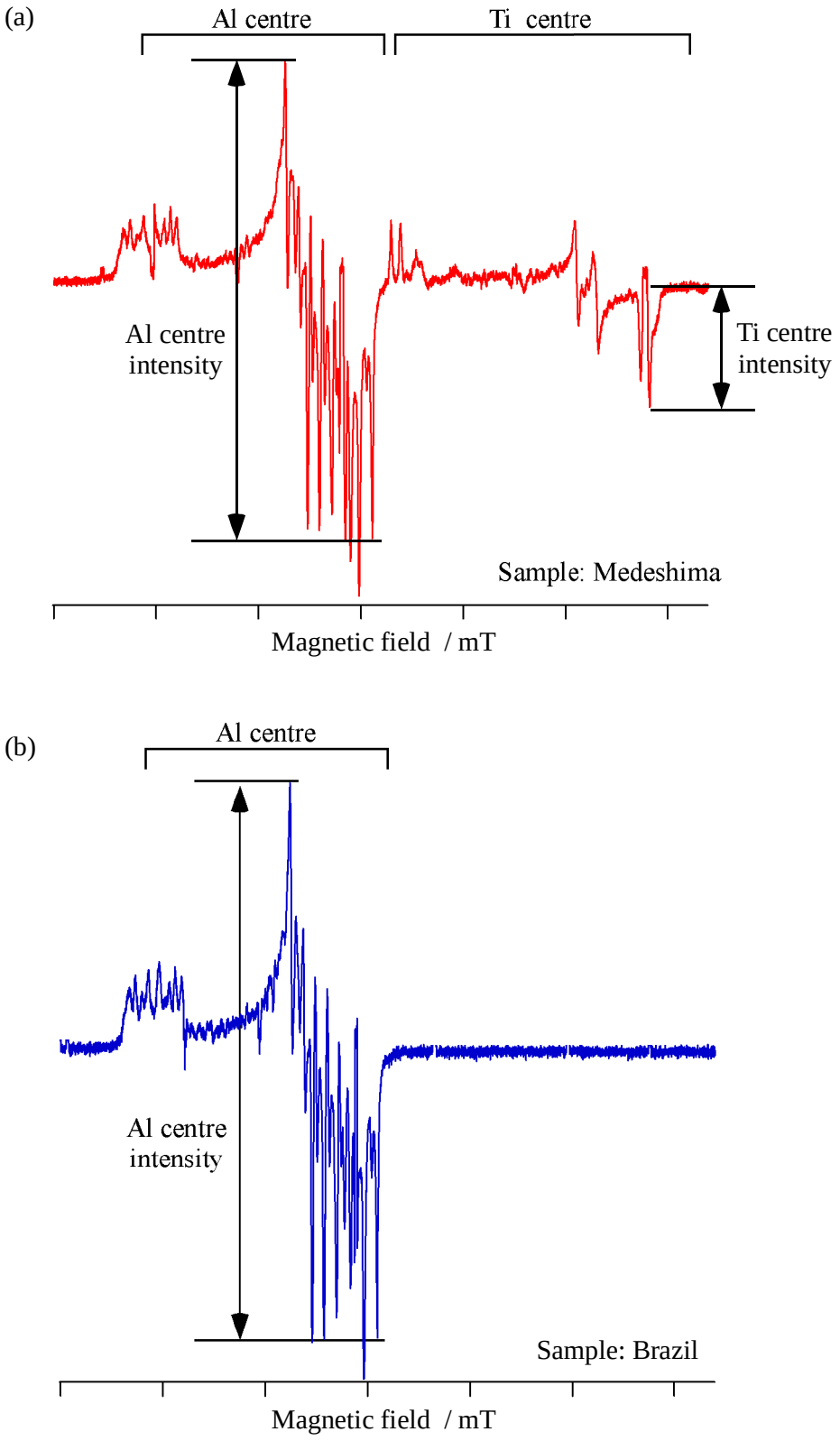

Fig. 2-6 Typical ESR spectra from RTL-quartz (Medeshima) (a) and BTL-quartz (Brazil) (b). Samples were irradiated of 20 kGy by γ-ray.

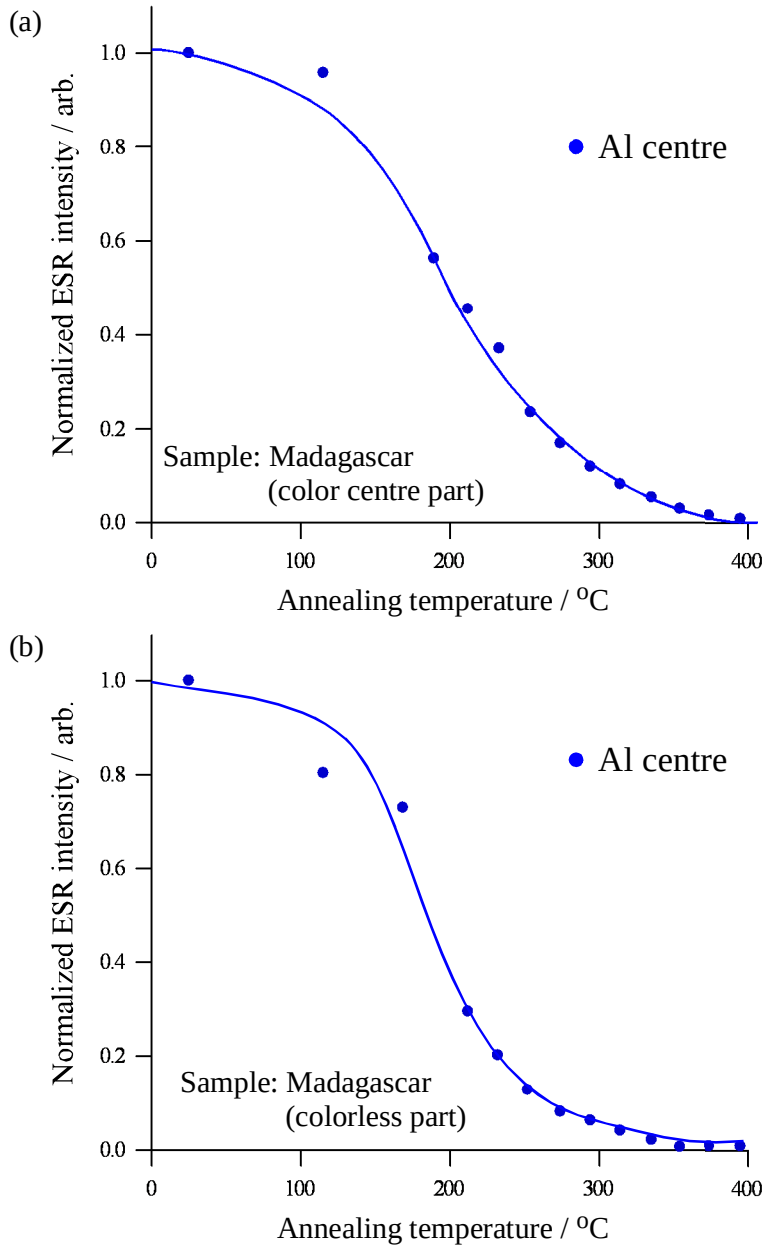

Fig. 2-7 Isochronal annealing experiments of Al centre on BTL-quartz samples.
Each marker showed signal intensity after heating the sample at particular temperature.
Solids lines were obtained by calculation based on the first order decay kinetics.
All grain samples were irradiated of 1.2 kGy by X-ray.

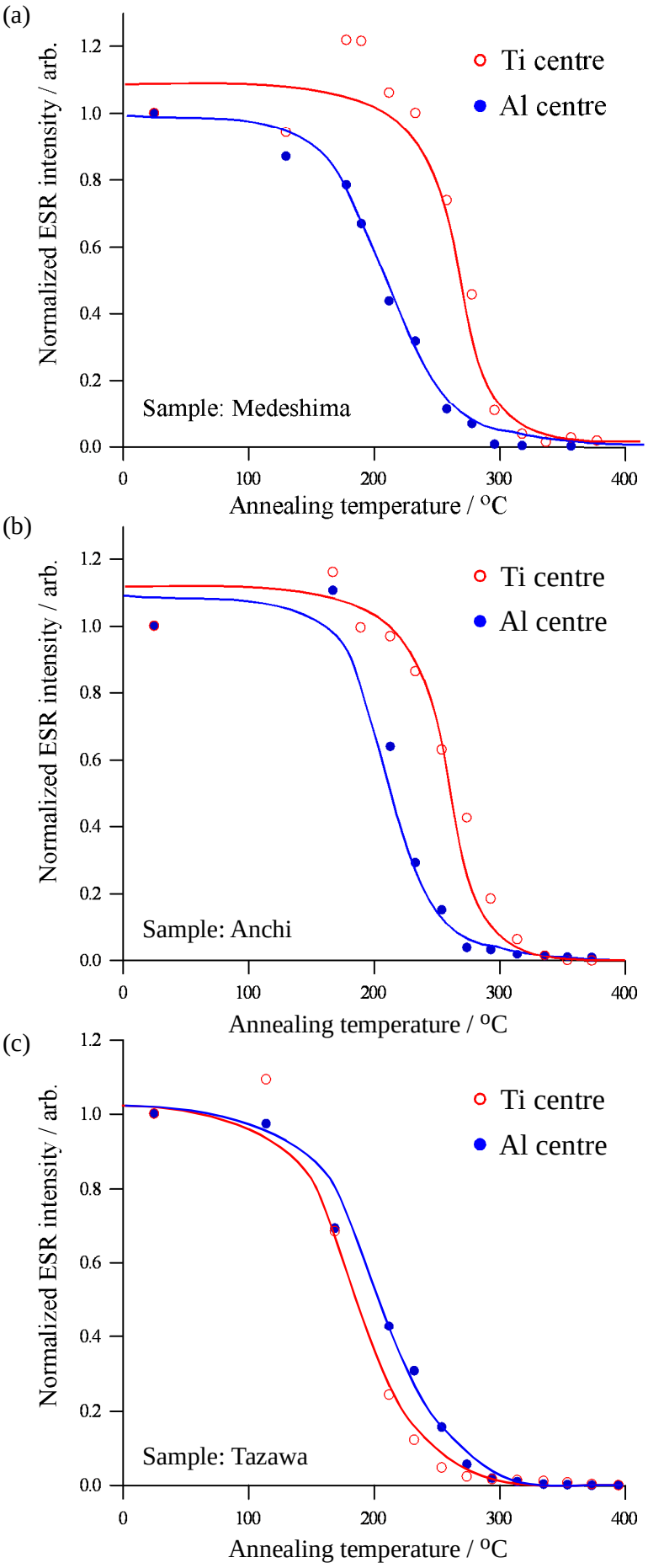

Fig. 2-8 Isochronal annealing experiments of Al and Ti centre on RTL-quartz samples.
Each marker showed signal intensity after heating the sample at particular temperature.
Solids lines were obtained by calculation based on the first order decay kinetics.
All grain samples were irradiated of 1.2 kGy by X-ray.

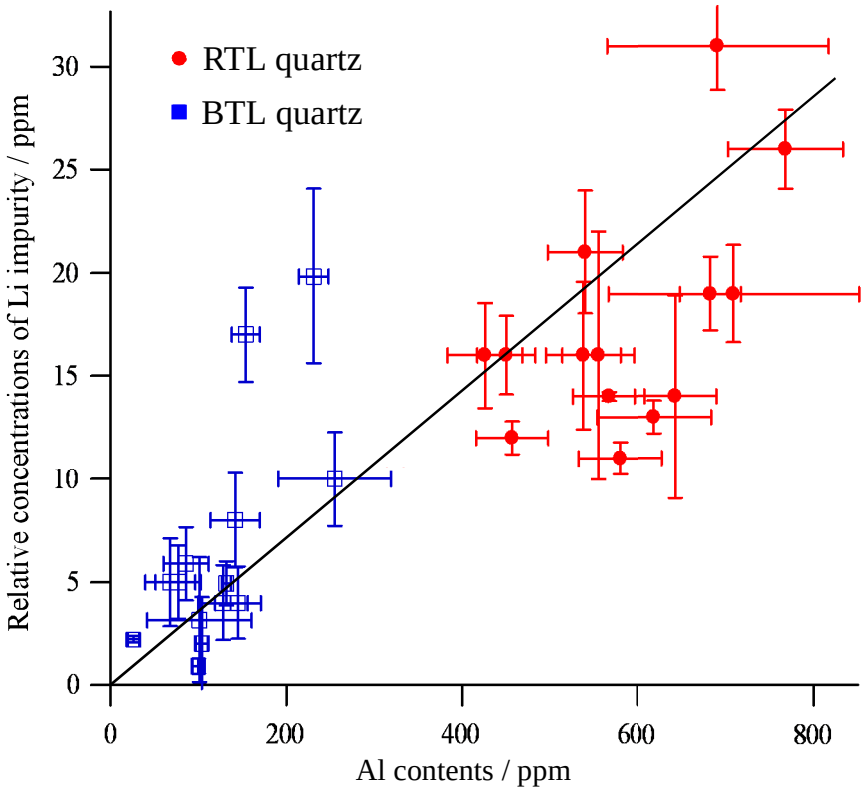

Fig. 2-9 Amounts of Al-impurities plotted as a function of the Li content in natural quartz samples. Solid line showed one-to-one relationship.

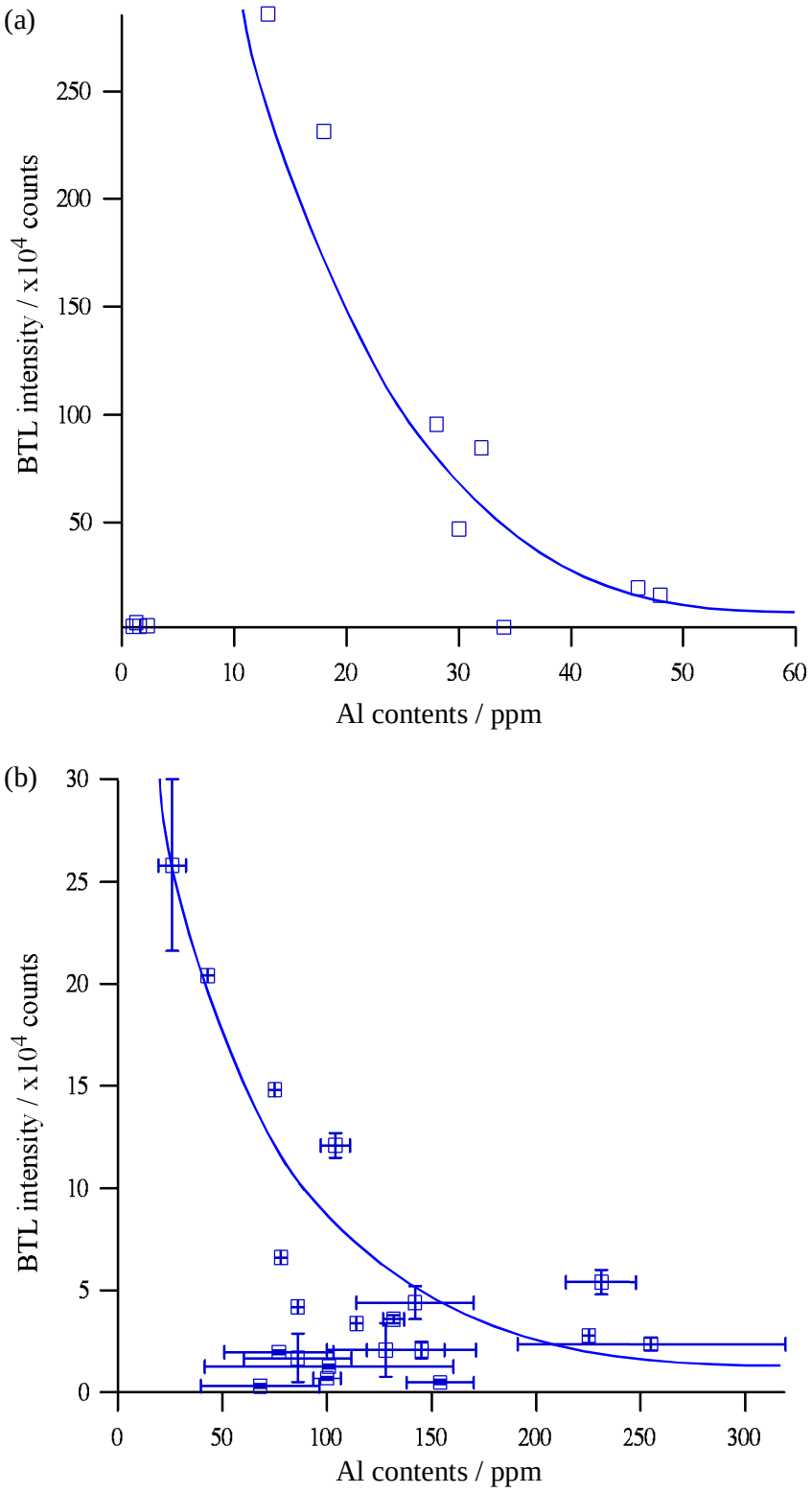

Fig. 2-10 Relationships of the BTL sensitivities with the Al content for synthetic quartz (a) and natural quartz (b). The quartz samples were irradiated with a fixed dose of 20 Gy. BTL sensitivities were integrated from 250 to 400°C.

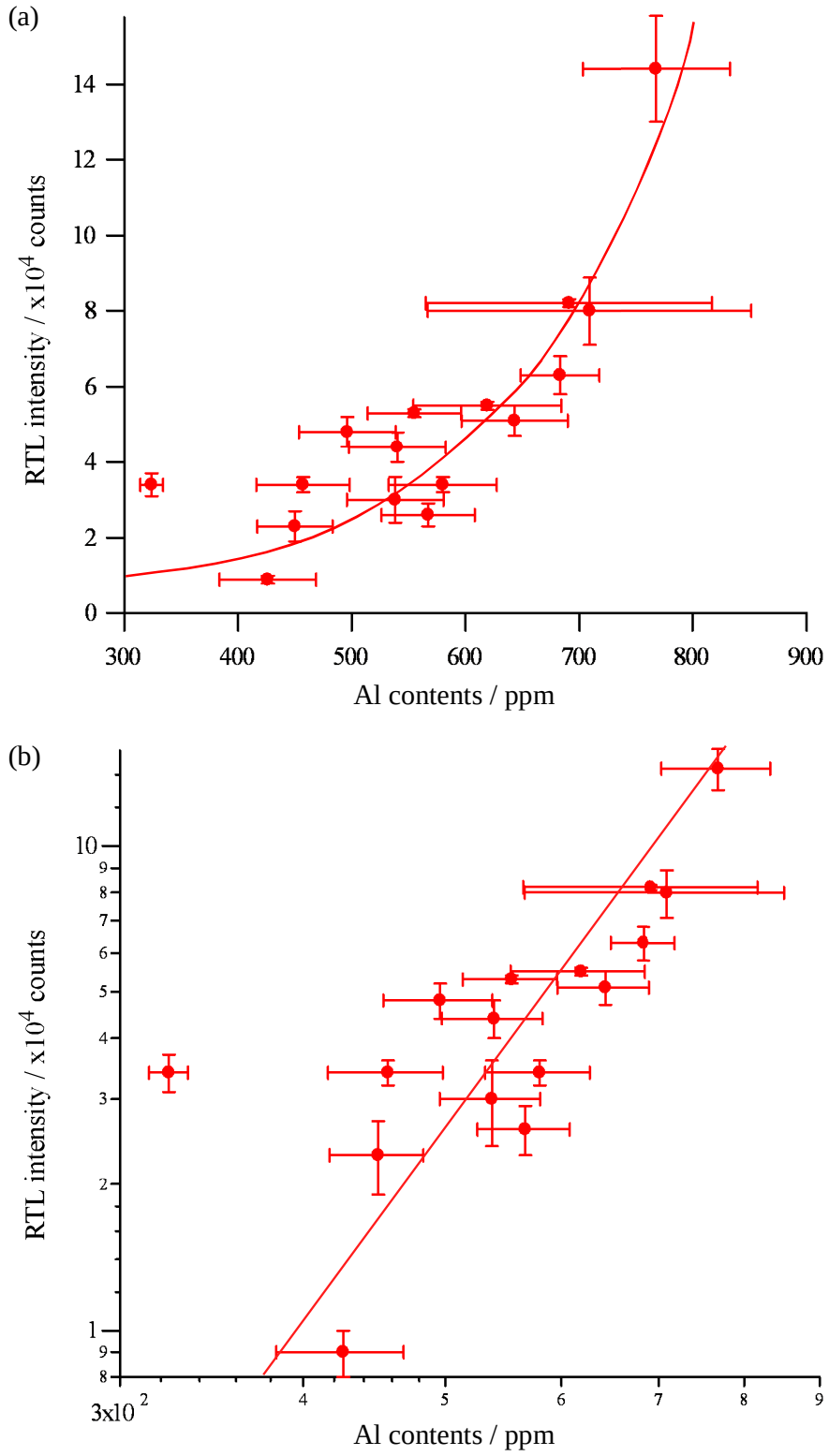

Fig. 2-11 RTL sensitivities plotted against the Al content for natural quartz samples (a) and log-log plot (b).
The quartz samples were irradiated with a fixed dose of 20 Gy. RTL sensitivities were integrated from 350 to 380^{o}C.

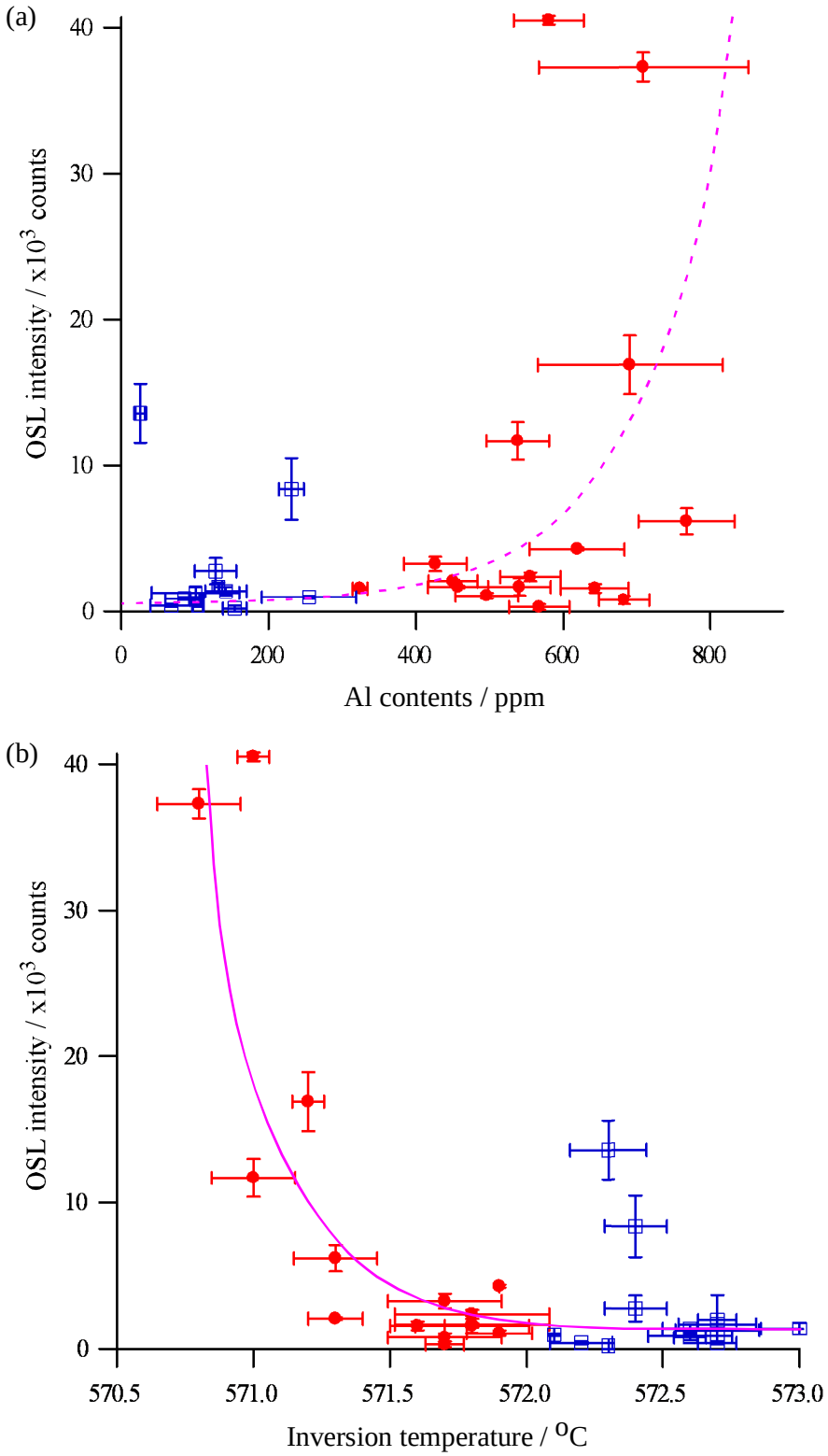

Fig. 2-12 OSL sensitivities for the natural quartz samples as a function of Al content (a) and of α–β phase inversion break temperatures (b).
The quartz samples were irradiated with a fixed dose of 20 Gy.
OSL sensitivities were integrated initial part for 1 sec of decay curves.

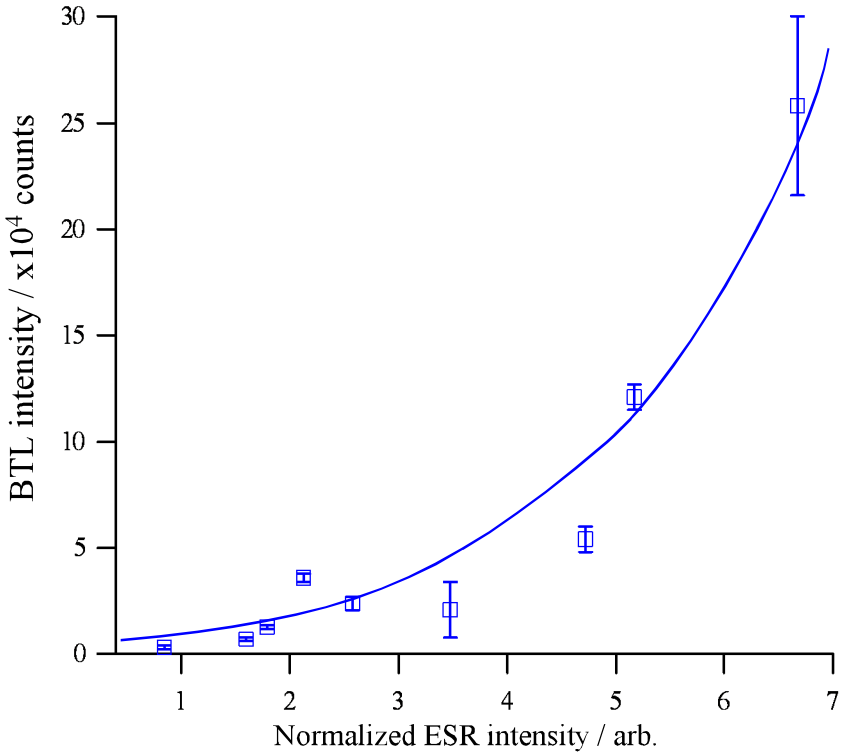

Fig. 2-13 A relationship between the BTL sensitivities and $[AlO_4/h]^o$ centre intensities in natural quartz samples.

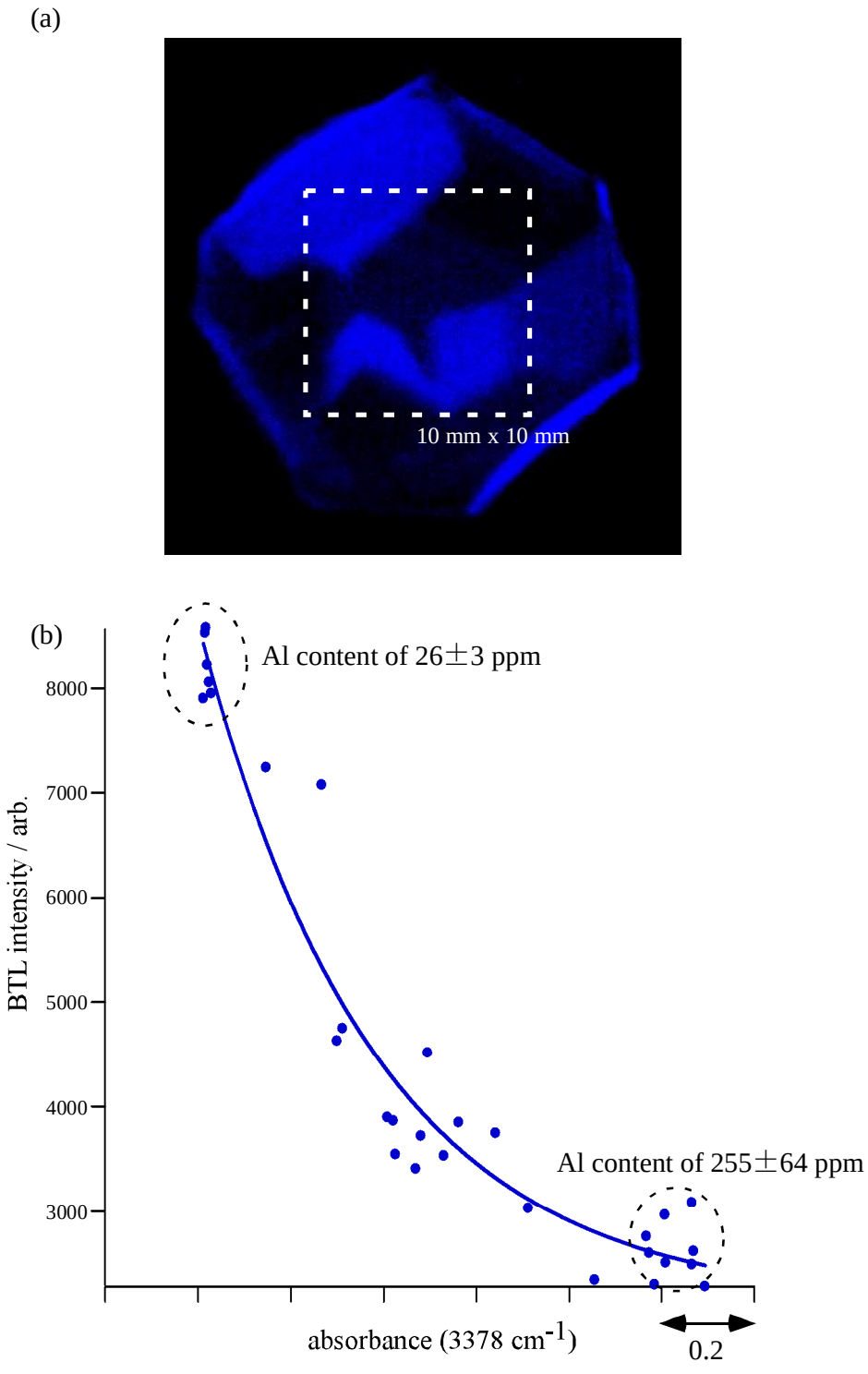

Fig. 2-14 Typical IR absorption spectra from Madagascan quartz sample.
This quartz sample was irradiated with g-ray of 20kGy.
These spectra were measured at liquid nitrogen temperature (-196°C)

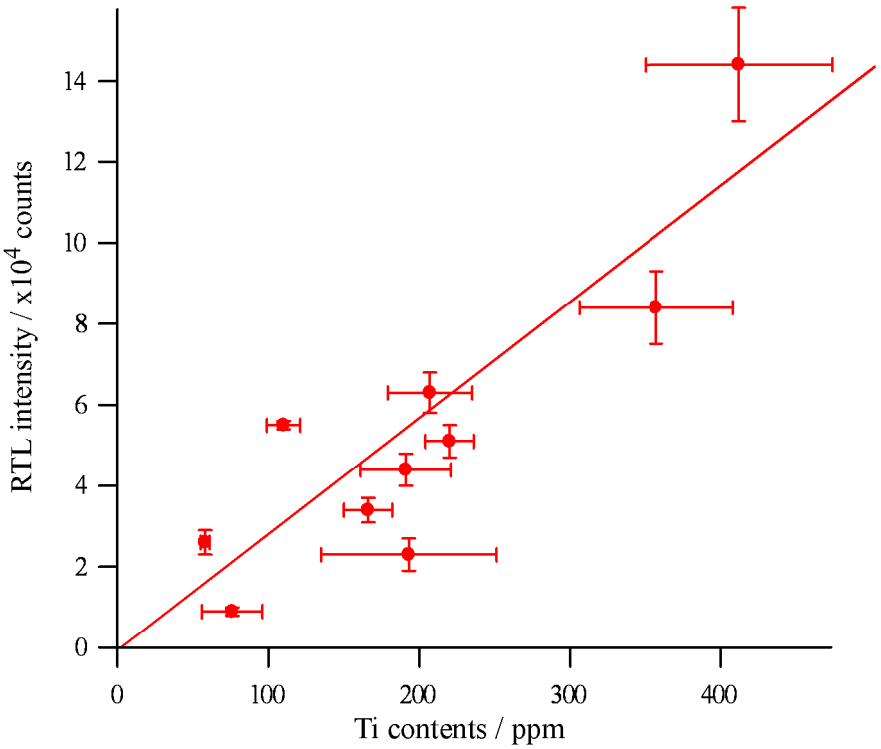

Fig. 2-15 RTL sensitivities plotted against the Ti content for natural quartz samples. The quartz samples were irradiated with a fixed dose of 20 Gy. RTL sensitivities were integrated from 350 to 380^{O}C.

† *Chapter 3* †

Determination of internal radioactivity in quartz grains using a multiple pulse time interval analysis (MTA) technique and its contribution on annual dose for RTL dating

Abstract

Pulse occurring time and pulse interval data, provided from a liquid scintillation counting (LSC) pulses, were followed to a multiple pulse time interval analysis (MTA) technique to determine a small amount of radioactive nuclides in quartz grains. By comparing γ-ray spectrometry, the LSC/MTA method has following advantages for the radioactivity determination: (i) requirement of a small samples for measurements (approximately ~2 g), (ii) contribution of negligible small background, (iii) ^{216}Po- and ^{214}Po-decay rates in ^{238}U- and ^{232}Th-decay series were easily distinguished from scintillation α-pulses without energy information, and (iv) even 0.1 ppm of ^{238}U and ^{232}Th in quartz grains were detected due to a high counting efficiency for liquid scintillation counting.

Using LSC/MTA method, one volcanic quartz sample was found to contain relatively high radioactive nuclides (^{238}U: 0.41±0.05 ppm; ^{232}Th: 0.28±0.02 ppm) compared to other quartz origins. The internal dose rate contribution on annual dose for this sample reached 10~20 %. As a result, some volcanic quartz samples should consider the internal dose rate contribution to annual dose when an external dose rate is relatively low level. Taking into consideration of internal radioactivity, the age of volcano activity was successfully evaluated from the RTL-measurements.

1. Introduction

The main minerals used in luminescence dating are quartz and feldspar. In particular, for accurate equivalent dose determination, the quartz grains are preferred, since the electron traps associated with TL and OSL have been recognized to be deep enough to store electrons without any fading for a half million years or more (Aitken, 1998). The accumulated electrons are proportional to annual dose and elapsed time after the most recent heating or bleaching events. An annual dose absorbed by a white mineral is evaluated according to a function of the radioactivity both in a grain (internal dose rate) as well as in a surrounding material (external dose rate). These dose rates can be mainly calculated from the concentrations of ^{40}K, ^{238}U and ^{232}Th series as natural radioactive nuclides using conversion factors (Adamiec and Aitken, 1998). In the case of quartz samples, it is usually a good approximation to assume that the internal dose rate is negligibly small contribution because of low radioactivity content in quartz sample (Aitken, 1985). However, when the external dose rate is relatively low level, such as in volcanic ash layer (Table 3-1), the contribution of internal dose rate should be taken into account on the evaluation of annual dose. In addition, the volcanic quartz sample may contain higher concentrations of radioactive nuclides as well as other impurity concentrations (see Chapter 2) when comparing to other quartz samples, such as hydrothermal origin, vein quartz and sediment quartz.

Generally, a high-resolution γ-ray spectrometry and/or a neutron activation analysis are useful tools for the determination of relatively high radioactivity, since these techniques can measure the activities of several individual radioactive nuclides. In a low level radioactivity analysis, a liquid scintillation counting (LSC) is a preferable method because of high counting efficiency for alpha particles (nearly 100%) in spite of poor energy resolution. Therefore, U- and Th-series may not be selectively identified from the mixture of natural radioactive nuclides by means of alpha energy spectra. To overcome this situation, multiple pulse time interval analysis (MTA) technique (Hashimoto et al., 2004) using a new PCI board having 1 μs time resolution (Yawata et al., 2006) has been applied to scintillation pulse analysis for the determination of ^{238}U and ^{232}Th in quartz samples.

In this chapter, the LSC combined with MTA technique (hereafter defined LSC/MTA method) was developed to determine a small amount of radioactive nuclides in quartz. By using this

method, the radioactivity in both quartz and surrounding soil were determined from several samples. Then, the application to RTL dating was achieved to a volcanic ash layer, taking into consideration to the internal dose rate contribution to annual dose.

2. Samples and sample preparation

For dating sample, a volcanic ash originated in the Toya-volcano activity, which have been estimated the age of at around 90-120 ka (Machida and Arai, 1992), was employed (in this chapter defined this sample as Toya sample). Fig. 3-1 shows sampling site of Toya sample. In addition, three quartz samples collected from another volcanic ash, sediment and a vein quartz rock were prepared. All quartz samples were extracted by a standard procedure (Hashimoto et al., 2005) and then were engaged to TL-spectrometry (see Chapter 2 in details). The Toya and another volcanic quartz samples showed typical RTL properties, while other quartz samples gave rise to typical BTL properties. In particular, the TL characteristics of Toya quartz sample are in concordance with the results of Ganzawa et al. (1997, 2005), by whom Toya sample was collected from different sites.

3. Annual dose estimation

3-1. Principle of multiple pulse time interval analysis (MTA)

A one of the delayed coincidence method, called a pulse time interval analysis (TIA) method, has been developed to determine natural radionuclides by a selective extraction of correlated events from the random events. The correlated events are defined successive α–α or β–α decay events within millisecond or microsecond orders. These correlated decay events are follows;

$^{220}\mathrm{Rn} \xrightarrow{\alpha} {}^{216}\mathrm{Po}(T_{1/2}:145\mathrm{ms}) \xrightarrow{\alpha} (\text{Th-series})$, $^{221}\mathrm{Fr} \xrightarrow{\alpha} {}^{217}\mathrm{At}(T_{1/2}:32.3\mathrm{ms}) \xrightarrow{\alpha} (\text{Np-series})$,

$^{219}\mathrm{Rn} \xrightarrow{\alpha} {}^{215}\mathrm{Po}(T_{1/2}:1.78\mathrm{ms}) \xrightarrow{\alpha} (\text{Ac-series})$, $^{214}\mathrm{Bi} \xrightarrow{\beta} {}^{214}\mathrm{Po}(T_{1/2}:164\mu\mathrm{s}) \xrightarrow{\alpha} (\text{U-series})$,

$^{213}\mathrm{Bi} \xrightarrow{\beta} {}^{213}\mathrm{Po}(T_{1/2}:4.2\mu\mathrm{s}) \xrightarrow{\alpha} (\text{Np-series})$.

On the other hand, cosmic rays and α/β(γ) rays, having non-successive decay events within a fixed time, are dealt with as random events. The TIA method is fundamentally based on the analysis of the pulse time interval to distinguish objective correlated events from the random events.

The TIA method could be distinguished into the two kinds of methods on the basis of the data-treatment of the pulse time intervals. One is a single time interval analysis (STA), which treats the pulse time intervals between just adjacent pulses (Hashimoto et al., 1992; Sanada et al., 2006). Another is multiple pulse time interval analysis (MTA), which deals with all pulse time intervals within a fixed time (Hashimoto et al., 1992; Yawata et al., 2006). Previously, it has been proved that the MTA technique is superior to the STA technique because the correlated events can be surely distinguished from the random events, which bring on horizontal line (Hashimoto et al., 2004). Therefore, MTA method will be dealt with for the determination of radioactive nuclides in this chapter.

Theoretical MTA distribution was introduced from the view point of probability of decay events within differential time dt (1, 10, 100 μs, 1, 5, 10 ms). A conceptual expression of the MTA is illustrated in Figs. 3-2 and 3-3. A fixed time (t_f) is defined as $t_f = \sum_{dt}^{1000} dt$. According to definition of correlated events, probability of correlated events within a fixed time ($P_i(t)$; Fig. 3-4) are defined following equation

$$P_i(t) = \sum_{i=1}^{k} W_i \cdot \left[\exp(-\lambda_i \cdot t) - \exp\left\{-\lambda_i \cdot (t+dt)\right\}\right]$$

$$= \sum_{i=1}^{k} W_i \cdot \left\{1 - \exp(-\lambda_i \cdot dt)\right\} \cdot \exp(-\lambda_i \cdot t) \quad \cdots(1),$$

where W_i is the decay probability of parents nuclides at t=0, and λ_i represents the decay constant of the correlated daughter nuclide. In this equation, if the dt value is less than one tenth of $T_{i1/2}$ (=ln $2/\lambda_i$) of an objective nuclei, Eqs. (1) can be approximated as follows.

$$P_i(t) = \sum_{i=1}^{k} W_i \cdot \lambda_i \cdot \exp(-\lambda_i \cdot t) dt \quad \cdots(2)$$

On the other hand, probability of random events (R) is defined the rate of random events within dt. Accordingly, R represent following equation

$$R = r \cdot dt \quad \cdots(3),$$

where r is probability that non-correlated events occur within the dt.

Combining Eqs. (1) and Eqs. (2), probability of total pulse occurrence within a fixed time is deduced

$$P_{Total}(t) = P_i(t) + R$$

$$= \sum_{i=1}^{k} \{W_i \cdot \lambda_i \cdot \exp(-\lambda_i \cdot t)\} dt + r \cdot dt \quad \cdots(4)$$

Consequently, MTA distribution is introduced by multiplying total counts N to Eqs. (4)

$$N \cdot P_{Total}(t)dt = N \cdot \sum_{i=1}^{k} \{W_i \cdot \lambda_i \cdot \exp(-\lambda_i \cdot t)\} dt + N \cdot r \cdot dt \quad \cdots(5)$$

In general, since only one correlated event is contained within a fixed time, Eqs. (5) is approximated to

$$N \cdot P_{Total}(t) = N \cdot \{W \cdot \lambda \cdot \exp(-\lambda \cdot t) + r\} dt \cdots(6)$$

Theoretical MTA distribution is demonstrated in Fig. 3-5. The number of correlated events is obtained from the initial exponential decay curve over the noise (indicated in a horizontal line), which is attributed to probability of random events (R). The correlated events are easily identified from the exponential decay time, since the decay time is depended on half life of daughter nuclides, such as ^{216}Po ($T_{1/2}$:145 ms), ^{217}At ($T_{1/2}$:32.3 ms), ^{215}At ($T_{1/2}$:1.78 ms), ^{214}Po ($T_{1/2}$:164 μs) and ^{213}Po ($T_{1/2}$:4.2 μs). Based on an assumption of radioactive equilibrium, the radioactivities of U-series, Th-series, Ac-series and Np-series can be evaluated.

3-2. System

3-2-1. LSC and TIA measurements

For the purpose of determination for a small amount of radioactive nuclides, a LSC (ORDERA 8100AB) called PERALS (McDowell, 1992) and a new high-speed multiple pulse time data registration, processing and real-time display system (ZN-HTS2) were used (Yawata et al., 2006). The PERALS apparatus equips with a pulse shape discrimination (PSD) circuit to reject pulses caused by β-particles and γ-rays to extract pure α-pulses. After adjusting the PSD level to an optimal condition (see Fig. 3-6), the spectrometer provides a output signal (TTL level), composing of two kinds of pulses; such as original pulses containing α/β(γ) pulse and α pulse as output signal (McDowell, 1992).

Each α/β(γ) pulses and α pulses from PERALS were fed into an original 32 bit PCI board installed with a new system. All channel and pulse occurring time data are stored to First-in First-out (FIFO) RAM, followed to transfer into temporary CPU RAM by direct memory access (DMA). Both data registration (into main RAM) and calculation of MTA distribution together with real-time display simultaneously process using two software. The MTA distribution data are output into an "Excel" format. Details of the new system are depicted in Fig. 3-7.

3-2-2. γ-ray spectrometry

The γ-ray detector is an intrinsic high-purity germanium crystal (HPGe) manufactured by EG&G ORTEC. The counting efficiency of the HPGe has been calibrated with several commercial calibration sources (Japan Radioisotope Association), which are constructed from the homogeneously dispersed multi radioactive nuclides. Table 3-2 shows the nuclei of the source and the activity at the reference date (i.e. 20 February 2003). The relative uncertainty on the activity is from 3.8 to 4.7%. These sources have an U-8 shape of a container with a total volume of 10, 20, 30, 40 and 50 ml (epoxy matrix: density of approximately 1.0 $g \cdot cm^{-3}$). The source dimensions are: from 10 to 50 mm height and 50 mm diameter. Fig. 3-8 shows a typical γ-ray energy spectra obtained with the U-8 container standard source for an 40000 sec measurement time. Since these spectra clearly show a drop in the efficiency at energies below 20 keV, the efficiency below 100 keV suffers from considerable uncertainty. However, this part of the spectrum does not give important information for dating applications. Fig. 3-9 shows the counting efficiency plot against γ-ray energies from each calibration sources. The curves are fitted to the following equation: $F(x) = \frac{1}{a \cdot x^b + c \cdot x^d}$, where a, b, c and d is a constant. From these fitting curves, the counting efficiencies for 1460 keV (^{40}K), 352 keV (^{214}Pb) and 238 keV (^{212}Pb) are obtained, taking into account of the correction factor of both γ-ray self-absorption and sum peaks. The ^{238}U and ^{232}Th concentrations in samples are estimated under an assumption of radioactive equilibrium within uranium and thorium decay chains.

3-3. External and internal dose rate estimation

For LSC/MTA method, a portion of Toya sample (bulk and quartz sample) and quartz samples (~2 g) were powdered and then completely dissolved in aqua regia and HF for 12 h at 110°C, respectively. To estimate recovery percentage during extraction procedure, ^{225}Ra solution as a yield tracer with a given activity was added into this solution. The scintillator solutions including ^{226}Ra, ^{224}Ra and ^{225}Ra were prepared by liquid-liquid extraction. The extraction procedure is depicted in Fig. 3-10. The solution containing radium isotopes was evaporated to dryness, and the residue was dissolved again in doubly distilled water (DDW). After adding 2.5M NaOH to adjust the pH to over 10, radium was selectively extracted into an extractive scintillator cocktail (ETRAC RADAEXα, ORDERA Inc.). This scintillator cocktail had already been converted to the sodium salt form by shaking with a 4M $NaNO_3$/0.2M NaOH solution. A 1.0 ml scintillator solution, containing all radium isotopes, was transferred to a standard glass test tube (ϕ=8.0mm, *l*=75 mm), and 60 mg di-(2-ethylhexyl) phosphoric acid (HDEHP) was added to stabilize until the second MTA-measurement of the Np-series nuclides to be made after 14 days, which need to attain almost maximum growth of $^{221}\mathrm{Fr} \xrightarrow{\alpha} {}^{217}\mathrm{At}(T_{1/2}: 32.3\mathrm{ms}) \xrightarrow{\alpha}$ and $^{213}\mathrm{Bi} \xrightarrow{\beta} {}^{213}\mathrm{Po}(T_{1/2}: 4.2\mu\mathrm{s}) \xrightarrow{\alpha}$ in Np-series. The scintillator solution was purged for 5 minutes with dry nitrogen gas to expel dissolved ^{222}Rn and oxygen which leads to oxygen-quenching in liquid scintillation counting (LSC) (Hashimoto et al., 1999). After then, to disturb ^{222}Rn and ^{220}Rn escape from scintillator solution, silicon stopper (ϕ=8.0 mm) was tightly sealed in a glass test tube not leaving any space. The LSC/MTA measurements were carried out twice to measure radioactivities of ^{214}Po and ^{216}Po, and to estimate radioactivity of ^{225}Ac, which is daughter of ^{225}Ra, reaches maximum about 14 days after radium extraction (Fig. 3-11). From the ^{225}Ac activity, the chemical recovery of radium isotopes during extraction was evaluated.

For γ-ray spectrometry, the dried Toya ample (~30 g), which was heated on a hot plate at 110°C for 48 h, was packed in a U-8 container and then measured for 80000 sec. The water content is expressed as weight of water divided by dry sample weight.

Based on ^{238}U, ^{232}Th and ^{40}K radioactivity, the external and internal dose rate were calculated using conversion factors (Adamiec and Aitken, 1998). In addition, the contribution of cosmic rays was

employed 0.18 mGy·a^{-1}, since the Toya sample was collected from approximately 42.8°N 140.9°E (Prescott and Hutton, 1994)

4. Equivalent dose determination using single-aliquot regenerative-dose (SAR) protocol

4-1. Preheat plateau of equivalent dose

In order to estimate the equivalent doses, RTL/SAR protocol was attempted using an automated luminescence measuring system, since the Toya quartz grains showed RTL properties. The measuring system was adjusted to optimal detection- and irradiation-conditions for RTL-measurements (see Chapter 1 in details).

In the SAR protocol, thermal treatment, namely preheat and cut heat, are needed to empty any shallow traps, particularly those electrons trapped by laboratory irradiations. Wintle and Murray (2006) had proposed that the SAR measurements are tried on a number of different aliquots using a different preheat temperatures from 160 to 300°C (namely equivalent dose preheat plateau). Once the results from test dose measurements, monitoring luminescence sensitivity changes in both natural and regenerated signals, are effective at each preheat temperature, the estimated equivalent doses should demonstrate an absence of preheat temperature dependence. Therefore, the plateau ranges as a function of preheat temperatures can be applied for the equivalent dose determinations. However, a poor preheat plateau that was reported by Choi et al. (2003) means that the SAR protocol may be inappropriate for equivalent dose estimation when using the quartz samples. For Toya quartz sample, the range of preheat temperatures from 160 to 300°C for 5 min and cut heat temperature of 200°C were investigated with regarding to equivalent dose preheat plateau.

4-2. Equivalent dose determination and dose recovery test

The dose-response curve for each aliquot was constructed by the RTL glowcurves which were integrated over the 350 to 380°C range as seen in Fig. 3-12. In all RTL measurements, the samples were measured from 50°C to 450°C at heating rate 1°C/sec. Resultant equivalent doses from 30 aliquots analyses were plotted into a radial plot (Galbraith, 1990).

To check the luminescence reproducibility as a dosimeter, dose recovery test (Roberts et al., 1999) was carried out using 10 aliquots analyses. In this test, as-received aliquots were given to a laboratory dose of 100 Gy by γ-ray (^{137}Cs) at the Radioisotopes Center in Niigata University, after removal of naturally accumulated luminescence signals by heating. The given dose was chosen to be close to the expected natural dose. Then, the SAR protocol was applied to each aliquot sample. The ratio of the measured dose to the given dose (100 Gy) was calculated for the individual aliquots, defined the dose recovery ratio. If the SAR protocol is working correctly, this ratio must be unity. So, the ability of the SAR protocol to measure accurately this dose is tested directly. In addition, the dose recovery test also provides information on the maximum precision that can be achieved in the absence of heterogeneity by natural variations of dose rate. These data can be used to confirm whether the quartz samples originated from a single source.

5. Results and discussion

5-1. Crosscheck between LSC/MTA method and γ-ray spectrometry

In order to check the reliability of LSC/MTA method for the radioactivity determination, the estimated radioactivities in Toya sample using LSC/MTA method were compared with those from γ-ray spectrometry. The evaluated concentrations of ^{238}U and ^{232}Th are summarized in Table 3-3.

The evaluated data from LSC/MTA method agreed well to those from γ-ray spectrometry within experimental errors. As a result, ^{238}U and ^{232}Th concentrations in samples are recognized to be quantitatively determined using LSC/MTA method as well as using γ-ray spectrometry. In the MTA technique, since the probability that non-correlated events occur within micro- and milli-seconds (r: see the Eqs. (3)) is sufficiently low, the correlated events associated with ^{216}Po (U-series) and ^{214}Po (Th-series) can be exhibited on the negligible small background as seen in Figs 3-13, 3-14. On the other hand, the γ-ray spectrometry can evaluate the radioactivity of ^{238}U, ^{232}Th and ^{40}K simultaneously and is easier to estimate radioactivity from view points of the chemical extraction procedures and the use of yield tracer. Accordingly, both the LSC/MTA method and the γ-ray spectrometry were utilized for the determination of radioactivities in quartz and in surrounding material, respectively.

5-2. Annual dose for Toya sample

The evaluated radionuclide concentrations (^{238}U, ^{232}Th and K_2O (^{40}K)) and external/internal dose rate in Toya sample are listed in Table 3-4. In addition, this Table also contains the estimated radioactive nuclides in three other quartz samples.

The radioactivities in volcanic products are closely related to composition of magma solution in the absence of contamination of other sources. Actually, the estimated concentrations of radioactivity in Toya sample are in concordance with that in Toya pyroclastic flow deposits (Ganzawa et al., 2005; U: 1.61~1.77 ppm, Th: 4.77~4.98 ppm, K_2O: 2.09~2.25 %), which were collected from different site. Using the conversion factors (Adamiec and Aitken, 1998), the external dose rate was evaluated as 1.07 ± 0.04 mGy･a^{-1}, taking into consideration of both cosmic ray contribution and moisture content of 18.7 %.

For internal radioactivity, the Toya quartz grains contained ^{238}U of 0.41±0.05 ppm and ^{232}Th of 0.28±0.02 ppm, whereas other quartz samples gave a small amount of radioactive nuclides as seen in Table 3-4. The internal dose rate was estimated to be 0.17 ± 0.02 mGy･a^{-1} under an assumption of k-value, which means the effectiveness for creation of luminescence hole and electrons by α-particles (Aitken, 1985) to be 0.03. As a result, the annual dose was estimated to 1.24 ± 0.06 mGy･a^{-1}. Surprisingly, for Toya sample, the internal dose rate contribution on annual dose reached 10~20 %. This means that annual dose in Toya sample should consider the internal dose rate contribution. High radioactive impurities in Toya quartz grains might also be attributed to quartz crystallization process with rapid cooling step as mentioned in Chapter 2. Since the radioactive nuclides during the rapid formation of quartz crystals, such as in the volcanic eruption, can not be excluded as well as other impurities, the volcanic quartz might give higher internal radioactivity compared with other quartz samples.

Generally speaking, Japanese volcanic products or layers usually contain low radioactivity compared with other soil and rock samples. As a result, TL/OSL-dating for Japanese volcanic products should take care of contribution of internal radioactivity for the evaluation of the internal dose rate as annual dose, because of the relatively low external dose rate.

5-3. Equivalent dose and age estimation of Toya sample

The equivalent doses of Toya quartz sample are plotted as a function of preheat temperatures as seen in Fig. 3-15. A preheat plateau from 160 to 300^{o}C with a mean value of 123.4 ± 18.1 Gy is certified to Toya quartz sample. This large plateau also implies that the most intense RTL glow peak (350-380^{o}C), which is available for the equivalent dose determination, is independent of the preheat temperatures. In the equivalent dose determination, the preheat condition at 240^{o}C for 5 min and cutheat of 200^{o}C were chosen.

Using above preheat and cutheat conditions, the equivalent doses are plotted into a radial plot as seen in Fig. 3-16. This plot is composed approximately of 30 aliquots. Based on the radial plot, a few sample data, which have equivalent doses outside the ±2 standard error band, were excluded from the equivalent dose determination. However, most of equivalent doses provided around one equivalent dose without large dispersion, implying this Toya sample is originated from one volcanic event (Galbraith and Laslett, 1993). As a result, the equivalent dose of Toya quartz grains was evaluated to be 120.0 ± 16.2 Gy. The error was derived from two sigma experimental error range. On the basis of the equivalent dose and the annual dose for Toya sample, the age was estimated to 96.8 ± 13.9 ka (Table 3-5). That is, the age of Toya activity was 96.8±13.9 x10^{3} years ago since TL age indicates elapsed time after the last heating events. This result was in good agreement with the expected age from independent age control (Machida and Arai, 1992; Ganzawa et al., 2005).

In dose recovery test, the dose recovery ratio (measured dose/given dose) was 1.00 ± 0.06 from ten aliquots analyses. Since the estimated ratio was unity, the Toya quartz samples, which accumulated over 100 Gy, can be suitable for analysis using conventional SAR protocol (Murray and Wintle, 2000). In addition, the maximum precision of equivalent dose determination, which is strongly influenced on measuring conditions including luminescence intensity and thermal background (see the Chapter 1), was estimated to be ±6%. As a result, the scatter in equivalent doses from natural sample (13.5%) might be attributed to heterogeneous irradiation by natural nuclides.

From these results, it was confirmed that RTL dating to volcanic activity can be applied to up to 10 ka due to a high RTL dose saturation level beyond 100 Gy. This means that the lifetime of RTL sources (trapped hole and electrons; see the Chapter 2) over 10 ka was experimentally proved to give

high stability during storage period. However, RTL technique has not been applied to sedimentary deposit dating due to a hard bleaching component of RTL peak (Franklin et al., 1995), resulting in a high RTL residual level after bleaching (Lai and Murray, 2006). In contrast, fast component of OSL has been recognized to be saturated around 100 Gy (~10 ka) (Wintle and Murray, 2006), although OSL ages directly indicated the time of deposit. Recently, Westaway and Roberts (2006) developed a dual-aliquot regenerative-dose (DAP) protocol for RTL dating to estimate the optical age by subtracting the unbleachable dose (one half part) from the total dose (another half part). Using isothermal RTL measurements, they could obtain the optical ages of 35-190 ka from cave deposits that compared favorably with independent age estimates. In future, the RTL phenomena should be useful tool for optical dating over 10 ka sediments as well as thermal dating due to high signal stability and absence of dose saturation in the range from 100-1000 Gy.

6. Conclusions

In order to determine internal radioactivity of quartz grains, LSC/MTA method was developed. By comparing γ-ray spectrometry, it was clarified that the LSC/MTA method has following advantages for the radioactivity determination: (i) requirement of a small amount of samples for measurements (approximately ~2 g), (ii) contribution of negligible small background, (iii) ^{216}Po- and ^{214}Po-decay rates were easily distinguished from scintillation pulses without α-energy information, and (iv) even 0.1 ppm of ^{238}U and ^{232}Th in quartz grains were detected due to a high counting efficiency for α- and β -particles.

Using LSC/MTA method, one volcanic quartz sample contained relatively high radioactivity compared to other quartz origins. The high radioactivity might be attributed to the rapid crystallization process, such as volcanic eruption. As a result, it was found that some volcanic quartz sample should consider the internal dose rate contribution to annual dose. Taking into consideration of internal radioactivity, the age of Toya volcano activity was evaluated to be 96.8±13.9 ka using RTL-measurements.

• *7. Reference*

Adamiec G., Aitken M., Dose-rate conversion factors: update. Ancient TL, **16**, 37-50 (1998).

Aitken M.J., Thermoluminescence Dating. Academic press, London, 61-86 (1985).

Aitken M.J., An introduction to optical dating. Oxford university press, 39-47 (1998).

Choi J.H., Murray A.S., Jain M., Cheong C.S., Chang H.W., Luminescence dating of well-sorted marine terrace sediments on the southeastern coast of Korea. Quat. Sci. Rev., **22**, 407-421 (2003).

Franklin, A.D., Prescott, J.R., Scholefield, R.B., The mechanism of thermoluminescence in an Australian sedimentary quartz. J. Lumin., **63**, 317-326 (1995).

Galbraith R.F., The radial plot: Graphical assessment of spread in ages. Nucl. Tracks and Raiat. Meas., **17** 207-214 (1990).

Galbraith, R.F., Laslett, G.M., Statistical models for mixed fission track ages. Nucl. Tracks Radiat. Meas. **21**, 459-470 (1993).

Ganzawa Y., Watanabe Y., Osani F., Hashimoto T., TL color images from quartzes of loess and thephra in China and Japan. Radiat. Meas., **27**, 383-388 (1997).

Ganzawa Y., Furukawa H., Hashimoto T., Sanzelle S., Miallier D., Pilleyre T., Single grains dating of volcanic quartz from pyroclastic flows using red TL. Radiat. Meas., **39**, 479-487 (2005).

Hashimoto T., Noguchi M., Washio H., Yamamoto Y., Uezu Y., Principle of single and multiple time interval analysis applicable to radioactive nuclides with half-lives of millisecond order. J. Radioanal. Nucl. Chem., **159**, 375-387 (1992).

Hashimoto T., Yoneyama Y., Sato K., Komatsu Y., Pulse time interval analysis (TIA) combined with liquid scintillation counting for the determination of environmental α-nuclides-preparation and utilization of ^{225}Ra as a Yield Tracer. J. Radioanal. Nucl. Chem., **239**, 619-629 (1999).

Hashimoto T., Sanada Y., Uezu Y., Simultaneous determination of radionuclides separable into natural decay series by use of time-interval analysis. Anal. Bioanal. Chem., **379**, 227-233 (2004).

Hashimoto T., Yawata T., Takano M., Comparison of naturally accumulated radiation doses and dating of archaeological burnt materials and usefulness of RTL-dating from quartz extracts. Geochem. J., **39**, 201-212 (2005).

Lai Z.P., Murray A.S., Red TL of quartz extracted from Chinese loess: Bleachability and saturation dose. Radiat. Meas., **41**, 836-840 (2006).

Machida H., Arai F., Atlas of tephra in and around Japan, University of Tokyo Press, 94-165 (1992)

McDowell W.J., Photon/electron-rejecting alpha liquid scintillation (PERALS) spectrometry: a review. Radioact. Radiochem., **3**, 25-52 (1992).

Murray A.S., Wintle A.G., Luminescence dating of quartz using an improved single-aliquot regenerative-dose protocol. Radiat. Meas., **32**, 57-73 (2000).

Prescott J.R., Hutton J.T., Cosmic ray contributions to dose rates for luminescence and ESR dating: Large depths and long-term time variations. Radiat. Meas., **23**, 497-500 (1994).

Roberts, R.G., Galbraith, R.F., Olley, J.M., Yoshida, H., Laslett, G.M., Optical dating of single and multiple grains of quartz from Jinmium rock shelter, northern Australia: Part II, results and implications. Archaeometry, **41**, 365–395 (1999).

Sanada Y., Kobayashi H., Furuta S., Nemoto K., Kawai K., Hashimoto T., Selective detection of correlated decay events in Rn progeny with micro-second life using pulse time interval analysis. Radioisotopes, **55**, 727-734 (2006).

Westaway K.E., Roberts R.G., A dual-aliquot regenerative-dose protocol (DAP) for thermoluminescence (TL) dating of quartz sediments using the light-sensitive and isothermally stimulated red emissions. Quat. Sci. Rev., **25**, 2513-2528 (2006).

Wintle A.G., Murray A.S., A review of quartz optically stimulated luminescence characteristics and their relevance in single-aliquot regeneration dating protocols. Radiat. Meas., **41**, 369-391 (2006).

Yawata T., Sakaue H., Itou S., Hashimoto T., Usability of a new multiple high-speed pulse time data registration, processing and real-time display system for pulse time interval analysis. J. Nucl. Sci. Tech. (in Japanese), **5**, 221-228 (2006).

Table 3-1 Typical concentration of natural radionuclides in volcanic ash and archaeological samples.

Sample	^{238}U (ppm)			^{232}Th (ppm)		
Volcanic products						
Crystal ash (CA-1, Nagano)	0.4	±	0.07	1.7	±	0.22
Volcanic pumice (Numazawa volcano)	0.9	±	0.06	1.3	±	0.09
Ash layer (Sawanishi, Fukushima)	1.5	±	0.07	1.6	±	0.09
Ash layer (Toya, Hokkaido)	1.4	±	0.07	5.8	±	0.22
Ash layer (Medeshima, Miyagi)	0.8	±	0.09	2.3	±	0.30
Pyroclastic flow deposits (Nishiyama, Niigata)	1.7	±	0.08	1.7	±	0.10
Archaeological samples						
Roof tile (Shinyakushiji, Nara)	4.1	±	0.15	13.4	±	0.46
Jomon pottery (A-5, Okumiomote)	1.7	±	0.09	10.1	±	0.36
Jomon pottery (A-8, Okumiomote)	1.8	±	0.08	10.9	±	0.31
Jomon pottery (A-14, Okumiomote)	1.6	±	0.11	10.5	±	0.41
Jomon pottery (A-18, Okumiomote)	1.7	±	0.09	9.6	±	0.41
Jomon pottery (A-23, Okumiomote)	1.1	±	0.11	8.5	±	0.42
Jomon pottery (B-12, Okumiomote)	2.5	±	0.11	11.6	±	0.51
Jomon pottery (B-18, Okumiomote)	2.2	±	0.12	6.3	±	0.48

Table 3-2 Characteristics of the commercial calibration sources as given by the manufacturer (Japan Radioisotope Association)

Nuclide	γ-ray energy (keV)	Half-life	Activity (Bq/kg)	Branching Ratio (%)	Total Uncertainty (%)
^{109}Cd	88	462.6 d	53.6	3.63	4.2
^{57}Co	122	271.7 d	3.04	85.6	3.8
^{139}Ce	166	137.6 d	3.08	79.87	4.0
^{137}Cs	662	30.04 y	4.27	85.1	4.6
^{54}Mn	835	312.1 d	4.85	99.98	4.6
^{88}Y	898	106.7 d	4.66	94.0	4.1
^{60}Co	1173	5.271 y	5.87	99.86	4.0
^{60}Co	1333	5.271 y	5.87	99.98	4.0
^{88}Y	1836	106.7 d	4.66	99.36	4.1

Table 3-3 Evaluated concentrations of ^{238}U and ^{232}Th in Toya sample.

Method	Nuclides	Sample mass	^{238}U (ppm)	^{232}Th (ppm)
γ-ray spectrometry	^{214}Pb and ^{212}Pb	~ 30 g	1.02 ± 0.07	5.75 ± 0.22
LSC/MTA method	^{216}Po and ^{214}Po	~ 2 g	0.89 ± 0.11	5.93 ± 0.16

Measuring time: 80000 sec

Table 3-4 Evaluated radionuclides and dose rate.

Sample		Method	^{238}U (ppm)	^{232}Th (ppm)	K_2O (%)	Dose rate (mGy･a^{-1})	Annual dose (mGy･a^{-1})
Toya sample	surrounding material	γ-ray spectrometry	1.02 ± 0.07	5.75 ± 0.22	1.22 ± 0.05	1.07 ± 0.04	1.24 ± 0.06
	in quartz	LSC/MTA method	0.41 ± 0.05	0.28 ± 0.02		0.17 ± 0.02	
Volcanic quartz (Tazawa, Japan)	in quartz	LSC/MTA method	0.11 ± 0.01	0.13 ± 0.03		0.05 ± 0.01	
Sediments quartz (BDH, UK)	in quartz	LSC/MTA method	0.16 ± 0.03	0.17 ± 0.10		0.07 ± 0.02	
Vein quartz (Brazil)	in quartz	LSC/MTA method	0.08 ± 0.004	0.05 ± 0.001		0.03 ± 0.01	

Table 3-5 Estimated age from quartz grains extracted from Toya volcanic ash.

Number of aliquots	Equivalent dose (Gy)	External dose rate ($mGy \cdot a^{-1}$)	Internal dose rate ($mGy \cdot a^{-1}$)	Annual dose ($mGy \cdot a^{-1}$)	Estimated age (ka)	Predicted age (ka)
33	123.4 ± 18.1	1.07 ± 0.04	0.17 ± 0.02	1.24 ± 0.06	96.8 ± 13.9	90-120*

*Machida and Arai, 1992

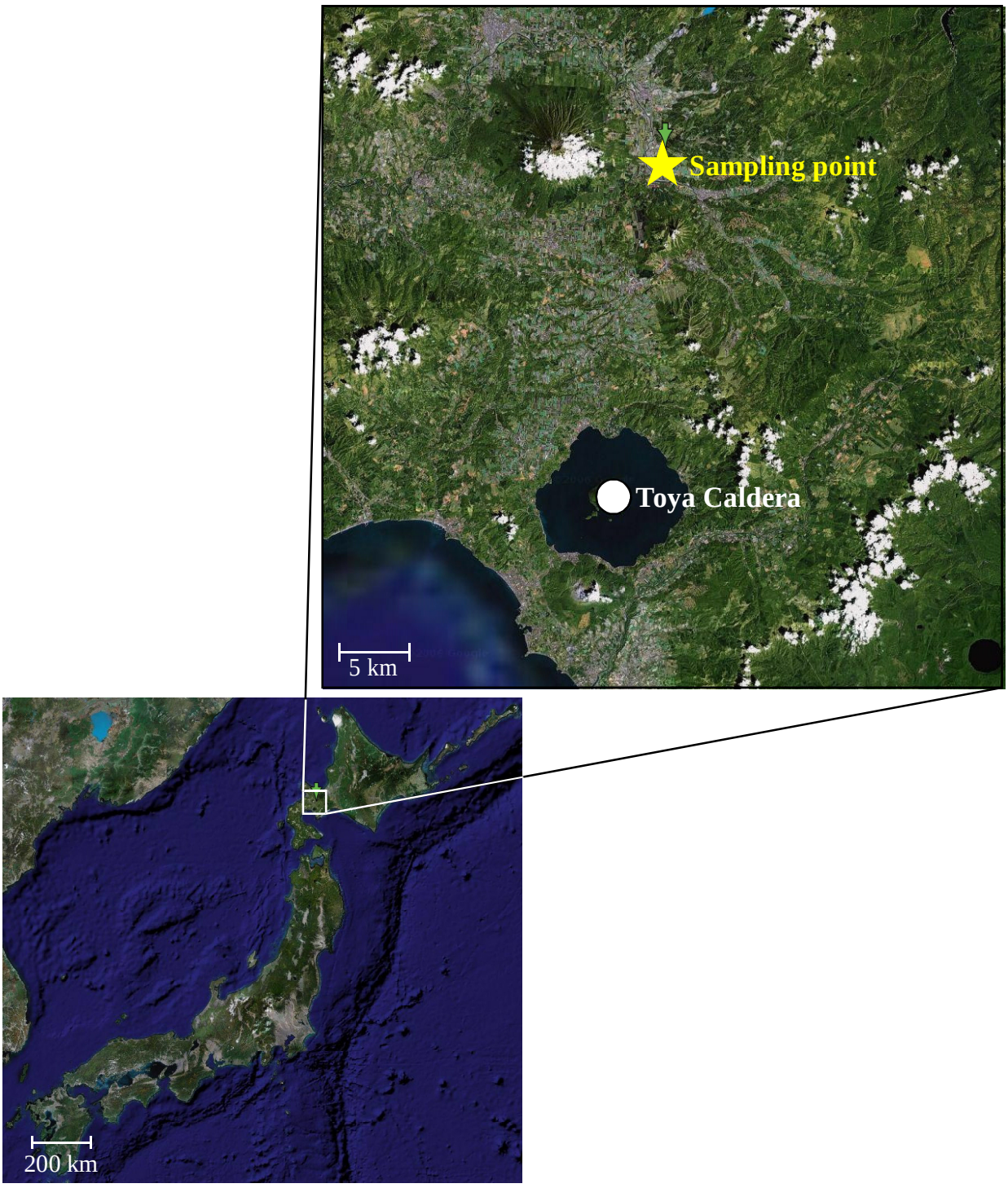

Fig. 3-1 Sampling location of volcanic ash, Toya, Hokkaido, Japan.

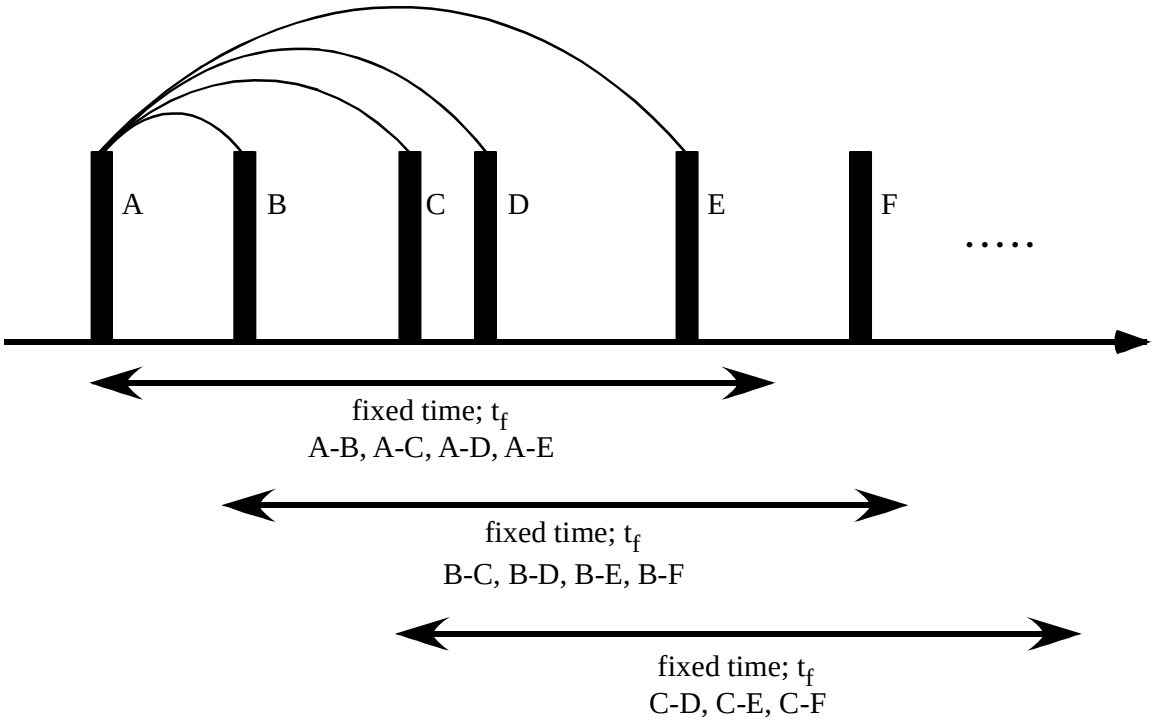

Fig. 3-2 Diagram for extraction procedure of multiple pulse time interval analysis (MTA).

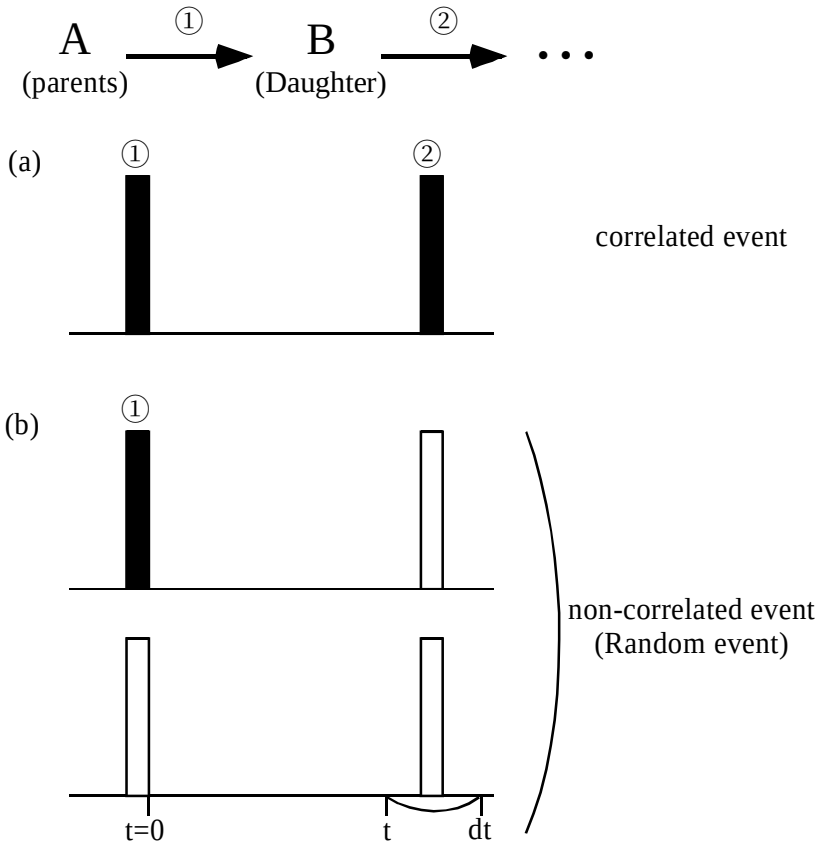

Fig. 3-3 Probability of MTA distribution. (a)correlated event, (b) non-correlated events.

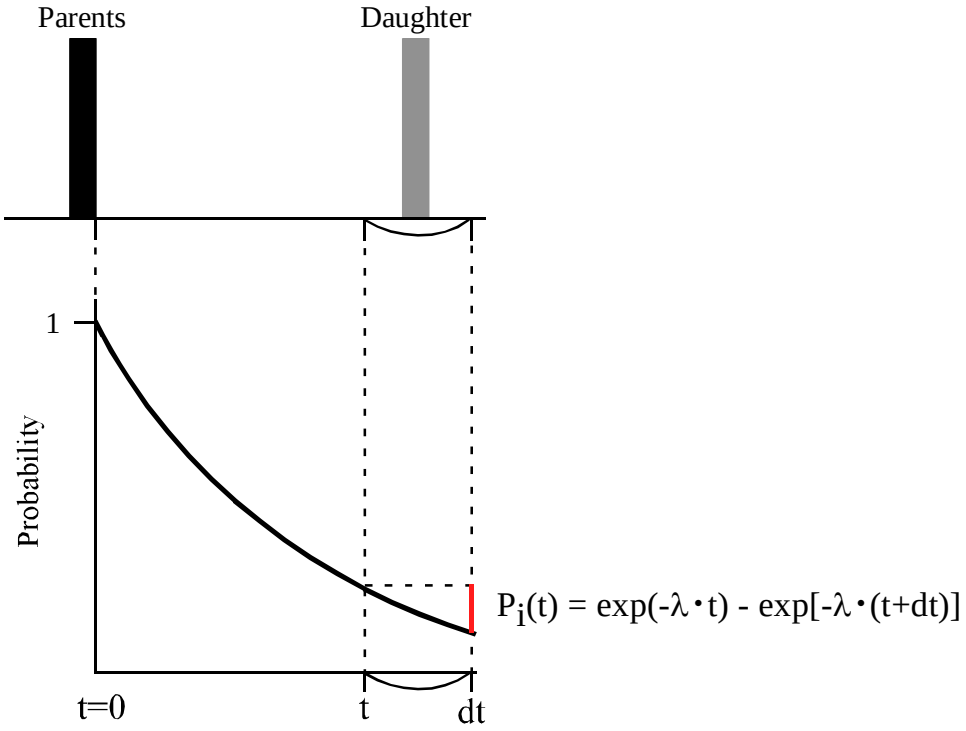

Fig. 3-4 Theoretical probability of successive decay events within short time (dt).

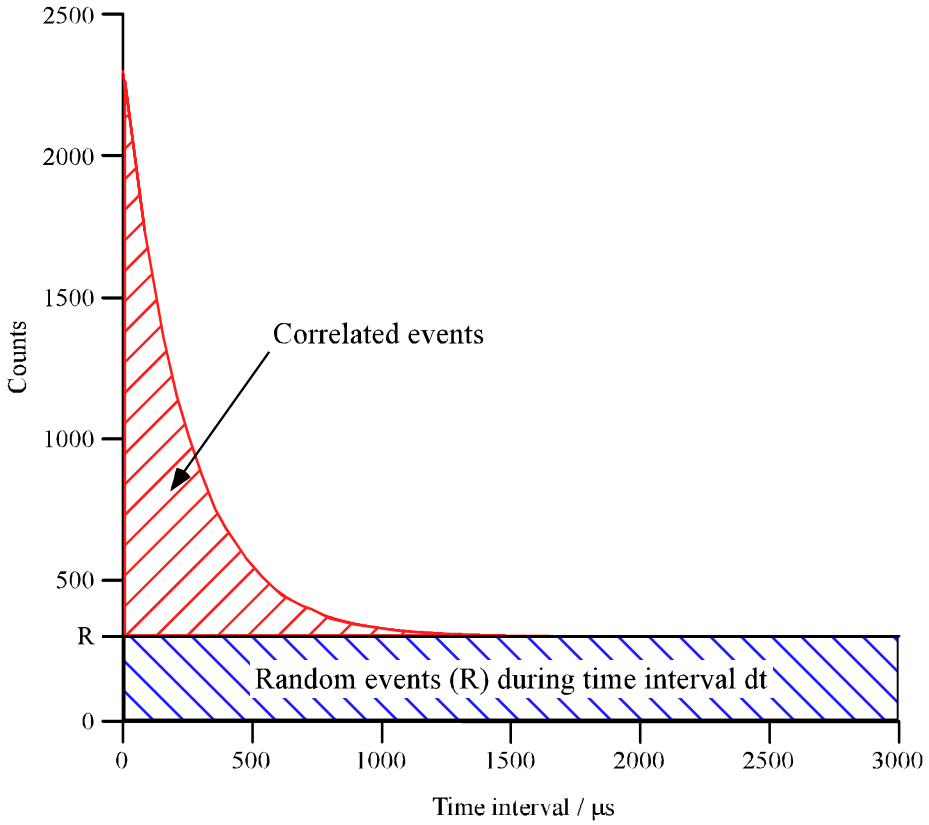

Fig. 3-5 Theoretical pulse time interval distribution by applying multiple pulse time interval analysis (MTA).

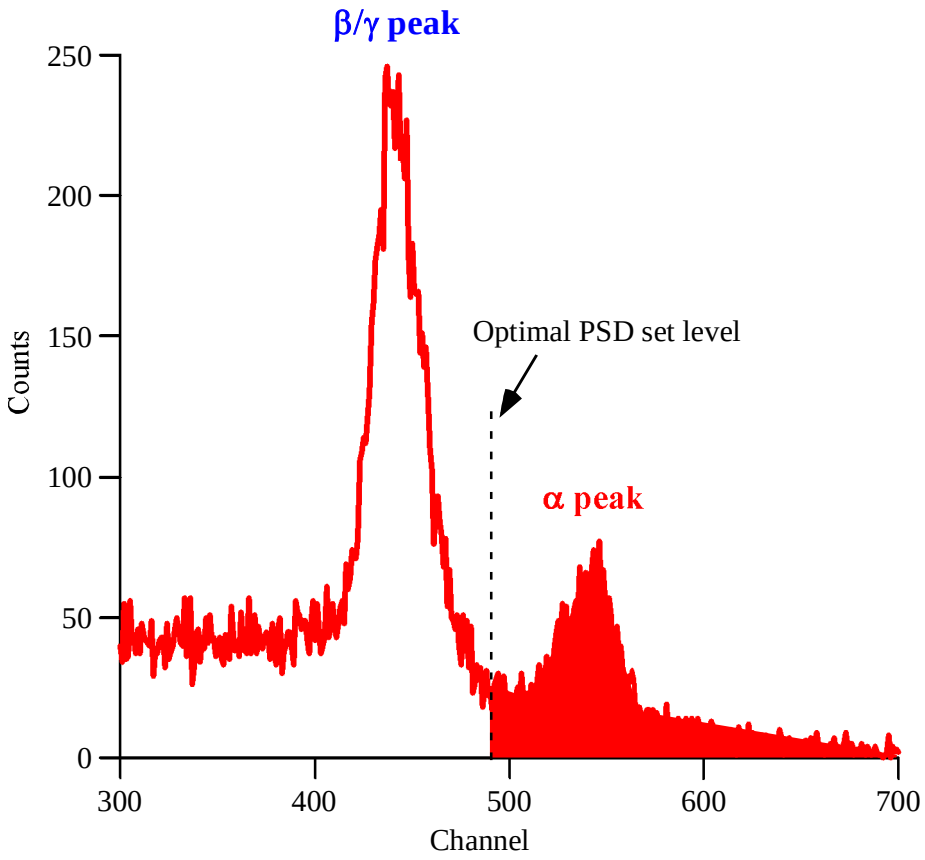

Fig. 3-6 PERALS pulse shape spectrum.

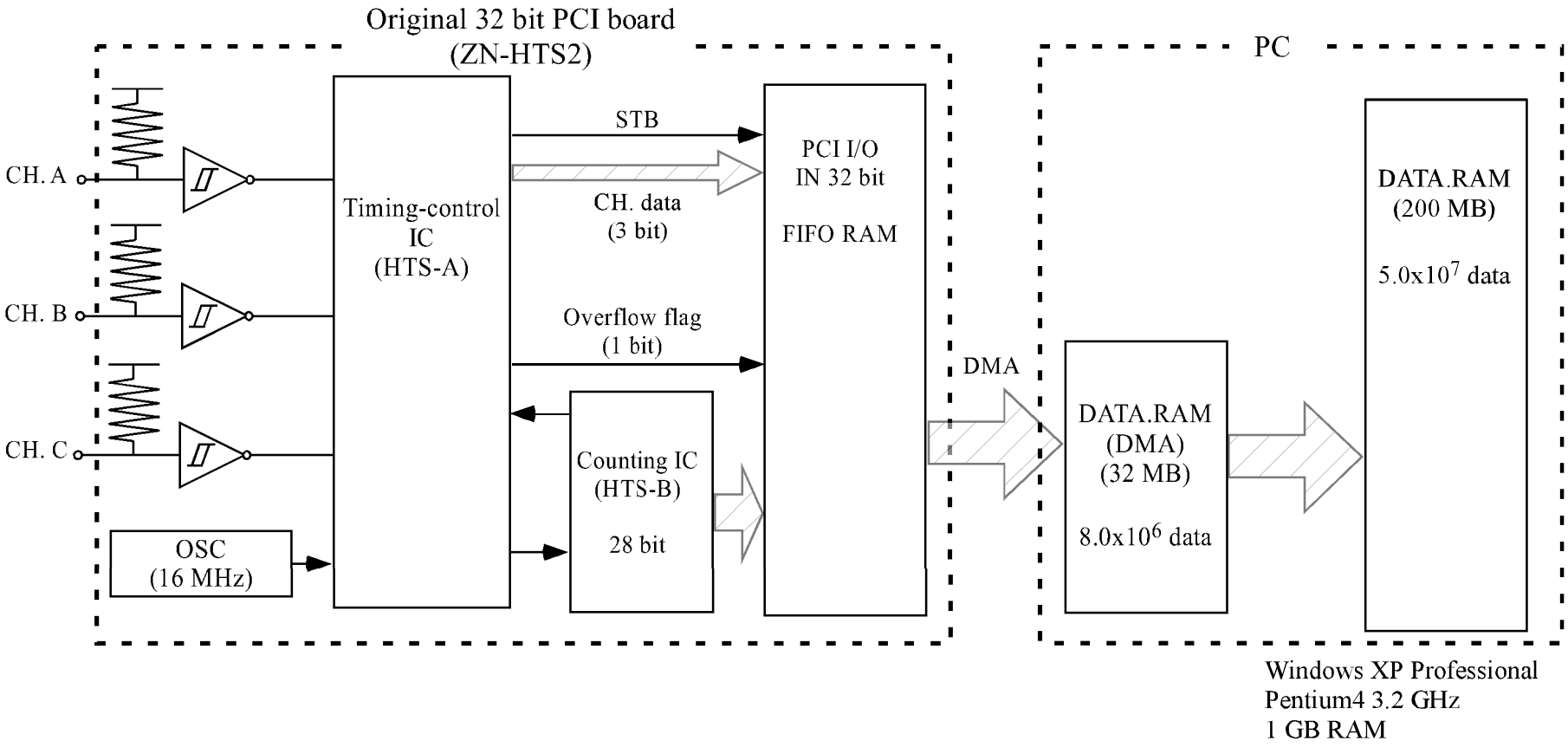

Fig. 3-7 Conceptual view of high-speed multiple pulse time data processing and real-time display system. Three input channels can provide simultaneously three different pulses and every data will be changed into pulse occurring times. All channel and pulse time data were transferred to FIFO RAM at 1 s rate, followed to transfer into temporary CPU RAM (32 MB) by DMA. Two process, data registration (into main RAM (200 MB)) and calculation of pulse time intervals along with real-time TIA-distribution display simultaneously processed using two softwares.

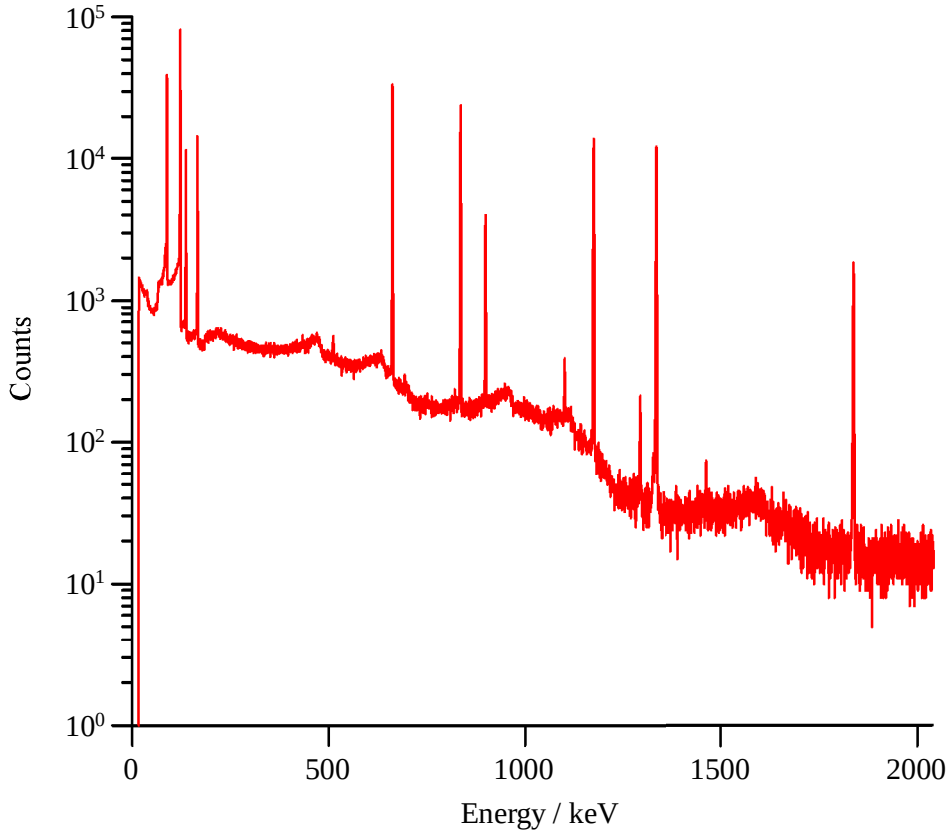

Fig. 3-8 γ-ray energy spectrum obtained with the U-8 container standard source for 40000 sec measurement time.

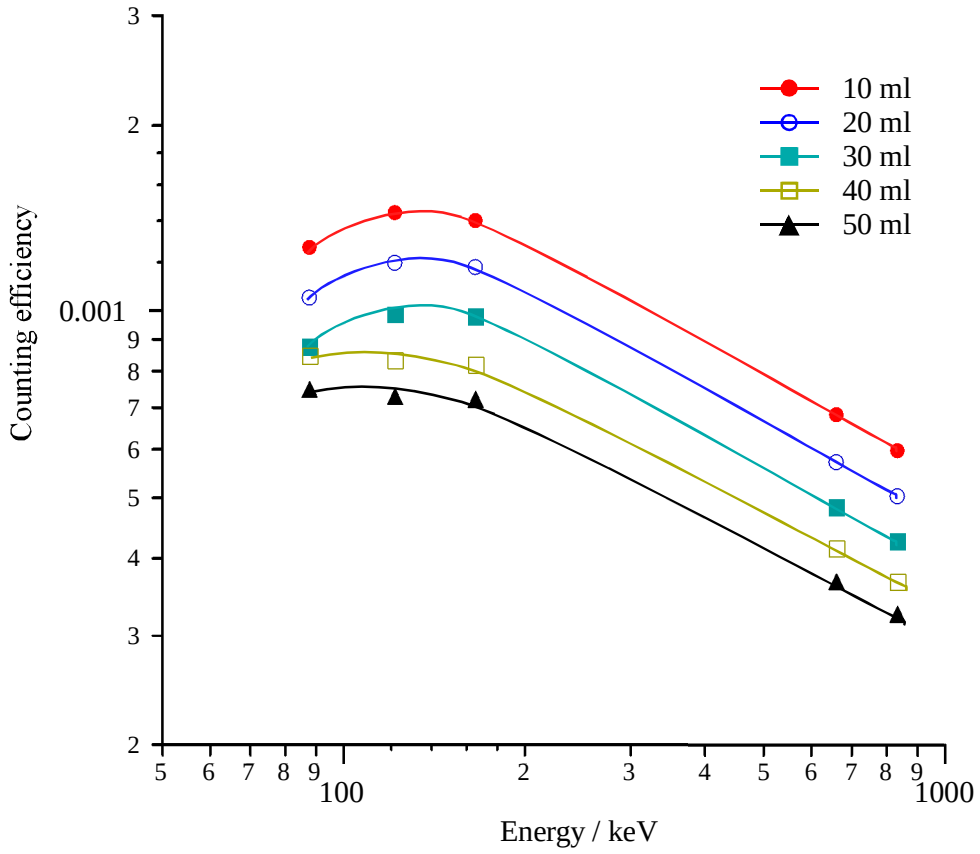

Fig. 3-9 Counting efficiency plot against γ-ray energies from each calibration sources.

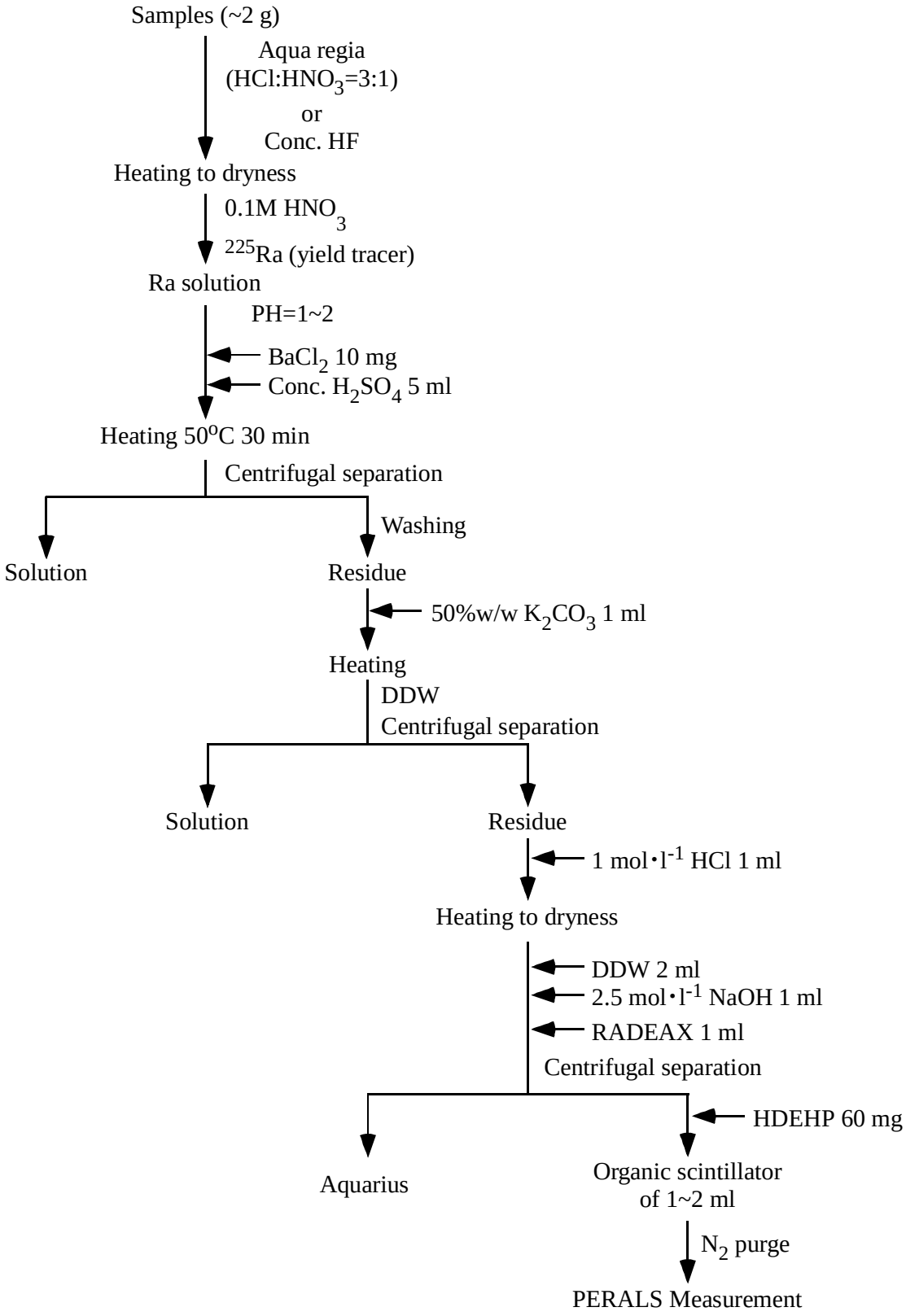

Fig. 3-10 Chemical Ra extraction procedure from natural samples.

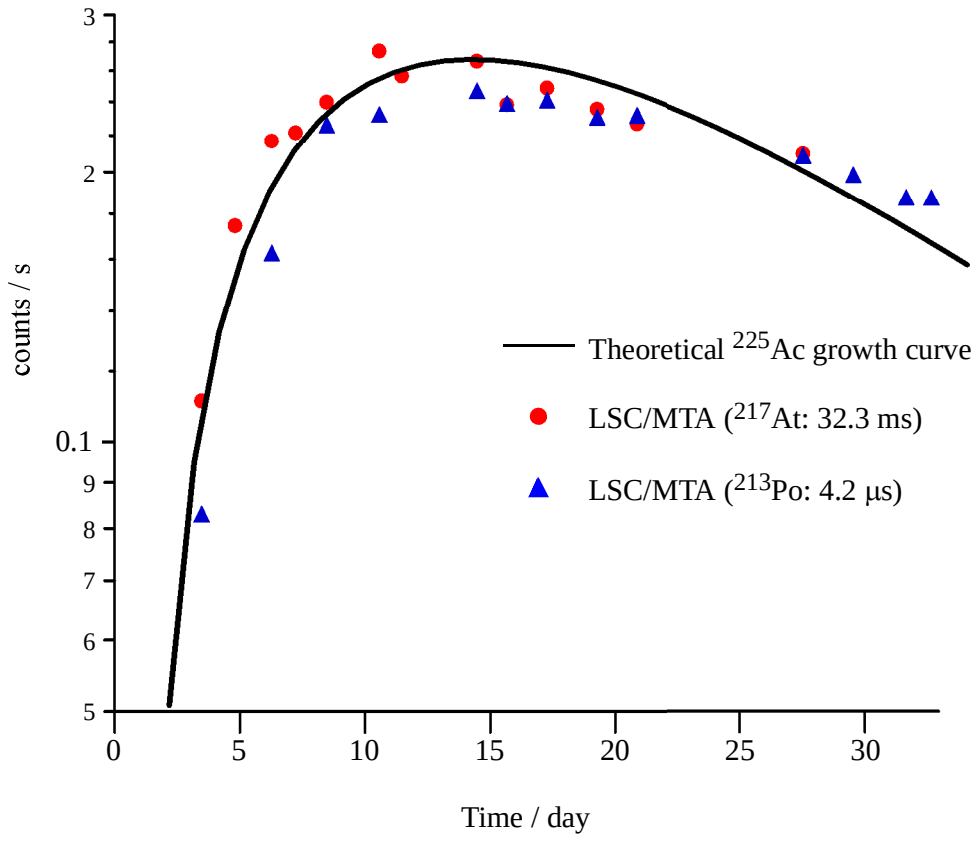

Fig. 3-11 Growth of ^{225}Ac estimated by LSC/MTA with theoretical growth curve.

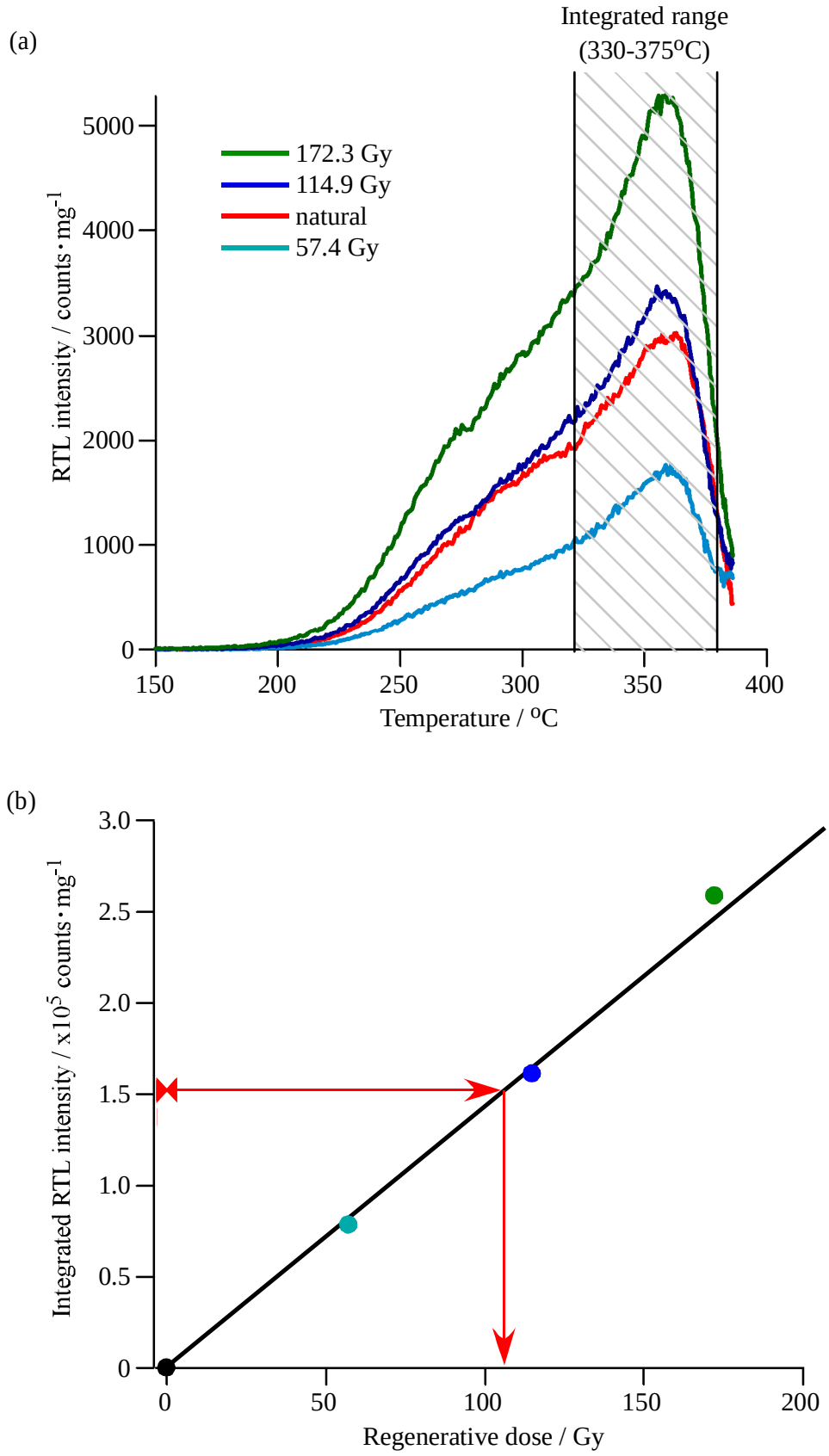

Fig. 3-12 RTL-glowcurves (a) and dose-response curve (b) of Toya sample. Integration range was 330-375°C.

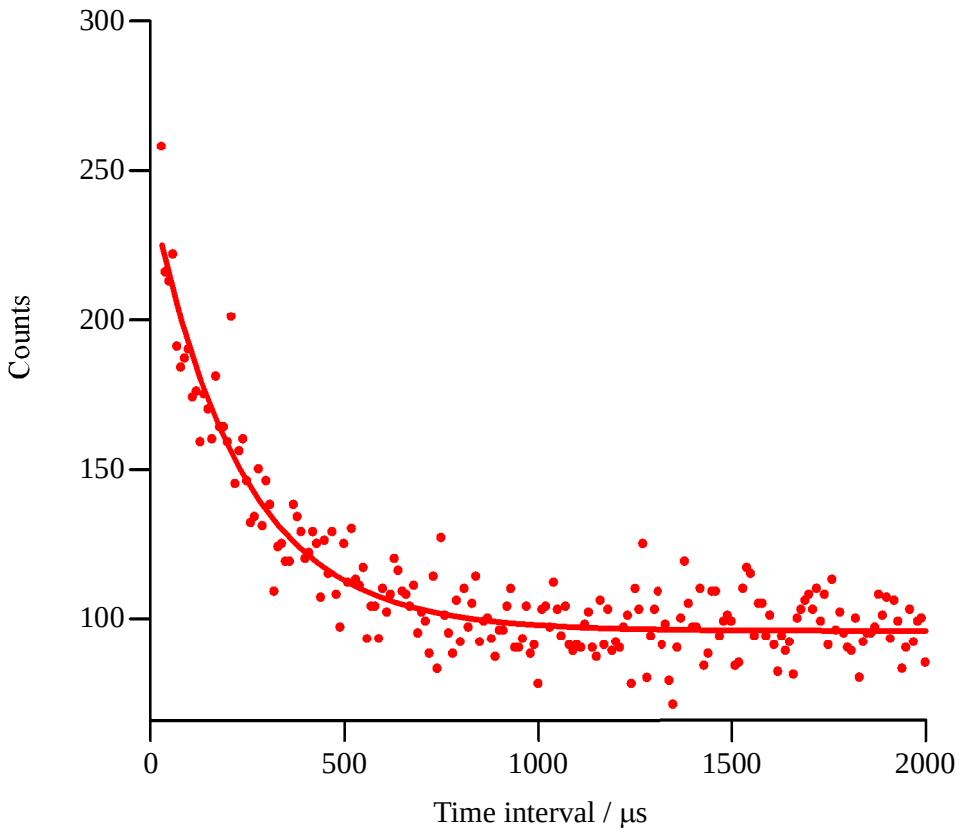

Fig. 3-13 MTA distribution associated with ^{216}Po.
Sample: Toya sample
Measurement time: 340000 sec

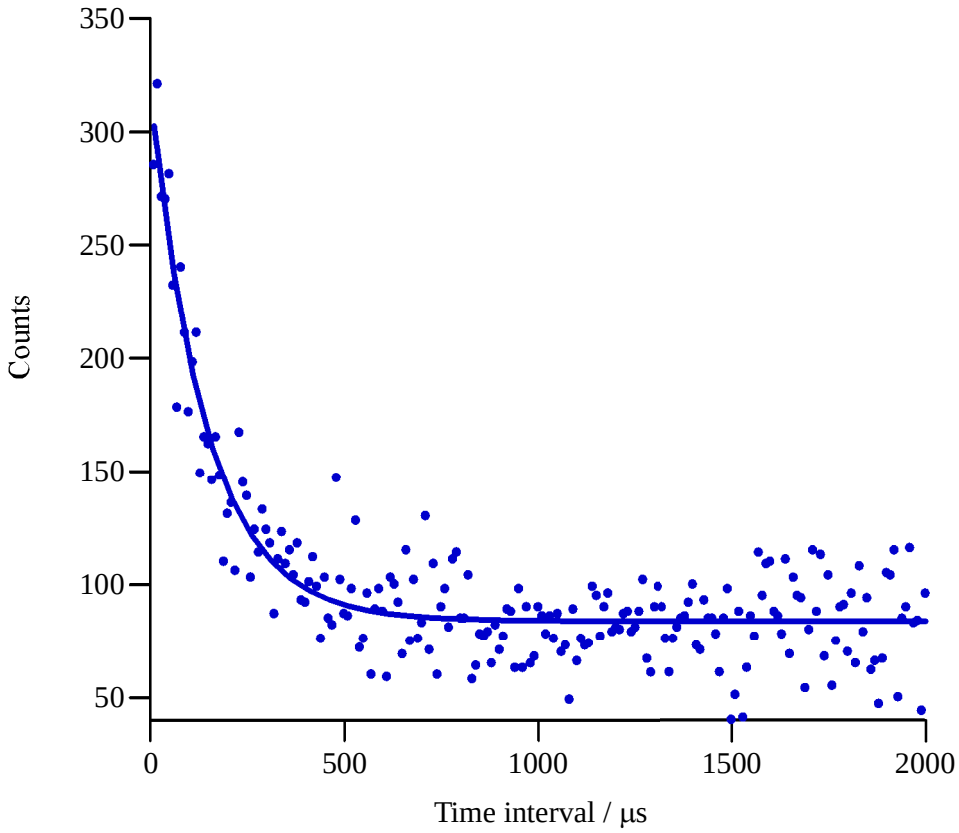

Fig. 3-14 MTA distribution associated with ^{214}Po.
Sample: Toya sample
Measurement time: 340000 sec

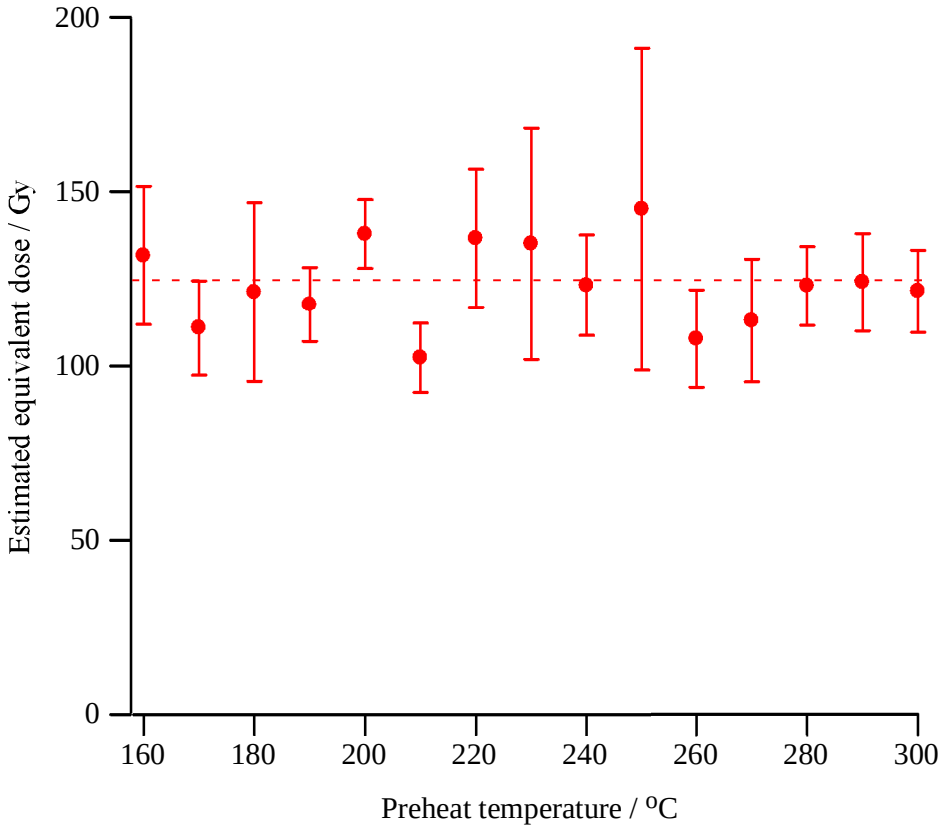

Fig. 3-15 Equivalent dose preheat plateau from Toya quartz grains.
The preheat time was fixed for 5 min.
The cutheat temperature was employed at 200°C.
Dotted line indicates a mean equivalent dose of 123.4 Gy.

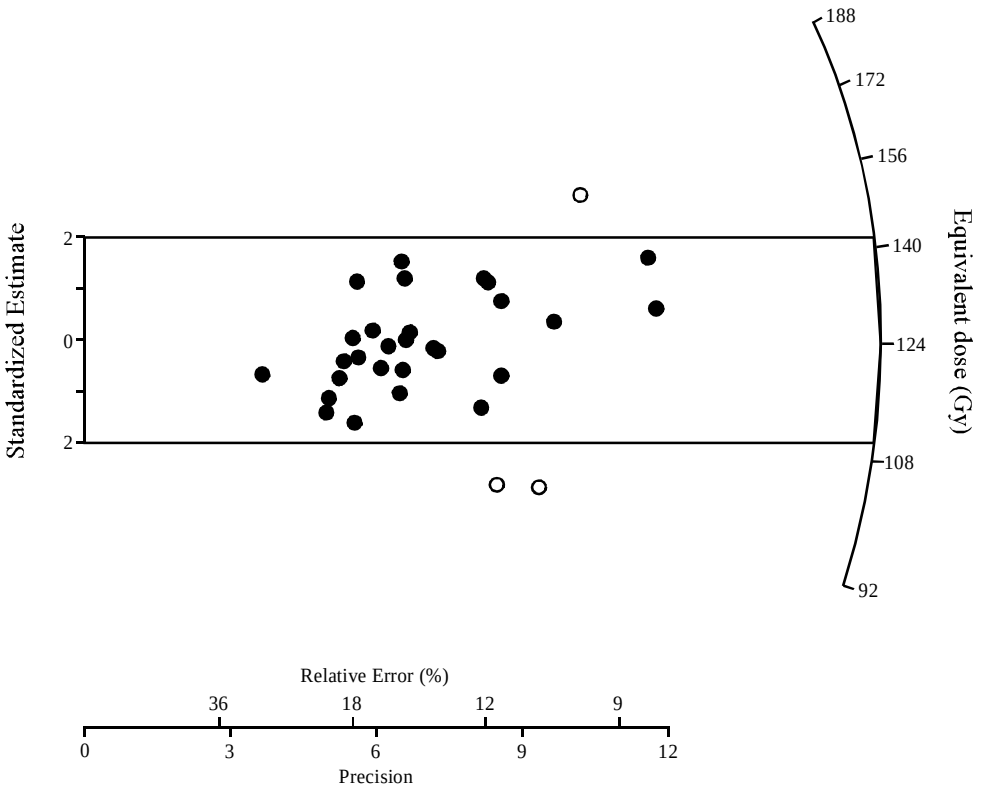

Fig. 3-16 Radial plot from Toya quartz grains.
This plot comprised of data from approximately 30 grains.